

Adolescent Idiopathic Scoliosis:
Classifying, Assessing, and Monitoring using Surface Topography Asymmetry
Analysis

by

Amin Komeili

A thesis submitted in partial fulfillment of the requirements for the degree of

Doctor of Philosophy

in

Structural Engineering

Department of Civil and Environmental Engineering
University of Alberta

© Amin Komeili, 2014

Abstract

The radiation dose and the associated lifetime risk of developing cancer is a problem justifying the use of surface topography (ST) as an alternative to radiographs for monitoring scoliosis. The current ST methods mainly rely on marker placement and fail to describe the 3D aspect of the scoliosis deformity. This thesis describes research and development of a novel method for assessing, quantifying, and monitoring the torso deformities based on their symmetry and curvature.

We present a new 3D asymmetry analysis that discloses the area of abnormality in a geometry using contours of deviation. Its application in biomedical image analysis of torso to quantifying and monitoring torso deformity is described. The deformity patterns of the analyzed torsos are categorized using the classification system. The reliability of the classification system along with its correlation to the radiograph measurement is investigated.

Internal characteristics observed in radiographs such as magnitude, number, and location of the scoliosis curve are estimated using the ST measurements. The difference of ST measurements between two successive acquisitions, with one year gap between, is used to determine the change of the thoracic/thoracolumbar and lumbar scoliosis curves. The capability of the ST measurements in classifying the scoliosis curves into progression and non-progression group is assessed with the aim of replacing some of the X-ray acquisition used to monitor patients with adolescent idiopathic scoliosis.

Preface

Some of the research conducted for this thesis forms part of a research collaboration, led by Dr. Samer Adeeb at the University of Alberta.

The setup of the technical apparatus and surface topography data acquisition referred to in chapter 2 was completed by Dr. Eric Parent research group, with the assistance of Ms. Lindsey Westover and Dr. Doug Hill. The data collection, asymmetry analysis and concluding analysis in chapter 2 to chapter 6 are my original work, as well as the literature review in chapter 1.

A journal paper has been published in the Journal of Engineering in Medicine from the developed technique in chapter 2 of this thesis as S. Hill, E.F. Sepulveda, A. Komeili, A. Travota, E. Parent, D. Hill, E. Lou, S. Adeeb, “Assessing asymmetry using reflection and rotoinversion in biomedical engineering applications,” Proceedings of the Institution of Mechanical Engineers, Part H: Journal of Engineering in Medicine, 2014 228: 523-529. S. Hill, E.F. Sepulveda, and I were responsible for the data collection and asymmetry analysis. Dr. D. Hill, Dr. E. Lou, Dr. E. Parent, and Dr. S. Adeeb contributed to concluding the results and assisted with manuscript composition.

A version of chapters 2 and 3 of this thesis has been published as A. Komeili, L. Westover, E. Parent, M. Moreau, M. El-Rich, S. Adeeb, “Surface Topography Asymmetry Maps Categorizing External Deformity in Scoliosis,” The Spine J. 2014, Jun 1;14(6):973-83. I was responsible for the data collection and conducting the asymmetry analysis. Ms. L. Westover and Dr. M. Moreau assisted with the data collection. Dr. E. Parent, Dr. M. El-Rich, and Dr. S. Adeeb contributed to concluding the results and assisted with manuscript composition.

A version of chapter 4 of this thesis has been submitted to the Journal of Spine Deformity as A. Komeili, L. Westover, E. Parent, M. El-Rich, S. Adeeb, “Correlation between a Novel Surface Topography Asymmetry Analysis and Radiographic Data in Scoliosis.” I was the primary author and was involved with the development of the concepts and data analysis. Ms. L. Westover, Dr. E. Parent, Dr. M. El-Rich, and Dr. S. Adeeb contributed to the manuscript composition

A version of chapter 5 of this thesis has been submitted to The Spine Journal as A. Komeili, L. Westover, E. Parent, M. El-Rich, S. Adeeb, “Monitoring for Idiopathic Scoliosis Curve Progression Using Surface Topography Asymmetry Analysis of the Torso in Adolescents.” Dr. S. Adeeb and I developed the classification technique. Ms. L. Westover, Dr. E. Parent, and Dr. M. El-Rich assisted in concluding the results and contributed in manuscript composition and manuscript edits.

The research project, of which this thesis is a part, received research ethics approval from the University of Alberta Research Ethics Board.

Dedication

To my parents Ensi and Mehdi and my beloved wife Hadis for making many sacrifices to give me the opportunity and ability to pursue my dream.

Acknowledgements

I would like to thank all those who helped me during the four past years, gave me the strength to complete my PhD degree at University of Alberta.

I would like to start with Dr. Samer Adeeb. My academic journey at University of Alberta began in 2010 when he invited me to conduct research under his supervision. I am grateful to him for having started me on the academic path. Without his encouragement and support, this dissertation would not have been possible. Dr. Adeeb has always challenged me with thought-provoking ideas that helped me better understand the problems I was trying to solve. I thank him for his valuable input during our many discussions on a wide range of research topics.

I would like to express my immense gratitude to my wonderful co-supervisor, Dr. Marwan El-Rich. He taught me finite element software such as HypeMesh which was a great help in my project. Dr. El-Rich supervised my research progress by sharing his expertise with me when I needed it the most. For that, I am truly grateful and thank him very much.

I would also like to thank Dr. Eric Parent for allowing me to work in his lab and his editorial assistance in writing the manuscripts. He provided me wonderful feedbacks and comments during my PhD study. His point of view as a clinical scientist made the outcome of my research more practical in the clinic.

Many individuals contributed to the success of reliability tests and data acquisition in this study. Significant contributions were made by Dr. Kajsa Duke, Mr. Doug Hill, Dr. Marc J. Moreau, and Ms. Lindsey Westover. I gratefully acknowledge the financial support I have received from my supervisor, Scoliosis Research Society (SRS), Womens and Children's Health Research Institute (WCHRI), the Faculty of Graduate Studies and Research (FGSR), and the Graduate

Students Association (GSA) at the University of Alberta. I am grateful to all the academic, non-academic, and IT staff in the Civil Engineering Department for their generous and prompt support. I would like to thank all my friends and colleagues with whom I have spent a wonderful time while studying towards my PhD.

Contents

CHAPTER 1	1
1. INTRODUCTION	1
1.1 Motivation	1
1.2 Literature Review	2
1.2.1 Scoliosis	2
1.2.2 Radiographs	3
1.2.3 Surface Topography	5
1.2.4 Classification	11
1.2.5 Monitoring.....	14
1.3 Thesis Contributions	17
1.4 Thesis Objectives.....	19
1.5 Hypotheses.....	20
1.6 Thesis Outline	21
CHAPTER 2	23
2. ASYMMETRY ANALYSIS TECHNIQUE	23
2.1 Introduction.....	23
2.2 Materials and Methods.....	24
2.2.1 Clinical Data	24
2.2.2 Data Pre-processing	25
2.2.3 Best Plane of Symmetry	26
2.2.4 Deviation Colour Map.....	29

2.3	Results	30
2.4	Discussion	31
CHAPTER 3		33
3.	CLASSIFICATION AND RELIABILITY	33
3.1	Introduction.....	33
3.2	Materials and Methods.....	34
3.2.1	Clinical Data	34
3.2.2	Classification	34
3.2.3	Reliability.....	35
3.3	Results	40
3.3.1	Classification	40
3.3.2	Repeatability, Test-retest Reliability.....	42
3.3.3	Intra-observer Reliability	44
3.3.4	Inter-observer Reliability	45
3.3.5	One year follow-up test-retest reliability	46
3.4	Discussion	48
3.5	Conclusion	52
CHAPTER 4		53
4.	CURVE PREDICTIONS	53
4.1	Introduction.....	53
4.2	Materials and Methods.....	54
4.2.1	Clinical Data	54
4.2.2	Number, direction, and location of curves.....	56
4.2.3	Height of the apical vertebra	57
4.2.4	Curve magnitude.....	58

4.2.5	Statistical analysis.....	59
4.3	Results	62
4.3.1	Number, direction, and location of curves.....	62
4.3.2	Curve magnitude.....	66
4.4	Discussion	67
4.5	Conclusion	71
CHAPTER 5		73
5.	MONITORING SCOLIOSIS	73
5.1	Introduction.....	73
5.2	Materials and Methods.....	74
5.2.1	Clinical Data	74
5.2.2	Surface topography	77
5.2.3	Radiograph analysis	77
5.2.4	Statistical analysis.....	78
5.3	Results	79
5.4	Discussion	83
5.5	Conclusion	86
CHAPTER 6		87
6.	MAPPING THE TORSO DEFORMITIES TO THE SPINAL DEFORMITIES	87
6.1	Introduction.....	87
6.2	Material and Methods	88
6.2.1	Surface Curvature Analysis.....	88
6.2.2	Mapping Technique.....	90
6.2.3	Monitoring the Worsening and Progression of Scoliosis Curve	93

6.3	Results	97
6.3.1	Surface Curvature Analysis.....	97
6.3.2	Validation of the Mapping Function	99
6.3.3	Predicting the Change of Cobb Angle.....	101
6.4	Discussion	106
6.5	Conclusion	108
CHAPTER 7		110
7.	SUMMARY AND CONCLUSION	110
7.1	Conclusion	110
7.1.1	3D Markerless Asymmetry Analysis.....	110
7.1.2	Classification System	111
7.1.3	Measurements.....	112
7.1.4	Curve Monitoring.....	115
7.2	Future Work.....	118
APPENDIX A INSTRUCTION MANUAL FOR CLASSIFICATION		122
APPENDIX B ENTROPY AND INFORMATION GAIN		126
REFERENCES		130

List of Tables

Table 1-1- King's classification and the description of each group.....	12
Table 3-1- Theoretical contingency table of an inter-observer test- Distribution of n subjects into two categories by Observer A and Observer B.....	38
Table 3-2- The developed signatures of the torso.....	41
Table 3-3- Test-retest reliability: comparing the classification of the first and second baseline scans of 15 torsos.....	44
Table 3-4- Intra-observer reliability of torso classification by the four observers.....	45
Table 3-5- Distribution of classification decisions by each pair of observers from the sample of 4 observers when rating 46 subjects into (A) 3 groups or (B) 6 subgroups	46
Table 3-6- The Lenke curve type, Cobb angle and treatment of 15 patients with one year follow-up data	48
Table 3-7- Reliability result of classifying the first and one year follow-up scan of 15 torsos.....	48
Table 4-1- Distribution of the curves based on the location of curve and Cobb angle value.....	55
Table 4-2- Determining the location of curve (T-TL, L) based on the subgroup category	57
Table 4-3- Calculation of the sensitivity and specificity.....	62
Table 4-4- The observers' classification of the number and location of the curves.	64
Table 4-5- Percentage of agreement (P%) and agreement coefficient (K) between the observers classification and radiograph measurements.	64
Table 5-1- Subjects and curves that were excluded from the analysis	76

Table 5-2- Distribution of the monitored curves based on the location of
curve and Cobb angle value.....76

Table 6-1- Cobb angle, curve count, and BMI distribution of the subjects.99

List of Figures

Figure 1-1- The numbered vertebrae and five regions of the spinal column [16].....	3
Figure 1-2- a) Single right thoracic scoliosis curve, b) double scoliosis curves, c) triple scoliosis curves	5
Figure 1-3- Posterior view. Acromial angle, superior angle, inferior angle, and posterior superior iliac spine are shown in red	7
Figure 1-4-Lenke classification [76].	13
Figure 1-5- Utilizing the scoliometer in forward bending position to measure the axial trunk rotation.	17
Figure 2-1 - Supported position of the patient in the frame.....	25
Figure 2-2- Set of vertices (point cloud) recorded by four VIVIVD 910 3D laser scanners (a) before cropping, b) after cropping.	26
Figure 2-3- Solid surface and point cloud represent the original and reflected torsos, respectively.	28
Figure 2-4- The torso DCM of a patient with AIS from different views.....	31
Figure 2-5- Back view of 5 torso DCMs of normal subjects.	31
Figure 3-1- The DCMs of the analyzed torsos for (a) patient with AIS and (b) healthy subject.....	35
Figure 3-2-a) Small and mild colour patches on the edge of section 1. b&c) Severe deformation at the edge of section 1. d) Deformation extended to the centre of section 1. e) Small scattered colour patches. f) Two colour patches exist in the section 3.....	37
Figure 3-3- First (a) and second baseline scan (b) for a patient with AIS (Cobb=31°).....	43
Figure 3-4- DCMs of a patient with AIS; (a) First scan (Cobb= 21°R-T; 38°L-TL), and (b) one year follow-up scan (Cobb= 18°R-T; 34°L-TL)....	47

Figure 4-1-a) Full DCM of an analyzed torso from back, side, and front view, b) Colour patches isolated from the DCM	56
Figure 4-2- a) Vertical distance between the point with maximum deviation and PSIS measured from the DCM, b) vertical distance between apical vertebra and PSIS measured using corresponding radiograph.....	58
Figure 4-3- The prediction of the location of apical vertebra using the vertical position of the point with maximum deviation in the colour patch (a) 102 T-TL and 34 L curves, (b) 57 T-TL and 20 L curves with Cobb>25°, (c) 24 validation sample subjects using regression line..	65
Figure 4-4- Classification trees to identify the degree of scoliosis using root mean square (RMS) and maximum deviation (MaxDev) of the colour patch for T-TL and L curves.....	67
Figure 4-5- Estimated location of apical vertebra on the DCM of a patient with AIS, and exact location of the apical vertebra on the superimposed corresponding X-ray. (•): Located on the radiograph, (◦): located on the DCM.....	71
Figure 5-1- Isolated colour patch of two torsos with the corresponding radiograph. The Cobb angles was measured from the corresponding radiograph.	79
Figure 5-2- Variation of Δ RMS, Δ MaxDev and Δ A% versus Δ Cobb for 97 T-TL and 30 L curves during 12±3 months follow-up. Dashed line represents the boundary between progression and non-progression based on the radiograph.....	81
Figure 5-3- Classification tree to detect curve progression $\geq 5^\circ$ using change of root mean square (Δ RMS) and change of maximum deviation (Δ MaxDev) of the colour patch for thoracic\thoracolumbar (T-TL) and lumbar (L) curves.	82
Figure 5-4- Identifying the curves with progression for patient with BMI<25 with frequency table that shows the number of cases for each category of the dependent variable.....	82
Figure 6-1- Uniform mapping versus non-uniform mapping between two plane curves.....	92

Figure 6-2- Left: curvature analysis of baseline ST scan, the black curve indicates the median furrow midline, the yellow curve connects the vertebra body centres in the corresponding radiograph, and black arrows are the mapping vectors. Right: curvature analysis of same torso after one year, the black curve indicates the median furrow midline, the dashed curve represents the predicted vertebrae curve using the mapping vectors.96

Figure 6-3- The pseudo Cobb angle (PCA) is the angle between two tangent lines extended from the points of inflection. Left: the PCA of vertebrae curve in the baseline scan. Right: the PCA of predicted vertebrae curve in the follow-up scan.97

Figure 6-4- Curvature contour illustration of an analyzed torso. Black curve: Fourier series interpolation of the median furrow midline, yellow curve: Fourier series interpolation of the vertebrae body centres.98

Figure 6-5-Examples of surface curvature analysis of torsos which were excluded from the investigation. The median furrow midlines were not entirely exposed in the surface curvature contour.99

Figure 6-6- Left: The predetermined curve 1 and curve 2 are correlated through mapping vectors. Right: Comparison of exact and approximate mapping function.100

Figure 6-7- Comparing the changes of PCA (ΔPCA) with the changes of the corresponding Cobb angle ($\Delta Cobb$).101

Figure 6-8- Classifying the 43 $\Delta PCAs$ in of T-TL section into “Improved” and “Worsened” groups representing $\Delta Cobb \leq 0^\circ$ and $\Delta Cobb > 0^\circ$, respectively.103

Figure 6-9- Classifying the 11 $\Delta PCAs$ in L section into “Improved” and “Worsened” groups representing $\Delta Cobb \leq 0^\circ$ and $\Delta Cobb > 0^\circ$, respectively.103

Figure 6-10- Classifying the 43 $\Delta PCAs$ in T-TL section into “Progression” and “Non-progression” groups representing $\Delta Cobb \geq 5^\circ$ and $\Delta Cobb < 5^\circ$, respectively.105

Figure 6-11- Classifying the 11 $\Delta PCAs$ in L section into “Progression” and “Non-progression” groups representing $\Delta Cobb \geq 5^\circ$ and $\Delta Cobb < 5^\circ$, respectively.105

List of Abbreviations

$\Delta A\%$	Percentage change in the area of the colour patch
ΔCobb	Change of Cobb angle
ΔMaxDev	Change in maximum deviation of the colour patch
ΔPCA	Change of pseudo Cobb angle
ΔRMS	Change in root mean square of the colour patch deviation
2D	Two Dimension
3D	Three Dimension
AIS	Adolescent Idiopathic Scoliosis
BSR	Back Surface Rotation
CPU	Central Processing Unit
DCM	Deviation Colour Map
ICA	Independent Component Analysis
IG	Information Gain
ISIS	Integrated Shape Imaging System
L	Lumbar
MaxDev	Maximum deviation of the colour patch
PA	Posterior Anterior
PCA	Pseudo Cobb Angle
PSIS	Posterior superior iliac spine
Q angle	Quantec angle
QSYS	Quantec Spinal Imaging System

RMS	Root Mean Square of distances between matched points
ROM	Range of Motion
RSG	Raster Stereography
SD	Standard Deviation
ST	Surface Topography
STDEV	Standard Deviation
SVR	Support Vector Regression
T	Thoracic
TL	Thoracolumbar

List of Symbols

All dimensional parameters and symbols used in this work are listed below.

(\cdot)	Derivative with respect to t
(\prime)	Derivative with respect to T
$\alpha_0, \alpha_1, \alpha_2, \alpha_3$	Coefficient of mapping function
(ρ, θ, z)	Cylindrical coordinate system
(ρ, θ, ϕ)	Spherical coordinate system
κ_1	First principal curvature
κ_2	Second principal curvature
A_i, B_i, C_i, D_i	Coefficients of the Fourier series
a_i, b_i, c_i, d_i	Coefficients of the Fourier series
C_1	Weight factor
Dist	Distance between matched points
E, F, G	Coefficients of first fundamental form
H	Mean curvature
$H(x)$	Entropy
$H_{gini}(x)$	Gini index
K	Gaussian curvature
L, M, N	Coefficients of second fundamental form
N	Number of rows
P_{sym}	Best Plane of Symmetry
$P\%$	Percentage of agreement

P_{1+}	Probability of observer A to classify a subject in category1
P_{+1}	Probability of observer B to classify a subject in category1
P_{2+}	Probability of observer A to classify a subject in category2
P_{+2}	Probability of observer B to classify a subject in category2
P_a	Overall agreement probability
P_e	Chance-agreement probability
P_i	Point in the original torso
P'_i	Reflected point about the best plane of symmetry
q'_i	Corresponding point in the reflected torso
R^2	Coefficient of determination
S	Matrix of original torso vertices
S'	Matrix of reflected torso vertices
$SD(a,b,c,d)$	Sum of the Distances between corresponding points on the original and reflected torso
S_{Comb}	Optimization function for determining the unknown of mapping function
$S_{curvature}$	Optimization function for determining the unknown of mapping function
$S_{uniformity}$	Optimization function for determining the unknown of mapping function
$[t_{min}, t_{max}]$	Interval of the parametric variable

Chapter 1

Introduction

1.1 Motivation

The motivation for this thesis emanated from the significance of surface topography (ST) in the scoliosis clinic. Using ST the geometrical information of the torso was incorporated in the routine care and management of scoliosis patients [1]. This was born by the fact that cosmetic appearance of scoliosis patients' torso brought them to the clinic [2]. The traditional management of scoliosis, assessment of the spine in Posterior-Anterior (PA) radiograph, has never been an effective method to describe and quantify the torso shape. The initial aim of ST was to assess, quantify, and monitor the asymmetry of the torso in patients with scoliosis. Later, the limitations of the radiograph motivated researchers and clinicians to extend the implication of ST in predicting the spinal alignment.

Most of the traditional ST methods use anatomical landmarks, located by palpation, to develop geometric parameters. The large anthropometric variation in the population, operator experience, patient discontent, and smooth surface of the torso in the lumbar section complicated the implementation of the landmark based methods in the clinic [3]. Therefore, methods using marker placement involve uncertainty which limits practical applications. Other techniques that avoided using markers used 2D indices by assessing the plane cross section of the torso to assess

scoliosis. Each study developed some predictive indices which is appropriate to describe only a portion of scoliosis characteristics. Those methods that considered full torso for analysis failed to generate intuitive parameters, so the clinicians involved in the chain of care of scoliosis patients could not easily understand the physical meaning of the indices.

Increased exposure to radiation due to monitoring scoliosis using spinal radiographs magnified the importance of the ST in management of scoliosis. A practical ST method is expected to evaluate external asymmetry of the torso and meanwhile represent a high correlation with respect to radiograph data to be able to document the progression of scoliosis. Several ST systems have been investigated to be used as an alternative to radiography [4-8]. The previously established ST techniques introduced parameters that could predict some of the scoliosis curve characteristics. However, each developed technique has some limitations. To our best knowledge there is still a considerable need for a new ST method that, in addition to the developed features in the existing methods, could be easily implemented by scoliosis clinicians, and could represent descriptive outputs which are perceptible to patients and their families.

1.2 Literature Review

1.2.1 Scoliosis

The spine is made of bony segments called vertebrae that interlock with each other. These vertebrae are divided into seven cervical (C1-C7 located in the neck), twelve thoracic (T1-T12 located in mid back), five lumbar (L1-L5- located in low back) vertebrae, five sacrum vertebrae and three coccyx [9]. Scoliosis is a complex spine deformity characterized by lateral deviation of the spine usually associated with axial rotation of the vertebrae (Figure 1-2) [10]. Adolescent idiopathic scoliosis (AIS) is defined as a persistent lateral curvature of the spine of more than 10° associated with

the axial rotation in the upright (standing) position. Idiopathic means that the cause of the disease is unknown which exemplifies the complex nature of this type of disorder. The AIS is the most common category of scoliosis which occurs between the ages of 11-17 years and affects 2-4% of the population, predominantly females [11]. Visible symptoms such as uneven shoulders and waist, eccentricity of the head with respect to the pelvis, appearance of a raised hip, and leaning of entire body to one side, are often the concerns of the patients affecting the health-related quality of life [12, 13]. Patients also judge the effectiveness of the treatment by seeking cosmetic improvements in the appearance of the torso [2, 14, 15].

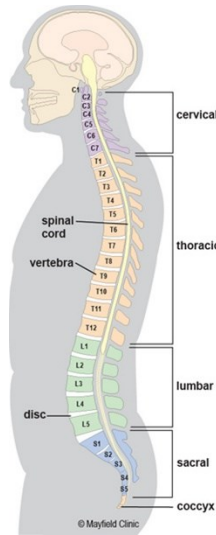


Figure 1-1- The numbered vertebrae and five regions of the spinal column [16]

1.2.2 Radiographs

The standard measure to evaluate, monitor, and guide the treatment decision of scoliosis is the Cobb angle, which is measured on a PA radiographic projection of the spine [17]. The Cobb angle is the frontal plane angle formed between the upper endplate of the most tilted vertebra above a curve and the lower endplate of the most tilted vertebra below the curve on a PA radiograph of the torso [18]. The definition of scoliosis curve progression is not consistent in the literature and varies

based on factors such as, incremental Cobb angle (5° and 10°), and the time spans of measurements for identification of progression [19-24]. However, in routine clinical application curve progression is usually defined as a change of 5° in the Cobb angle [25]. Treatment are adopted based on the considerations of severity and progression of the scoliosis curve. A scoliosis curve of 10 to $20-25^\circ$ is regarded as mild scoliosis and normally does not require any treatment but is monitored during regular check-ups by the clinician to detect if the curve is progressive [26]. Children with mild scoliosis are observed every three to nine months to notify clinicians in case of progression [26-29]. A scoliosis curve with $25^\circ < \text{Cobb} < 40-50^\circ$ is treated non-operatively by using a brace to prevent further curve progression [14]. For a patient with a Cobb angle that reached or exceeded 40° or 50° (severe scoliosis) correction and stabilization by orthopaedic surgery is recommended [21, 30].

In spite of the extensive applications of the Cobb angle, it has some limitations. One limitation lies in the method of measurement, in which curves are described by appearance of the projection of the spine on the PA radiograph films. Thus, Cobb angle does not fully reveal the 3D characteristics of the spinal deformity [31]. For instance, scoliosis may occur due to the axial rotation of the spine rather than lateral deformation. Some studies suggested that the Cobb angle, measured from PA radiograph, partially accounts for the out of plane rotation [32, 33]. The methods aiming to assess the axial rotation of the spine from PA X-ray were associated with suboptimal reliability [24, 34]. Another issue associated with the use of PA X-ray is the cumulative effect of ionisation which increases the risk of cancer [1, 35-37]. Patients with AIS, who undergo frequent X-ray monitoring, tend to be relatively young and their organs are more sensitive to ionizing radiation [1, 36, 38]. One study showed twofold excess risk for breast cancer for women treated for scoliosis between 1925 and 1965 [39]. Moreover, cosmetic external appearance of the torso with its

attendant social issues is the primary concern of the patients and the incentive reason to seek treatment rather than the alignment of the spine [13, 15, 40-43].

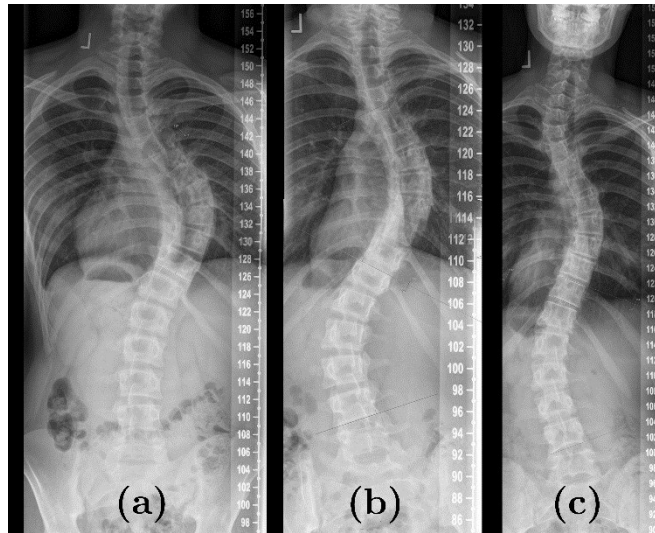


Figure 1-2- a) Single right thoracic scoliosis curve, b) double scoliosis curves, c) triple scoliosis curves

1.2.3 Surface Topography

Radiographs only quantify the internal deformity due to scoliosis. However, it is also important to assess the appearance of the torso because the abnormal shape of the torso is what often convinces patients to seek consultation at a scoliosis clinic [13, 42, 43]. An asymmetric torso is often more bothersome to patients in comparison to having a curved spine and has a psychological impact on their quality of life [40, 43]. Moreover, the interpretation of the radiographs sometimes turns out complicated, because radiographs represent a 2D projection of the 3D deformities. For instance, deformity related to spine rotation is not easily detected in standard PA radiograph. These limitations motivated researchers to develop 3D scanning systems [15, 28, 44-48], that use harmless visible light, for assessment of torso deformities. ST was introduced as a non-invasive method to investigate the 3D shape of the torso surface. It is also employed in some clinical applications to guide the planning of orthoses and

monitor scoliotic distortions [49]. The scoliosis researchers use information of torso deformity in part in hopes of reliably predicting underlying spine characteristics such as the shape, location and severity of the curve. Another objective of ST is to detect the scoliosis curve progression at an early stage without exposing patients to radiation risks.

The employed tools and methods in ST can be categorized into two groups: those that require direct measurements of the patient's back; and those utilizing reconstruction of surface shape from a photographic technique [50]. The later one provides more detail of the surface shapes to detect deformities and monitor the progression. The second group includes surface imaging systems such as Moire fringes [51], rasterstereography [52], and optics such as integrated shape imaging system (ISIS)[5], Quantec Spinal Image System (QGIS)[3, 15, 42, 53], the INSPECK system [28] and the MINOLTA VIVID digitizer based system [54].

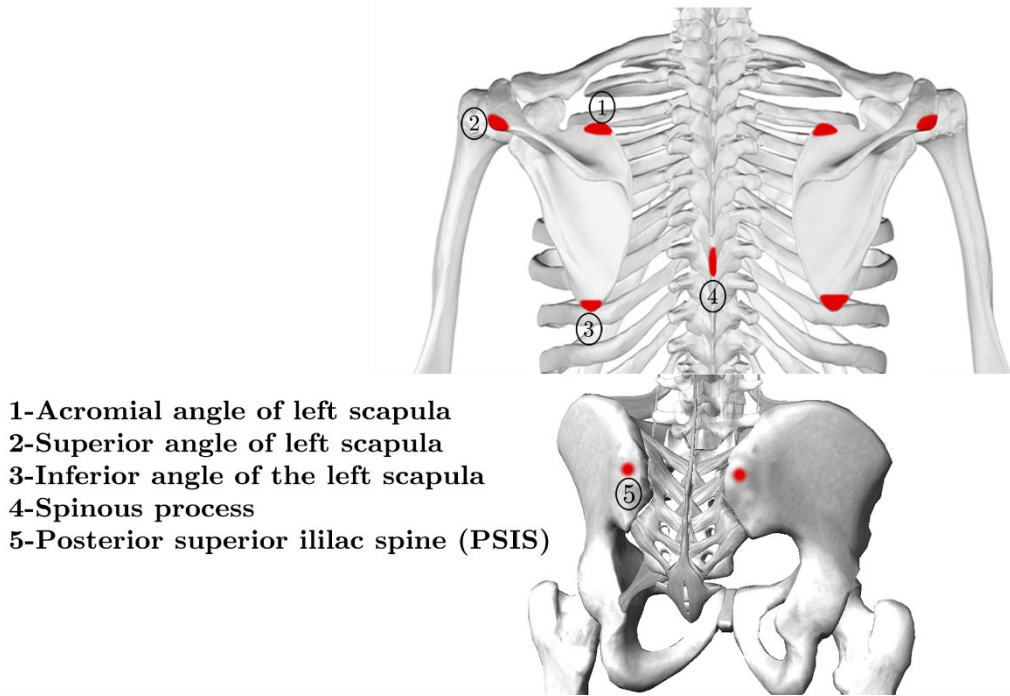


Figure 1-3- Posterior view. Acromial angle, superior angle, inferior angle, and posterior superior iliac spine are shown in red

Several ST methods have been developed to measure torso deformities. Most of them extensively involve manual landmark placing in multiple anatomic locations such as the spinous processes, the acromial angle of shoulders, superior and inferior angles of the scapulae, and posterior superior iliac spine (PSIS) (see Figure 1-3). Examples of obtained parameters using marker based assessments include the cosmetic score [55], Quantec spinal angle [15], posterior trunk symmetry index, and orthogonal map transformation [56]. Most parameters were based on either the distances or angles between the landmarks [5, 15, 57-61], or the geometric properties of 2D transverse cross sections of the torso [56, 60]. Jaremko et al. [59] (2002) developed 48 parameters from the local levels of the back surface (L5, L1, T9) to predict the magnitude of the Cobb angle. The indices were derived using the anatomical landmarks determined by the attending orthopaedic surgeon or staff radiologist. Using 5 developed torso indices the Cobb angle was correctly estimated within 10° in 88% (42/48) of subjects with coefficient of determination $R^2=0.83$ and a

standard deviation (SD) of 6.1° . Their cross sectional analysis of the torso deformity had several limitations, starting with controversial evidence regarding the definition of the indices. Moreover, their indices of torso asymmetry estimated the Cobb angle within 10° , which is a wide range for management of scoliosis [25]. Later, Bergeron et al. [62] (2005) extended Jaremko et al.'s [60] work and developed a ST method in which support vector regression (SVR) and principal components analysis were used to improve the prediction of the Cobb angle. Although their technique still required landmark placing, their results showed robust prediction of the spinal shape with mean norm error $\epsilon = \sqrt{\int [X(z) - x(z)]^2}$ of 4.1 ± 2.8 mm. Mínguez et al. [63] projected a grid over the patient's back and marked 14 anatomical points to calculate two topographic variables (DAPI and POTSI). These parameters explained 50% of the Cobb angle variance and 38% of the vertebral axial rotation variance. Also, cases with clinically relevant scoliosis (Cobb $>10^\circ$, vertebral axial rotation $>10^\circ$) were diagnosed among 86 subjects with 87% accuracy [63]. For those ST methods that require locating the anatomical landmarks on the torso by palpation, the line of spinous processes is the most direct available evidence of the position of the underlying spine. For example the "computer-Cobb angle" [64], which is similar to the Cobb angle except that curve endpoints are mathematically defined as points of inflection of the curve and curve endplates are replaced by perpendiculars to the point of inflection, was measured using the spinous process line. Although the computer-Cobb angle was smaller than the Cobb angle, it was shown that computer-Cobb angle is still correlated closely to the Cobb angle with coefficient of variation $R^2=0.59-0.88$ [65-67].

The ST methods that assess the torso deformities by measuring indices from manually placed markers have several limitations. Marker placing is a procedure that requires a trained operator which can introduce measurement error in the indices. The number and location of the anatomical points are limited which results in lack of

precision in presenting the entire torso deformities information recorded in surface scans. Moreover, there is a lack of agreement among the methods about the definition of the anatomical points [10].

To express the complete 3D torso scan in plain view, Ajemba et al. [56] mapped the spherical coordinate system (ρ, θ, φ) of the torso surface onto a normalized Cartesian coordinate system (x, y, z) using the orthogonal map. The torso was cut into r transvers cross sections where each cross section was represented by s evenly spaced points. Thus, each orthogonal map consisted of a $r \times s$ matrix of numbers where the elements of the matrix correspond to the horizontal distance R , between each of the s points per cross-section. The change rate of closures of the paths of maximal curvature at each incremental cross-section on the orthogonal map was defined as “twist” index. The “bend” index was defined as the radius of curvature of torso cross-section. They classified the torso deformities into mild, moderate and severe categories based on the developed “twist” and “bend” indices. The external deformity, internal deformity and clinical history of the patients were quantified with a developed scoring system to identify the boundaries of the classification (i.e., [twist and bend $<20^\circ$, Mild], [$20^\circ < \text{twist}$ and/or bend $<60^\circ$, Moderate], [twist and/or bend $>60^\circ$, Severe]). Their classification resulted in good correlation with the external deformity; however the obtained indices indicated poor correlation to the internal deformity and clinical history of the patient. Recently, a 4D ST system was used to automatically detect the location of the markers and estimate the Cobb angle [68, 69]. However, only 36% (9/25) of Cobb angles were estimated within $\pm 5^\circ$ ($R^2 = 0.69$; $P < 0.05$) [68].

There are other methods in the literature that estimated the vertebrae curve characteristics at a short-time or long-time interval using the clinical history of patients. Although some of them succeeded in reducing a portion of X-ray radiation in monitoring of scoliosis curve, these type of methods are not categorized as ST

technique because they don't assess torso surface deformities. For instance, in a more recent study Wu et al. [70] (2010) predicted the spine characteristics like Cobb angle, location and lateral deformation of the apical vertebra. Three or four 3D spine and ribcage models were reconstructed from consecutive X-ray images (with 6-month intervals) using six landmarks (superior and inferior bases of both pedicles and endplate centres). A generalized cross-validation extrapolation technique was employed to predict future progression at the next 6-month period. One limitation of their method was that at least three consecutive visits with 6 month interval were required to predict the shape of the forth curve at the next 6 or 12 months. Considering the fact that their data set included only 11 AIS patients with thoracic curve, the Cobb angle was extrapolated at the 6-month interval with a good accuracy of $4.7\pm 3.9^\circ$ and $R^2 = 0.9$. The apical vertebra location was estimated within the range of 0.4 ± 0.7 vertebral level and the accuracy of the apical vertebra lateral deviation prediction was $3.9\pm 3.8\text{mm}$ with $R^2 = 0.81$.

Previous ST studies led to valuable and promising results in assessing the torso deformities, however there are still obstacles that limit the common use of ST in the scoliosis clinics around the world such as unclear definition of trunk metrics, 2D measurements, poor inter- and intra-observer reliability, and obscure presentation of the torso deformities. Although some studies attempted to present the entire torso deformities in one view (e.g. [56]), to our best knowledge, the 3D presentation of the torso deformities in this study, using deviation colour map, provides the best and most intuitive illustration of the state and severity of the torso deformities without relying on any markers. Clearly such intuitive non-invasive tool to assess and monitor the scoliosis and to better quantify the 3D external deformities has potential to be highly useful.

1.2.4 Classification

The clinical relevance of radiograph measurements in evaluation of patients with AIS, in addition to the misperception in defining the degree of curve underlines the necessity for classification system. Categorizing scoliosis to different groups helps clinicians to better communicate and guides them in scoliosis management.

Scoliosis is classified based on the magnitude and the type of curves. The initial attempt in describing the curve pattern of patients with AIS on radiographs was made by Ponseti and Friedman in 1950 [71]. Ponseti classification consisted of three groups: single-curve, double-curve, and triple-curve. The location of the curves was identified in the cervico-thoracic, thoracic, thoraco-lumbar, and lumbar regions. The Ponseti classification did not consider the magnitude of curve as a parameter, thus it did not provide any guidance about treatment strategy.

Considering the curve pattern, magnitude, and flexibility of the scoliosis deformity, King et al. [72] described their classification system in 1983 for patients with AIS (Table 1-1). They provided some suggestions for the curves for which surgery was identified as the treatment. The King classification helped surgeons to decide the level of fusion and spine instrumentation of scoliosis patients. Although, King classification was widely accepted, it did not include all scoliosis curve patterns such as triple curves. The fair inter- and intra-observer reliability also challenged the repeatability of the King classification [73].

One of the most widely recognized classification systems that intended to guide the treatment of scoliosis is the Lenke classification [74, 75]. The Lenke system uses both coronal and sagittal radiographs and relies on the location of the curve and magnitude of the Cobb angle [76]. Six curve types (Number 1–6), a lumbar spine modifier (A, B, or C), and a sagittal thoracic modifier (–, N, or +) are considered in the Lenke classification scheme [76] (Figure 1-4). The location of the curves is defined as proximal thoracic, main thoracic or thoracolumbar/lumbar. Lenke classification

could address the low reliability associated with the King classification by producing high inter- (Kappa = 0.92) and intra-observer reliability (Kappa= 0.83) [76, 77]. The details of these reliability coefficients are described in Section 3.2.3. The Lenke classification is widely accepted and utilized by the majority of scoliosis surgeons worldwide to guide the surgical care [74, 75] but it does not consider surface deformity and is not meant for use in small curves.

Table 1-1- King's classification and the description of each group.

Type	Description
Type I	Thoracic and lumbar curve, the lumbar curve has higher magnitude and is more rigid.
Type II	Thoracic and lumbar curve, the thoracic curve has higher magnitude and is more rigid.
Type III	Single thoracic curve without lumbar curve
Type IV	Long thoracic curve with L4 tilted into the curve.
Type V	Double thoracic curve.

Curve Type				
Type	Proximal Thoracic	Main Thoracic	Thoracolumbar / Lumbar	Curve Type
1	Non-Structural	Structural (Major*)	Non-Structural	Main Thoracic (MT)
2	Structural	Structural (Major*)	Non-Structural	Double Thoracic (DT)
3	Non-Structural	Structural (Major*)	Structural	Double Major (DM)
4	Structural	Structural (Major*)	Structural	Triple Major (TM)
5	Non-Structural	Non-Structural	Structural (Major*)	Thoracolumbar / Lumbar (TL/L)
6	Non-Structural	Structural	Structural (Major*)	Thoracolumbar / Lumbar - Main Thoracic (TL/L - MT)

<p>STRUCTURAL CRITERIA (Minor Curves)</p> <p><i>Proximal Thoracic:</i> - Side Bending Cobb $\geq 25^\circ$ - T2 - T5 Kyphosis $\geq +20^\circ$</p> <p><i>Main Thoracic:</i> - Side Bending Cobb $\geq 25^\circ$ - T10 - L2 Kyphosis $\geq +20^\circ$</p> <p><i>Thoracolumbar / Lumbar:</i> - Side Bending Cobb $\geq 25^\circ$ - T10 - L2 Kyphosis $\geq +20^\circ$</p>	<p>*Major = Largest Cobb Measurement, always structural Minor = all other curves with structural criteria applied</p> <p>LOCATION OF APEX (SRS definition)</p> <table border="0"> <tr> <td>CURVE</td> <td>APEX</td> </tr> <tr> <td>THORACIC</td> <td>T2 - T11-12 DISC</td> </tr> <tr> <td>THORACOLUMBAR</td> <td>T12 - L1</td> </tr> <tr> <td>LUMBAR</td> <td>L1-2 DISC - L4</td> </tr> </table>	CURVE	APEX	THORACIC	T2 - T11-12 DISC	THORACOLUMBAR	T12 - L1	LUMBAR	L1-2 DISC - L4
CURVE	APEX								
THORACIC	T2 - T11-12 DISC								
THORACOLUMBAR	T12 - L1								
LUMBAR	L1-2 DISC - L4								

Modifiers			
Lumbar Spine Modifier	CSVL to Lumbar Apex		
	A		CSVL Between Pedicles
	B		CSVL Touches Apical Body(ies)
C	CSVL Completely Medial		

Thoracic Sagittal Profile T5 - T12	
= (Hypo)	< 10°
N (Normal)	10°- 40°
+ (Hyper)	> 40°

Curve Type (1-6) + Lumbar Spine Modifier (A, B, or C) + Thoracic Sagittal Modifier (-, N, or +)
Classification (e.g. 1B+): _____

Figure 1-4-Lenke classification [76].

A ST classification could have these benefits: (1) it could help clinicians to better communicate in clinic and decide proper treatment option; (2) it could facilitate development of more effective and accurate torso indices; (3) it could assist to reflect deformity of importance to patients. The Ponseti, King, and Lenke classifications are based on the spine shape in the sagittal and/or coronal radiograph. With regards to the torso classification of patients with AIS only few studies attempted to classify the curve type based on the torso features [26, 47, 56, 78]. Seoud et al. [78] studied 97 AIS patients who were candidates for surgery (Cobb $>40^\circ$). They categorized the torso deformities using the back surface rotation (BSR) index into three basic classes: thoracic major curves (union of types Lenke 1 and Lenke 2), double and triple major curves (union of types Lenke 3 and Lenke 4) and lumbar major curves (union of types Lenke 5 and Lenke 6). The prediction accuracy for the first, second, and third class was 57.1%, 73.8%, and 85.2%,

respectively. Liu et al. [42] investigated the QSIS scans of 249 patients with $\text{Cobb} < 30^\circ$ to develop ST indices. They divided patients based on the developed ST indices into three groups: Group 1 ($\text{Cobb} < 10^\circ$), Group 2 ($10^\circ < \text{Cobb} < 20^\circ$), and Group 3 ($20^\circ < \text{Cobb} < 30^\circ$). The patients with surgical magnitude scoliosis were excluded from their study. They examined the accuracy of classification using 31 patients with mild curve ($\text{Cobb} < 30^\circ$) as validation sample and they could correctly classify 80% of the patients. They suggested a radiograph may necessary if a patient changed its group; however the range of the Cobb angle in their groups was too wide to consider 5° curve progression and they did not test the prediction using longitudinal data. In a recent study conducted by Adankon et al. [79] (2012), the curve type of 165 patients with AIS having Cobb angle $> 35^\circ$ was automatically classified into thoracic major, double major, and lumbar/thoracolumbar categories with 95% classification accuracy. Although their method was robust and clinically meaningful, they did not report the functionality of their method for patients with $\text{Cobb} < 35^\circ$.

An effective ST classification system would be reliable, and would be meaningful in terms of the radiographic data. In addition, a classification system that utilizes the full torso scan contains more information about the 3D nature of the deformity than landmark-based classification systems. None of the current classification systems encompasses all curve types and curve magnitudes with high reliability rate. Hence, there is room for further improvements in the classification of the torso deformities in patients with AIS.

1.2.5 Monitoring

A primary concern of orthopedic surgeons is identifying whether a minor scoliosis curve will progress to severe deformity. Although specific factors have been associated with a higher risk of curve progression [80], unfortunately, there is currently no solid and reliable method to predict which patient with AIS will

progress. Therefore, a series of full spine radiographs are used in clinical practice to monitor patients with AIS. So, patients with AIS may have one or two radiographs every 6 months until the end of skeletal growth [28, 29]. The X-ray dose and the lifetime risk of development of cancer is a problem justifying research on alternatives to the use of radiographs for monitoring scoliosis [1, 81]. This concern is more crucial for patients with AIS compared to adult scoliosis patients, because the received radiation dose is higher for younger patients and growing organs are more susceptible to radiograph exposure. Therefore, the frequency of X-ray acquisition is limited to every 6 to 8 months, which represents a long interval in the case of progressive scoliosis in adolescent patients [78]. To overcome the problem of high cancer risk in the process of scoliosis monitoring, several studies have attempted to use ST measurements to predict the magnitude of the Cobb angle or to detect changes in the Cobb angle over time noninvasively with varying levels of success [3, 15, 21, 27, 82].

Korovessis et al. [83] predicted the magnitude of the Cobb angle for thoracic and lumbar curves in adult idiopathic scoliosis patients using a scoliometer (Figure 1-5). Several clinical factors, such as the scoliometer value, age, and sex, were correlated to the radiographic parameters, such as Cobb angle, using simple and multiple linear regression analysis. They developed two formulas to predict the Cobb angle of thoracic and lumbar curves with mean error of 5.63° and 5.79° , respectively. The outcomes of their study had low accuracy in predicting the scoliosis curve progression and there is no investigation to show that their equation is suitable for monitoring patients with AIS [84]. The QSISS was used by Thometz et al. [3] to assess the magnitude of the Cobb angle in 149 patients with AIS. The Quantec angle (Q angle) was measured from the surface data using 12 landmarks. The Q angle is the difference of the upper and the lower maximal tilting angle measured from a line detected by ST technique. A mean difference between the Cobb angle and the Q angle of $5.7 \pm 9.1^\circ$ and $4.9 \pm 7.4^\circ$ ($p < 0.05$) was obtained for thoracic and lumbar

curves, respectively. However, Thometz et al. only compared the Q angle with Cobb angle using cross-sectional data and did not investigate the Q angle in a long-term follow-up of scoliosis to quantify if Quantec use could help reduce need for radiograph.

Some studies aimed at qualitatively predicting the chance of progression in the scoliosis curve by associating factors to the risk of progression such as: age, sex (girls predominantly), growth rate [85], curve type (right thoracic and double curves in girls), curve magnitude [86], and axial rotations of vertebrae [87]. Using the Q angle, Goldberg et al. [15] monitored 59 scoliosis patients to detect a 10° Cobb angle scoliosis progression over one year period with a specificity of 45% and sensitivity of 100% (see section 4.2.5). Although their method identified all curves with $>10^\circ$ increase in the Cobb angle, the considered 10° as the criteria of progression is too wide for on-time diagnostic of scoliosis worsening condition for patients with AIS [24]. Theologis et al. [21] used the Integrated Shape Imaging System (ISIS) to detect $>5^\circ$ Cobb angle curve progression in 78 patients with single right thoracic curve. Only three of six ISIS parameters were useful to significantly detect ($P < 0.005$) progression at the 6-month follow-up. Schulte et al. [27] measured lateral deviation and axial rotation of vertebrae using raster stereography (RSG) technique but did not explain how the parameters were calculated. All 9 examined patients with AIS in their study had right thoracic curve with a 61% change in mean Cobb angle during the mean follow-up period of 8 years. They showed that the progression of RSG parameters were correlated to the radiographic ones in the long-term period. With regard to the evaluation of curve progression it was suggested that the RSG parameters should be interpreted with more caution because RSG parameters may underestimate the curve progression. No discussion was made about capability of the RSG parameters in monitoring the 5° Cobb angle curve progression during a shorter follow-up consistent with the interval of consecutive monitoring visits. Although RSG parameters were

from the first and latest follow-up scans (at least a 3 years interval), they concluded that RSG parameters could reduce one radiographic examination per year during the long-term follow-up of patient with AIS. Recently, Adankon et al. [82] used independent component analysis (ICA) to investigate the difference between ST measurements of two successive acquisitions and capture the local scoliosis deformations. The full torso was represented by 40 components using principal component analysis to reduce the dimensionality of the data. The torso data of 30 patients, whose data were collected at three clinical visits, was considered in their study. They analyzed 60 individuals for the progression/non-progression labelling between pairs of successive visits, including of 26 progressive individuals and 34 non-progressive individuals. Although their method did not visually illustrate scoliosis deformities, the progression of at least 5° curve progression was detected with sensitivity of 92% and specificity of %79.



Figure 1-5- Utilizing the scoliometer in forward bending position to measure the axial trunk rotation.

1.3 Thesis Contributions

As described, above ST has a potentially significant role in the reduction of radiation exposure and cancer risk for patient with AIS. It is of great interest to develop a ST method that clearly represents the deformity of the torso and successfully monitors the scoliosis curve progression. The main objective of the present thesis is to address following problems in detail:

- 1- Developing a ST method that describes asymmetry of patients with AIS and is convenient to implement by clinicians with different scoliosis backgrounds;
- 2- Classifying the asymmetry pattern of the torso of patients with AIS;
- 3- Monitoring scoliosis curve progression.

The following problems were addressed by proposing a new 3D markerless ST technique based on “asymmetry analysis”. In the first problem, we considered a novel ST data analysis method that is independent of marker placing. The goal was to minimize the human role in the execution of the method and to develop a ST technique which is not limited to a certain acquisition system and is compatible with other imaging systems (such as ISIS [5], QSIS [3, 15, 42, 53], and INSPECK system [28]) in the scoliosis clinics. We developed a novel 3D ST technique that is applicable to the task of assessing the torso deformity caused by scoliosis. In the second problem, we categorized the asymmetry pattern of the torso into three groups and six subgroups, by which a clear illustration of the spine state and better measurements were provided. In the last problem, we studied the capability of the proposed technique to detect $\geq 5^\circ$ curve progression to avoid some X-ray used for monitoring scoliosis over time.

To study the above three problems, we adopted an asymmetry analysis approach and considered the full torso as an entity to preserve all the information of the deformities caused by scoliosis. The 3D model of the torso is reconstructed using the coordinate of the torso recorded by VIVID 910 3D laser scanners. The developed asymmetry analysis captures external deformities including the lateral deformation and the axial rotation of the torso. The asymmetric regions of the torso caused by scoliosis are colour coded to visually illustrate the pattern and severity of deformities. In spite of the extensive mathematical algorithm in the procedure, the intuitive

descriptive results of our ST technique greatly influence the human perception of shape deformity.

While several classification systems have been developed from radiograph data, categorizing the external deformities is still relatively unexplored. In this thesis, the torso deformity is quantified and categorized into different groups based on the number and location of the asymmetries. For each group the torso measurements will be assessed separately. The change of asymmetry pattern was documented by comparing the baseline and one year follow-up scans of patient with AIS. The progression/improvement of the scoliosis curve is predicted from the change of torso asymmetry in order to eventually possibly decrease the number of X-rays used in monitoring scoliosis over time. The major original contributions of this dissertation are:

- 1- Employed markerless ST technique, instead of placing markers on the specific anatomical location of the back surface to analyze the torso of patient with AIS. This allows us to use all the information of torso.
- 2- Avoided 2D measurements such as indices that are calculated from torso cross-section properties. This is a more appropriate approach to quantify the asymmetry of the torso which manifests in 3D.
- 3- Explored the ability of the method in monitoring the scoliosis curve and suggested a practical solution to reduce radiation exposure in the clinical applications.

1.4 Thesis Objectives

The objectives of this thesis are:

- 1- To introduce a new 3D approach to ST which investigates the asymmetry of the torso for patients with AIS without the need of markers.

- 2- To present a classification system for patients with AIS into categories based on the asymmetry pattern of the torso and evaluate the corresponding inter-, intra-, and test-retest reliabilities.
- 3- To develop new surface indices which identify the curve type, curve magnitude, and location of a curve's apical vertebra.
- 4- To detect 5° or more scoliosis curve progression using the 3D markerless asymmetry analysis of patient with AIS.

1.5 Hypotheses

- 1- The proposed classification system categorizes the torso deformity into different groups such that for each group the torso measurements could be assessed separately. The markerless feature of this method eliminates the errors of marker placing. Therefore, it leads to a reliable results and presents an effective tool to assess the torso disorders.
- 2- To measure the deformities no specific plane has been considered, so the 3D deviation analysis considers the 3D deformities as well as the relative axial rotation of the vertebrae. Strong correlation will exist between the asymmetry of the torso and underlying spinal characteristics such as curve type, curve magnitude, and location of apical vertebra.
- 3- The main clinical application for these correlations would be to non-invasively monitor the scoliotic curve progression by detecting which curves progress over time and need an X-ray and which curves do not progress and do not need an X-ray.

1.6 Thesis Outline

Asymmetry analysis techniques are tools for assessing and describing 3D shapes. The output of torso shape asymmetry analysis can be processed to describe the state of the deformities for quantifying and tracking shape changes. This thesis presents a new 3D markerless asymmetry analysis of the torso and demonstrates its application to scoliosis management. This dissertation is organized as follows.

The developed 3D markerless asymmetry technique is described in Chapter 2. The selection criteria of the examined subjects, the description of our acquisition system and the asymmetry analysis technique are described in Section 2.2. The results of the asymmetry analysis for the torso of patients with AIS and the torso of normal subjects are given in Section 2.3.

The patterns of torso asymmetry due to the scoliosis deformities and the developed classification system are given in Chapter 3. Section 3.2.3 presents the theoretical framework of the reliability tests and investigates the reliability of the introduced classification system. Section 3.3 presents the results of the conducted reliability tests.

The application of the developed asymmetry analysis and its corresponding indices in quantifying the torso deformity is discussed in Chapter 4. Section 4.2 describes how the developed ST indices predict internal characteristics such as: number, direction, location, and magnitude of the scoliosis curve.

Chapter 5 investigates the capability of the 3D markerless ST asymmetry analysis to detect $\geq 5^\circ$ progression of the spine curvature in patients with AIS over a one year follow-up interval. The theoretical framework of the employed classification system is described in Section 5.2. The accuracy of the resulting classification tree is validated in Section 5.3.

Chapter 6 presents surface curvature analysis along with the developed mapping technique, an alternative tool for shape analysis. Section 6.2 comprised of:

1- surface curvature analysis; 2- considered criteria in construction of the mapping function; 3- pre-processing and reconstruction routines; and 4- application of the mapping function in monitoring the progression of the scoliosis curve.

Finally, Chapter 7 reviews the achievements of this study and presents the conclusion. This chapter also discusses the future work arising from this study.

Chapter 2

Asymmetry Analysis Technique¹²

2.1 Introduction

Current ST methods mainly rely on 2D measurements obtained from the distances between markers manually placed by a trained clinician on the patient's torso [57, 58]. The marker-based measurements involve uncertainty and fail to describe the 3D aspect of the scoliosis deformity. Thus, there is a considerable need for a new 3D markerless ST method that could replace some of the X-ray radiations and minimize human role in ST measurements. In this chapter a new 3D markerless ST technique based on "asymmetry analysis" is proposed. The developed technique is employed to analyze the ST scans of 100 patients with AIS. The asymmetry of the torso is exposed on the torso surface using the deviation analysis to capture a better vision of the torso deformities.

¹ A version of this chapter has been published in The Spine Journal, Amin Komeili, Lindsey Westover, Eric Parent, Marc Moreau, Marwan El-Rich, Samer Adeeb, "Surface Topography Asymmetry Maps Categorizing External Deformity in Scoliosis."

² A version of this chapter has been published in the Journal of Systems and Control Engineering. S. Hill, E.F. Sepulveda, A. Komeili, A. Travota, E. Parent, D. Hill, E. Lou, S. Adeeb, "Assessing asymmetry using reflection and rotoinversion in biomedical engineering applications," Proceedings of the Institution of Mechanical Engineers, Part H: Journal of Engineering in Medicine May 2014 228: 523-529.

The present chapter is organized as follows: Section 2.2.1 presents the inclusion criteria of samples and describes the tools that were used to collect the data. The pre-processing steps are explained in Section 2.2.2. The model description and governing equations of the asymmetry analysis and the specification of the deviation colour map are explained in Section 2.2.3 and 2.2.4, respectively. The results are presented in Section 2.3, and discussions are given in Section 2.4.

2.2 Materials and Methods

2.2.1 Clinical Data

Full torso scans of patients with AIS with different Lenke curve types were selected randomly from scans collected in an ongoing study on full torso ST at the Edmonton Scoliosis Clinic. Inclusion criteria for patients in this study were AIS, treated non-operatively, and having baseline and follow-up ST scans and corresponding out of brace radiograph within a 12 ± 3 month interval from baseline. The X-ray and ST scans were taken on the same day. Data was collected from all consenting consecutive volunteers attending routine visits to the scoliosis clinic. A typical visit consists of a ST scan, a radiograph, some questionnaires and a clinical visit with a surgeon. Approval for this study was obtained from the Health Research Ethics Board and all subjects signed informed consent.

Four VIVID 910 3D laser scanners (KONICA MINOLTA Sensing Inc.) were placed in the corners of a square room and distanced 3m from each other at the Edmonton Scoliosis Clinic in order to capture the coordinate of the torso. The subjects stood in a frame to control the location relative to the scanners (Figure 2-1) and the position of the feet, shins, as well as support the arms at 90 degrees of elevation [12, 88, 89]. A probe placed just above C7 offers feedback to the subjects to limit the postural sway from their natural standing position. The accuracy of each

scanner with the wide lens is ± 1.4 , ± 0.4 and ± 0.4 mm along the depth, width and height axes, respectively [12, 88, 89].

The scan system accuracy and torso surface reconstruction were validated by Jaremko [61] using a 22 cm x 22cm x 37.5 cm wooden block [90]. The block was scanned in four different positions. In each position, distances between the points located on each corner and each mid-side were calculated (a total of 8 distances). The difference in distances between scans (average across all 8 measures) was 1.8 ± 0.9 mm (maximum difference 2.8 ± 0.7 mm) for surface topography. This difference is more reliable compared to X-ray reconstruction with 2.8 ± 1.5 mm difference in distance between scans [61].



Figure 2-1 - Supported position of the patient in the frame.

2.2.2 Data Pre-processing

The four views from the cameras were merged together using the Polygon Editing Tool (Konica Minolta PET version 2.21) [91] to create a model of each subject's full torso. The data was exported as a point cloud and imported into the Geomagic software [92]. The points that covered the frame, arms, hips, head and neck were manually selected and deleted. The lower portion of the torso was cropped at the pants line. Pants were always aligned below the PSIS during scanning. The subject's

head was cropped at approximately the level of the shoulders. The arms were cut using a sagittal plane that was placed approximately through the corners of the acromion. For several patients, some surfaces were not properly captured by the cameras such as the top of the shoulders and the lateral side of waist. These zones created holes and spikes in the torso models. Additionally, the models had areas of overlapping points due to the merging process. In order to obtain a smooth cloud of points representing the torso geometry, the Geomagic built-in functions “Fill Single” were used to fill in the small holes and to remove the spikes and the overlapping points. Figure 2-2 shows the point cloud of a torso before and after cropping. After pre-processing the scans, the coordinates of the torso surface points were imported into Wolfram Mathematica (Wolfram Research, Inc., Mathematica, Version 8.0.4.0)[93].

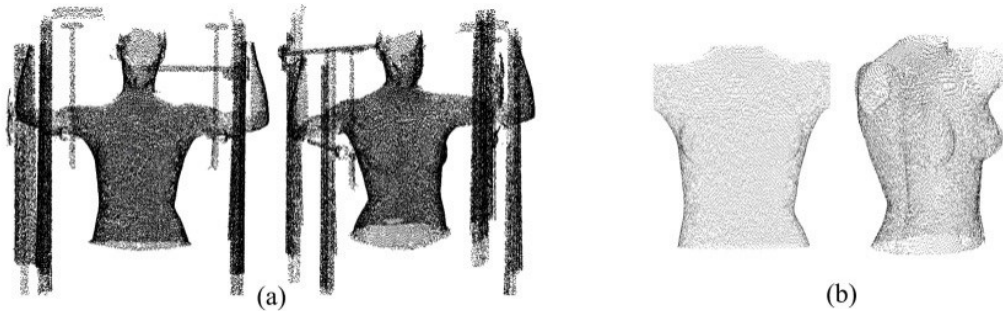


Figure 2-2- Set of vertices (point cloud) recorded by four VIVID 910 3D laser scanners (a) before cropping, b) after cropping.

2.2.3 Best Plane of Symmetry

Asymmetry of the torso is the prominent external symptom of the scoliosis which is first noticed by the patient. Therefore, our initial objective was to develop an analysis technique capable of assessing the asymmetry of the full torso. This analysis technique should also be independent of markers, reproducible, reliable, and encompasses the full torso data. The proposed asymmetry analysis consists of minimizing the distance between an object and its reflected image to find the “best

plane of symmetry” (P_{sym}). The P_{sym} can then be used to reflect the object and a colour deviation map is used to categorize the extent of the asymmetry of the torso.

In this study the scanned torso was named the “original torso” and the one that is reflected with respect to the P_{sym} was named the “reflected torso” (Figure 2-3). The origin of coordinate system was defined according to the origin of the data acquisition system. A subroutine was developed in Wolfram Mathematica [93] to find the best plane of symmetry approximately aligned with the mid-sagittal plane. The vertices of the original torso were saved in matrix S, which is $(n \times 3)$ matrix. The number of rows (n) in matrix S represents the number of points recorded by the scanners and the columns contain the Cartesian coordinates of a point. The P_{sym} was defined as:

$$ax + by + cz = d \quad (2-1)$$

where, a, b, c, and d are unknown constants to be determined. For each considered point $P_i = (x_i, y_i, z_i)$ in the original torso, its reflection about the P_{sym} is $P'_i(a, b, c, d) = (X_i, Y_i, Z_i)$, a function of a, b, c, and d. The original torso was reflected through the P_{sym} and was called S' where,

$$\begin{aligned} S' &= [X_i, Y_i, Z_i]_{n \times 3} \quad (i = 1, \dots, n) \\ X_i &= X_i(a, b, c, d) \\ Y_i &= Y_i(a, b, c, d) \\ Z_i &= Z_i(a, b, c, d) \end{aligned} \quad (2-2)$$

For each point $P_i = (x_i, y_i, z_i)$ in the original torso, its corresponding point $q'_i(a, b, c, d) = (X_i, Y_i, Z_i)$ on the reflected torso, should be determined to be able to compare the original torso with the reflected torso. The pair of (P_i, q'_i) is called “matched points”. The closest point approach was used to calculate the corresponding point q'_i which is the closest in distance to point P_i . The closest point technique minimizes the sum of distances between the matched points. The sum of absolute distances between matched points was calculated as:

$$SD(a, b, c, d) = \sum_{i=1}^n |\text{Dist}(P_i, q'_i)| \quad (2-3)$$

where, $\text{Dist}(P_i, q'_i)$ is the distance between matched points (P_i, q'_i) . The best plane of symmetry P_{sym} is calculated by finding $a, b, c,$ and d that minimize $SD(a, b, c, d)$. For a perfectly symmetric object, the calculated P_{sym} would be a true plane of symmetry and $SD=0$. However, here the object is the torso of the patient with AIS, which is not a symmetric geometry, thus the $SD \neq 0$ and there is a misalignment between the original and reflected torsos (Figure 2-3). Therefore, the calculated plane is referred to as the “best plane of symmetry”. The unknown coefficients $a, b, c,$ and d of P_{sym} were determined using “FindMinimum” command in Wolfram Mathematica [93] which searches for a local minimum in SD function.

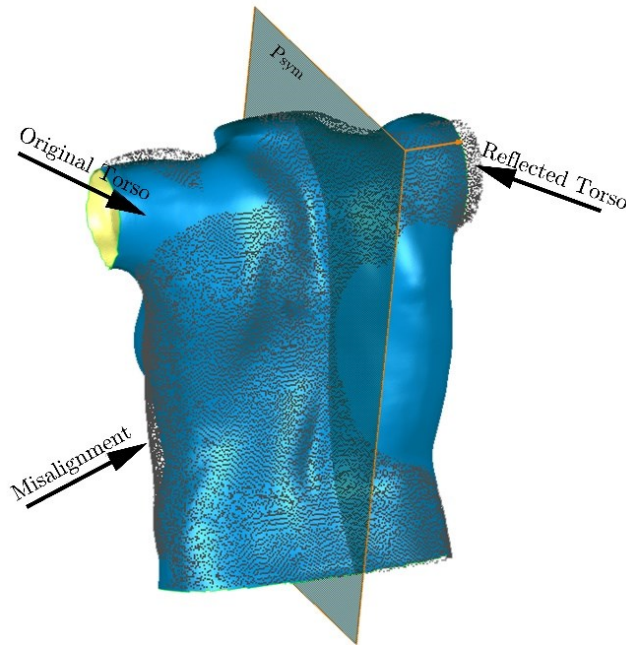


Figure 2-3- Solid surface and point cloud represent the original and reflected torsos, respectively.

2.2.4 Deviation Colour Map

The deviations between two aligned torsos, the original torso and the reflected torso, can be assessed using the shortest distance to the original torso measured radially from the points on the reflected torso. In this work, the original torso is regarded as a triangulated surface and the points on the original torso are the vertices of that surface. The maximum allowable size of this radius is the maximum deviation (MaxDev). The mean quadratic distance (RMS) of the individual point by point deviation is calculated as:

$$\text{RMS} = \sqrt{\frac{\sum(\text{deviation}_i^2)}{n}} \quad i = 1, \dots, n \quad (2-4)$$

where, n is the total number of points on the reflected torso. A deviation colour map (DCM) is a colour-coded representation of the deviations between the reflected torso and original torso.

The misalignment between the original and the reflected torsos is a measure of the asymmetry and can be visualized using a deviation contour map showing the distance between the two surfaces. The DCM was obtained using the built-in function “3D Compare” in Geomagic software and illustrated on the torso surface (Figure 2-4). The colour spectrum with a maximum and minimum deviation of $\pm 22\text{mm}$ which consists of nine colours was chosen to provide an appropriate balance for the amount of detail shown in the asymmetry maps and was standardized for all subjects (Figure 2-4). However, for subjects with a severe torso surface deformity, a larger range for the colour spectrum could be used to better visualize and locate the centres of the asymmetry regions. Analyzing five normal torsos showed that less than 3mm deviation is expected in normal, so the green colour in the DCMs presented $< \pm 3\text{mm}$ deviation and was considered as a range for normal (Figure 2-5).

2.3 Results

Blue colours indicate that the original torso is outside of the reflected torso (i.e. original torso covers the reflected torso) and red colours indicate that the original torso is inside of the reflected torso. Light blue and yellow represent mild (-3mm to -9mm and +3mm to +9mm) outward and inward deviations of the original torso, respectively. The dark blue and red colours indicate where the deviation of the original torso is higher than the maximum and minimum deviations specified in the colour mapping function (>22mm). In other words, a dark red or dark blue colour indicates a large deformation in that region. Finally, the grey colours on the edges of the model show the regions where the original torso points did not have corresponding points in the reflected torso (i.g. due to asymmetric cropping of the arms) (Figure 2-4). By virtue of the asymmetry analysis, every point in the asymmetry map with positive deviation (red colour) has a corresponding point with the same magnitude but negative deviation (blue colour). The colour pattern is symmetric across the best plane of symmetry. For example, a rib hump on the right side of a patient would be characterized by a blue colour deviation on the right side (since the original torso would be outside the reflected one) and a corresponding red colour deviation on the left side. A pair of corresponding blue and red colours in the asymmetry map is termed a “colour patch” (Figure 2-4). A subroutine was developed in Wolfram Mathematica [93], by which colour patches of the torso are separated to locally study the asymmetry of the torso.

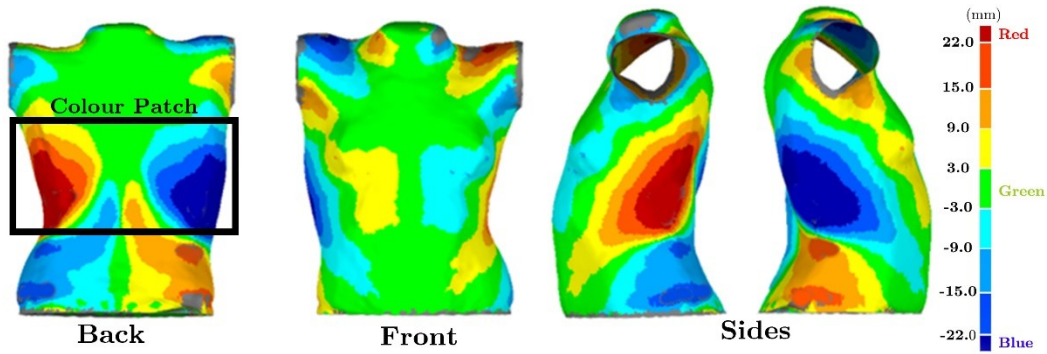


Figure 2-4- The torso DCM of a patient with AIS from different views.

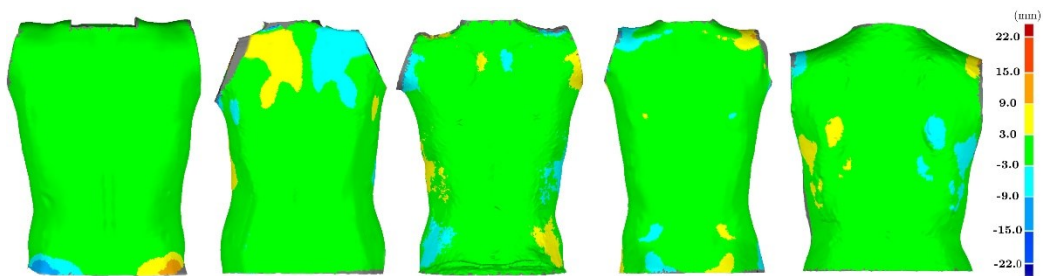


Figure 2-5- Back view of 5 torso DCMs of normal subjects.

2.4 Discussion

The developed ST technique documented a method of acquiring comprehensive information about the torso deformities without placing marker on the torso surface. The proposed asymmetry analysis takes advantage of considering full torso geometry in the analysis instead of using limited number of anatomical points to represent the torso. One factor that limits the implementation of the current ST methods in the clinics is the vague definition of the planes and anatomical points. Matching a collection of points between scans with the frequency of once every 6 months is a challenging task [94] for several reason such as: variation in the posture of the patients between scanning sessions, significant changes in the shape of torso due to growth or weight gain, skin slippage as the markers are being placed [94]. In the developed ST technique, however, no anatomical landmarks were defined. In

addition, our ST technique is independent from the location and type of coordinate system that the acquisition system is using. So proposed ST analysis could be employed to analyze the asymmetry of other body parts, such as breasts, and even other geometries beyond the scoliosis context.

Moreover, studies show that the cosmetic external appearance of the torso is the primary concern of the patients and any improvement in the shape of the torso would be an incentive reason to continue the treatment [14, 15]. The outcome of the asymmetry analysis produces an easy to understand and clear representation of the torso deformities by interlinking the severity of torso deformities to the colour intensity. Thus, the progression or improvement of the torso asymmetry is comprehensible by adolescent patients which could be a motivation for patients to continue the treatment.

In this research $0\pm 3\text{mm}$ deviation was considered normal and any deviation in this range was presented with green colour in the DCM of the torso. However, as Figure 2-5 illustrates, even the DCM of normal subjects may show some asymmetry signatures. Identifying asymmetry pattern of the healthy subjects was not the interest of this study, nonetheless the pattern of asymmetry for normal subjects could be investigated to screen out the normal subjects from the scoliosis subjects in the screening of scoliosis.

Chapter 3

Classification and Reliability¹

3.1 Introduction

In the context of scoliosis, classification systems provide clinicians and researchers a way to organize clinical information and coordinate torso deformities for easier investigation. The other importance of scoliosis classification systems lies in their ability to standardize communication among surgeons and to assist understanding the relevance of clinical data [95]. With regard to the vertebra classification of patients with AIS, the Lenke system [76] addressed many of the significant limitations of the King system [72] and has become the most widely recognized classification systems. Most of the current ST classifications, as described in Section 1.2.4, rely on marker placement and encompass only a portion of curve types and curve magnitude. Lack of physical meaning of the classification parameters has not yet satisfied the clinician's expectations. In this chapter the DCMs of torso are used to develop a classification system. In Section 3.2.1 the inclusion criteria of selecting samples and the employed tools used to collect the data are discussed. The classification system and definition of the groups are explained in Section 3.2.2. The

¹ A version of this chapter has been published in The Spine Journal. Amin Komeili, Lindsey Westover, Eric Parent, Marc Moreau, Marwan EL-Rich, Samer Adeeb, "Surface Topography Asymmetry Maps Categorizing External Deformity in Scoliosis."

reliability of the classification system and its correlation with respect to the Lenke classification is investigated in Section 3.2.3. The results of reliability tests for the developed classification system are presented in Section 3.3. Discussion and conclusion are given in Sections 3.4 and 3.5, respectively.

3.2 Materials and Methods

3.2.1 Clinical Data

Full torso ST scans were retrieved for 50 patients with AIS as described in Chapter 2 for the reliability analysis of the classification system. The mean Cobb angle was 34.1° (minimum 12° , maximum 67°). There were 13, 10 and 23 subjects with Lenke 1, Lenke 3 and Lenke 5 curve types, respectively. Four subjects with AIS were excluded because of poor accuracy in reconstruction of torso model or noisy data; thus 46 subjects with AIS remained for the analysis. A second scan was acquired a few minutes after the first scan and was used for assessing the reliability in 15 randomly selected subjects. Patients stepped out of the positioning frame and were repositioned between the first and second scans. An additional scan one year later was analyzed for some another 15 randomly selected subjects, among which 7 patients had been treated with braces and 8 did not receive treatment. The mean Cobb angle at the one year follow-up was 32.7° (minimum 14° , maximum 92°). Also, the ST scans of 5 normal subjects were analyzed to compare the similarities and differences of the DCM of normal subjects with AIS patients.

3.2.2 Classification

Asymmetry analysis was completed on 51 out of the original 55 subjects (46 AIS and 5 healthy subjects). The scheme of the DCMs for the 46 subjects who had the baseline and short follow-up scans were visually appraised by three scoliosis

professionals. The DCMs were compared based on the location, number and extent of the colour patches to identify possible categories for the surface classification. Categories were identified based on the number, extent and location of the colour patches present in the DCM of torsos. Figure 3-1 shows an example of the DCM obtained from the analysis for an AIS and a healthy subject. While the clarity and integrity of the classification were appraised by scoliosis professionals, the reliability of the classification were assessed by novice observers. The results of the reliability tests were evaluated to identify the problematic and ambiguous aspects of the classification definition. The groups were revised by applying appropriate modifications. Reliability of the new classifications was reassessed until the desired confidence was acquired.

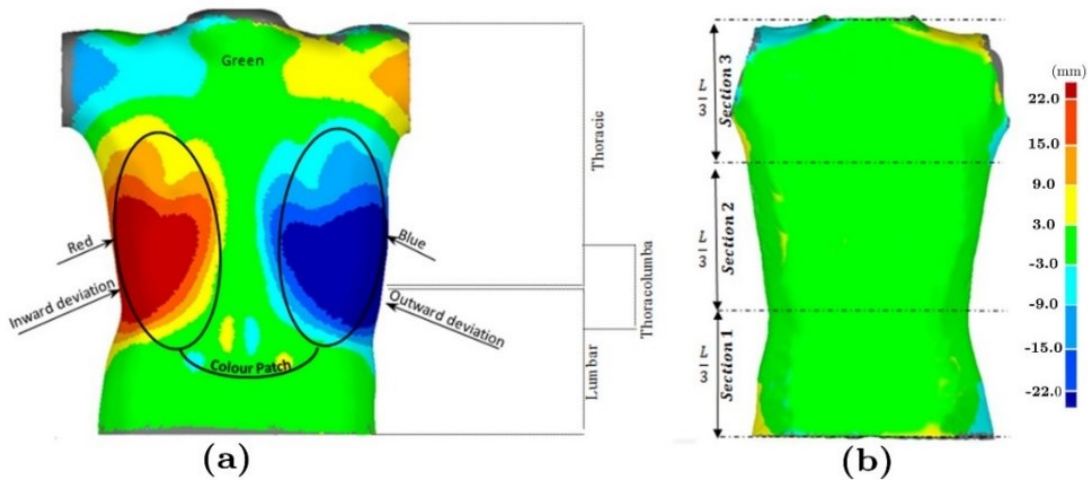


Figure 3-1- The DCMs of the analyzed torsos for (a) patient with AIS and (b) healthy subject.

3.2.3 Reliability

A good scoliosis classification system should be unambiguous, reliable, exhaustive, mutually exclusive, and should provide guidance for treatment strategy. In this thesis, the success of a classification system is evaluated by reliability tests such as

inter-and intra-observer tests. Inter-observer variation can be measured in any situation in which two or more independent observers are evaluating the same thing. Intra-observer variation is measured when stability of responses from the same observer answering the same thing at different time points are investigated. Repeatability or test-retest reliability refers to the variation in repeat measurements made on the two scans of same subject with few minutes interval under identical conditions. The Kappa coefficient is used to evaluate the results of the reliability tests for categorical variables.

The intra-observer, inter-observer, and test-retest reliability of classifying subjects with AIS into the proposed categories were evaluated. Eight observers were asked to classify patients based on the DCM. Three observers were experienced scoliosis researchers while the remaining five did not have specific knowledge about scoliosis. The ability to distinguish the colours was the only qualification criterion for the observers. The classification system was summarized in a two-page instruction manual (Appendix A) to ensure that the definitions of the classification system and procedure of categorization were understood by all observers. The content of the instruction manual was explained to the observers before performing the test.

In order to better differentiate the subgroups and clarify the definition of the colour patch some instructions were provided at the end of instruction manual. It was advised to start the classification by counting the number of colour patches. Figure 3-2 shows some cases where counting the patterns might be confusing. The following tips may help to distinguish the colour patches:

- 1- Small colour patches located on the edges and sides of the torso in section 1 are not counted (Figure 3-2(a)), unless they have a dark blue or red colour or are extended to the centre of section 1. (Figure 3-2(b), (c), (d)).

- 2- Small scattered colours may be due to abnormal muscle growth or inaccurate scanning, so they are dismissed (Figure 3-2(e)).
- 3- Only one curve is counted in the section 3, even if more than one colour patches in this section exist. (Figure 3-2(f)).

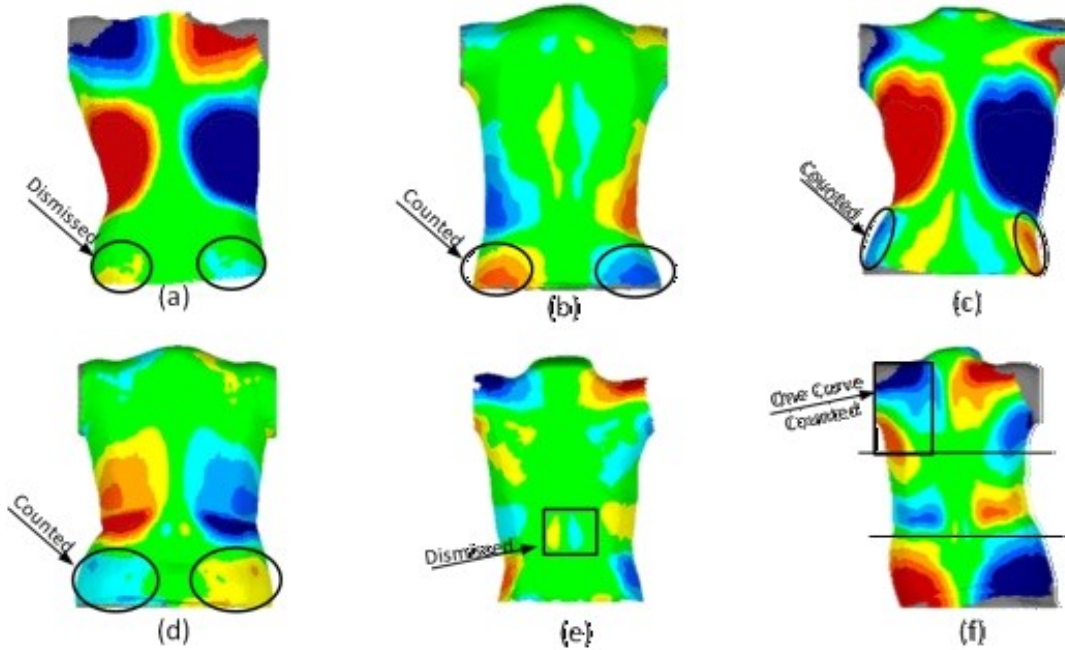


Figure 3-2-a) Small and mild colour patches on the edge of section 1. b&c) Severe deformation at the edge of section 1. d) Deformation extended to the centre of section 1. e) Small scattered colour patches. f) Two colour patches exist in the section 3.

While several reliability coefficients have been proposed in the literature, the Cohen’s Kappa (1960) became over time the most widely-used agreement index of its genre for categorical variables [96]. The calculation of Kappa is based on the difference between how much agreement is actually presented (“observed” agreement) and how much agreement would be expected to be present by chance alone (“expected” agreement). To explain the concept of Kappa coefficient the contingency table (Table 3-1) of a simple inter-observer reliability test is considered to describe the computational methods in their general form. The contingency table for an intra-

observer reliability test would be similar to Table 3-1 except that different trials of an observer are compared.

Table 3-1- Theoretical contingency table of an inter-observer test- Distribution of n subjects into two categories by Observer A and Observer B.

Observer A	Observer B		Total
	1	2	
1	n_{11}	n_{12}	n_{1+}
2	n_{21}	n_{22}	n_{2+}
Total	n_{+1}	n_{+2}	n

The contingency Table 3-1 is used to evaluate the extent of agreement between two observers (A and B) who have each classified n individuals into two non-overlapping category (1 and 2). Table 3-1 indicates that observers A and B both agreed on classifying n_{11} and n_{22} subjects into category 1 and category 2, respectively. Therefore, observers A and B agreed on the classification of $n_{11}+n_{22}$ subjects out of a total of n subjects and they disagreed on the classification of $n_{12}+n_{21}$ subjects. The overall agreement probability, which is denoted by P_a , is given by:

$$P_a = \frac{n_{11}+n_{22}}{n} \quad (3-1)$$

If P_a would be considered as extent of agreement between observers A and B, then it overestimates the inter-observer reliability due to possible chance agreement. In other word, observer A may ignore a particular subject's characteristics and could still categorize that subject into the exact same group as observer B. The Kappa coefficient adjusts the P_a , using the chance-agreement probability P_e , to identify the lucky agreement and remove it before evaluating of the percent of agreement. Based on the contingency Table 3-1, the probability for observers A to classify a subject into category 1 is:

$$P_{1+} = \frac{n_{11}+n_{12}}{n} \quad (3-2)$$

And the probability for observer B to classify a subject into category 1 is:

$$P_{+1} = \frac{n_{11}+n_{21}}{n} \quad (3-3)$$

Therefore observers A and B are expected to reach agreement on category 1 with probability $P_{1+} \times P_{+1}$. Likewise, they are expected to reach agreement on category 2 with probability $P_{2+} \times P_{+2}$, where:

$$P_{2+} = \frac{n_{21}+n_{22}}{n}, \quad P_{+2} = \frac{n_{12}+n_{22}}{n} \quad (3-4)$$

The chance-agreement probability P_e is the summation of the two chance agreement probabilities calculated with respect to the 2 response categories 1 and 2 and its formula is given by:

$$P_e = P_{1+}P_{+1} + P_{2+}P_{+2} = P_{1+}P_{+1} + (1 - P_{1+})(1 - P_{+1}) \quad (3-5)$$

Cohen [97] defined the Kappa coefficient as follows:

$$\kappa = \frac{P_a - P_e}{1 - P_e} \quad (3-6)$$

According to Cohen [97] Kappa's denominator represents "... the units for which the hypothesis of no association would predict disagreement between the judges.", and its numerator represents "... the percent of units in which beyond-chance agreement occurred ...". The magnitude of Kappa is standardized to the range of 0 to 1, where 1 is perfect agreement, 0 is exactly what would be expected by chance. Poor, fair, moderate, good and excellent agreements are indicated by the ranges 0-0.20, 0.21-0.40, 0.41-0.60, 0.61-0.80, and 0.81-1.00, respectively [96]. In this study the reliability of the developed classification system was assessed using inter and intra-observer reliability tests and the degree of agreement was reported using the Kappa coefficient.

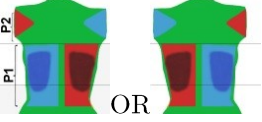
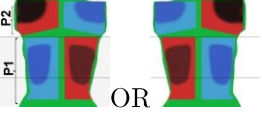
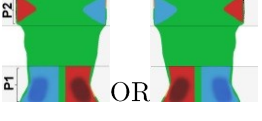
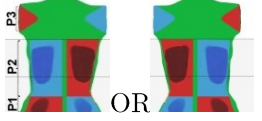
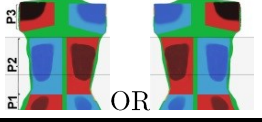
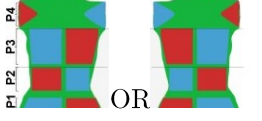
3.3 Results

3.3.1 Classification

Three broad classification groups and a total of six subdivided subgroups were identified among the DCMs by the scoliosis professionals (Appendix A). The three groups (Groups A, B and C) were identified based on the number of colour patches on the DCM of torso. As defined in Section 2.2.4 a pair of corresponding blue and red colours in the DCM is termed a colour patch. The location of each colour patch is described in reference to the bottom third (section 1), middle third (section 2) or top third (section 3) of the torso (Figure 3-1). A schematic and a description of each Group and its subgroups are shown in Table 3-2. Group A contains three subgroups, each having two colour patches along the torso height. In subgroups A1 and A2 the centre of the largest colour patch is located in the thoracic or thoracolumbar region whereas it is in the lumbar region in subgroup A3. Subgroup A2 has asymmetry extending to the scapula while subgroup A1 does not. Group B with its subgroups B1 and B2 is characterized by having three colour patches along the height of torso with the centre of the largest colour patch located in thoracolumbar or lumbar regions. Subgroup B2 has asymmetry in the scapula area while subgroup B1 does not. Group C which includes subgroup C1 has four colour patches through the torso height.

As described in Section 2.2.4, the asymmetry analysis determines the distance from each point in the original torso to its corresponding point in the reflected torso, and displays these distances in the form of a deviation colour map. The STDEV of these distances is also calculated for each analysis. The STDEV values for the AIS subjects classified in Group A, Group B, and Group C were $7.6\pm 3.1\text{mm}$, $8.3\pm 2.8\text{mm}$, and $6.5\pm 3.5\text{mm}$, respectively. The STDEV for the five healthy subjects was $3.4\pm 0.8\text{mm}$.

Table 3-2- The developed signatures of the torso

	Subgroup	Description of individual colour patches
Group A (2 Asymmetry patches)	A1 	First Patch: located in sections 1* and 2 with the centre of deformation close to the boundary between sections 1 and 2 representing thoracic/thoracolumbar curves. Second Patch: located in section 3 and characterizes shoulder asymmetry
	A2 	First Patch: same as subgroup A1. Second Patch: located in section 3 with the centre of the patch located close to the scapula
	A3 	First Patch: located strictly in section 1 representing lumbar curves Second Patch: located strictly in section 3 and characterizes shoulder asymmetry
Group B (3 asymmetry patches)	B1 	First Patch: located strictly in section 1 representing lumbar curves Second Patch: located in sections 1 and 2 with the centre of deformation located close to the boundary between sections 1 and 2 representing thoracic and thoracolumbar curves Third Patch: located in section 3 and characterizes shoulder asymmetry
	B2 	First and Second Patches: same as subgroup B1. Third Patch: located in section 3 with the centre of the patch located close to the scapula
Group C (4 asymmetry patches)	C1 	First, Second and Third Patches: located in and between sections 1 and 2 Fourth Patch: located strictly in section 3 and characterizes shoulder asymmetry
*Sections 1, 2 and 3 represent the bottom, middle and top thirds of the torso respectively.		

3.3.2 Repeatability, Test-retest Reliability

When comparing two torso surface data of a same patient, for instance through the follow-up, it is important to ensure that the differences are due to real change of the torso deformities not to the change associated to a difference in patient's posture or growth between acquisitions. In addition, before we could correlate surface asymmetry to spinal deformity, we need to validate that each stage of processing, that transformed raw torso surface data into indices of torso asymmetry, was reasonably accurate and reliable. The goal of the repeatability test is to assess how consistent is the result of asymmetry analysis within individuals.

The asymmetry analysis involves human manipulation in the pre-processing step including merging the recorded point clouds of the torso by each camera and cropping the model. Therefore, the measurement error due to patient sway and human intervention should be assessed. The ST scans of 8 randomly selected patients were merged and cropped by two users to assess the repeatability of the method. This analysis includes the error due to the model preparation and error in data acquisition. The prepared models were analyzed and obtained DCMs were compared. The asymmetry maps showed similar patterns between the two corresponding torsos for all patients. The average RMS and MaxDev variation were 1.1% (range: 0.-2.9%) and 2.3% (range: 0.5-4.7%), respectively.

Although the position of the patient with respect to the cameras was attempted to be controlled using the frame, there is still potential variability in the ST scans within an individual due to sway, different posture and etc. The test-retest reliability of the classification was assessed by comparing the second baseline scan of the 15 selected patients, which was recorded few minutes after the first scan, with the first scan. This analysis includes the error due to the effect of patient posture and reconstruction. The 15 pairs of torso models were randomized and five observers were asked to classify the 30 models. The intra-observer test-retest kappa coefficient and

the percentage of agreement (P%) between the two scans were determined for each observer where $P\% = P_a * 100$. The reliability was reported as the average of the five calculated kappa coefficients and the five calculated P% values. Figure 3-3 shows typical asymmetry maps of the first and second baseline scans of a patient with AIS. The average percent difference in STDEV of DCMs between the first and second baseline scan among the 15 analyzed subjects was 5% (minimum 1% and maximum 15%) and the asymmetry maps showed similar patterns between the two scans for all patients. The intra-observer test-retest reliability in subgroup classification using the first and second baseline scans of 15 torsos was 85% agreement (range: 80% to 93%), with a mean kappa value of 0.83 (range: 0.70 to 0.92), indicating good to excellent reliability (Table 3-3). For the group classification, the percent agreement increased to 92% (range: 80% to 100%) with a mean kappa value of 0.99 (range: 0.32 to 1) demonstrating that the majority of the torsos were classified in the same category using the first and second baseline scans. Moreover, the high value of P% and the small difference in the STDEV (5%) between the first and second baseline scans confirms the repeatability of the method.

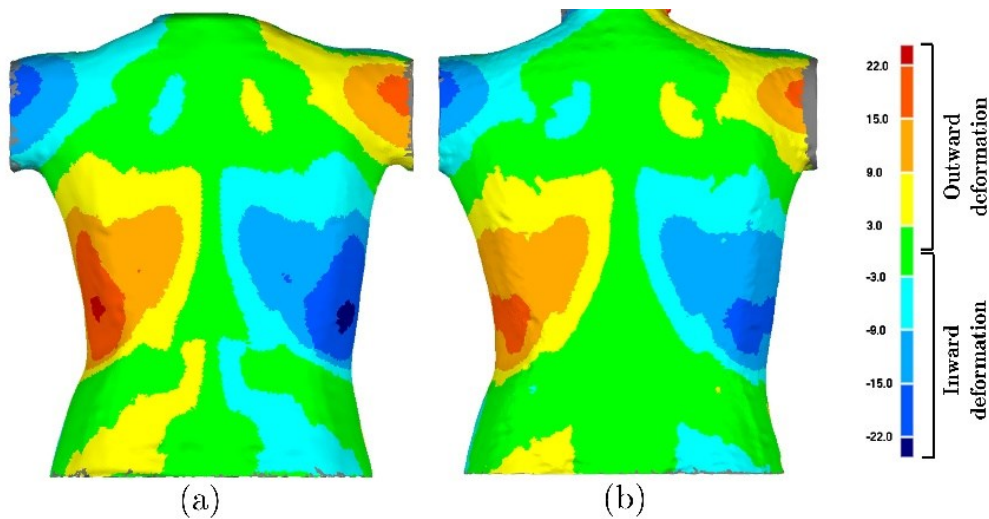


Figure 3-3- First (a) and second baseline scan (b) for a patient with AIS (Cobb=31°)

Table 3-3- Test-retest reliability: comparing the classification of the first and second baseline scans of 15 torsos

Observers	Group Classification				Subgroup Classification			
	P%	K	95% CI	Strength of agreement	P%	K	95% CI	Strength of agreement
1*	100%	1	1.00-1.00	Excellent	93%	0.91	0.74-1.00	Excellent
2	87%	0.62	0.15-1.00	Good	80%	0.70	0.41-0.99	Good
3	80%	0.32	-0.28-0.92	Fair	80%	0.73	0.48-0.98	Good
4*	93%	0.89	0.67-1.00	Excellent	80%	0.75	0.51-1.00	Good
5*	100%	1	1.00-1.00	Excellent	93%	0.92	0.76-1.00	Excellent
Average	92%	0.99		Excellent	85%	0.83		Excellent

*: Scoliosis professional observers

P%: Percentage of agreement

3.3.3 Intra-observer Reliability

To determine intra-observer reliability, four observers classified the group of 46 AIS subjects two times, leaving at least three days between each trial to minimize memory bias. The kappa coefficient and the P% between the two trials were determined for each observer. The reliability was reported as the average of the four calculated kappa coefficients and the four calculated P% values.

The average kappa coefficient for the intra-observer reliability of the four observers who classified twice the DCM of 46 subjects with AIS in the three broad groups was 0.85 (range 0.68 to 0.92) indicating good to excellent reliability (Table 3-4). When considering the six subgroups the kappa coefficient showed good intra-observer reliability (average 0.74, range 0.70 to 0.78) indicating that the observers were able to consistently classify the subjects into the same category (Table 3-4).

Table 3-4- Intra-observer reliability of torso classification by the four observers

Observers	Group Classification				Subgroup Classification			
	P%	K	95% CI	Strength of agreement	P%	K	95% CI	Strength of agreement
1*	96%	0.92	0.81-1.00	Excellent	80%	0.75	0.61-0.90	Good
2	91%	0.84	0.69-0.99	Excellent	83%	0.78	0.65-0.92	Good
3	83%	0.68	0.48-0.87	Good	78%	0.72	0.57-0.87	Good
4	93%	0.88	0.74-1.00	Excellent	76%	0.70	0.55-0.85	Good
Average	91%	0.85		Excellent	79%	0.74		Good

* Scoliosis professional observer
P% Percentage of agreement

3.3.4 Inter-observer Reliability

To determine inter-observer reliability, four observers classified the group of 46 AIS subjects. The multi-observer kappa coefficient and the P% were determined.

Noticeable inter-observer reliability was found among the four observers in classifying the 46 subjects with AIS into both the three groups and the six subgroups. For the three group classification, the multi-observer kappa value was 0.62 and the percentage of agreement was 80%, indicating good reliability. For classification into the six subgroups, the corresponding values were 0.52 and 59%, respectively, indicating moderate reliability.

To assess the discrepancy in classification between observers, the frequency of their classification can be shown in matrix format. The classifications by each pair of observers for the 46 subjects were compared (six comparisons in total for four observers) and summarized in Table 3-5 A and B. The diagonal components of the matrix indicate the number of times two observers agreed on the classification for a particular subject. The off-diagonal components indicate when two observers disagreed on the classification for a particular subject, and the location of the entry in the matrix indicates where the discrepancy occurred. For example in Table 3-5 A, there were 39 instances when one observer classified a subject into Group A and another observer classified the same subject into Group B.

Table 3-5- Distribution of classification decisions by each pair of observers from the sample of 4 observers when rating 46 subjects into (A) 3 groups or (B) 6 subgroups

A: Group Classification

	Group A	Group B	Group C	Total
Group A	137			137
Group B	39	70		109
Group C	8	10	12	30
Total	184	80	12	276

B: Subgroup Classification

	Sub-group A1	Sub-group A2	Sub-group A3	Sub-group B1	Sub-group B2	Sub-group C1	Total
Subgroup A1	33						33
Subgroup A2	22	62					84
Subgroup A3	7	3	10				20
Subgroup B1	7	5	9	37			58
Subgroup B2	4	9	5	16	17		51
Subgroup C1	2	2	4	6	4	12	30
Total	75	81	28	59	21	12	276

3.3.5 One year follow-up test-retest reliability

The one year follow-up ST scan was acquired approximately 12±3 months after the baseline scans and analyzed for 15 selected subjects. Table 3-6 shows the Lenke curve type, Cobb angles at baseline and one year, and the treatment received during the one year interval for each subject. The mean curve progression for these patients was 4° (minimum -10°, maximum 25°) with a STDEV of 6.04°. None of the patients changed Lenke curve type during the one year interval. Subjects were not selected on the basis of whether or not they had progressed during the follow-up to reflect the likelihood that classification would change in the population seen longitudinally at our clinic. Since the Lenke curve types did not change over the one year span, the pattern of torso asymmetry was expected to stay the same as well. The 30 models

from the 15 pairs of torso models (first baseline and one year follow-up) were randomized and five observers were asked to classify each DCM. The kappa coefficient and the P% for the classification based on baseline and one year scans were determined for each observer. The one year test-retest reliability was reported as the average of the five calculated kappa coefficients and the five calculated P% values to reflect the stability of the classification over a one year interval.

Table 3-7 shows the intra-observer test-retest reliability results of the classification based on the first baseline and one year follow-up scans of 15 torsos for each of five observers. The mean kappa value of group and subgroup classifications were 0.70 (range: 0.56 to 0.84) and 0.71 (range: 0.29 to 0.82), respectively. Figure 3-4 shows the DCM of a subject for each of the two scans within a one year interval.

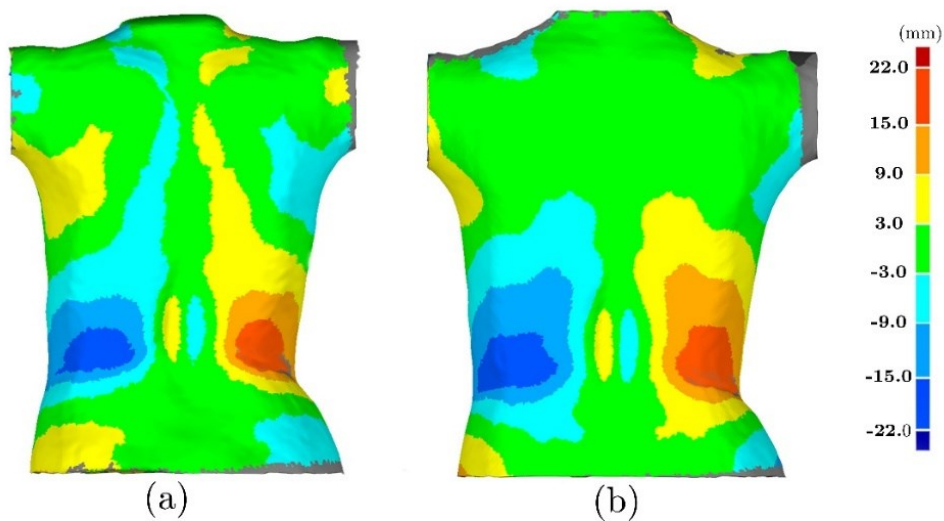


Figure 3-4- DCMs of a patient with AIS; (a) First scan (Cobb= 21°R-T; 38°L-TL), and (b) one year follow-up scan (Cobb= 18°R-T; 34°L-TL).

Table 3-6- The Lenke curve type, Cobb angle and treatment of 15 patients with one year follow-up data

ID	Lenke Type	Baseline Curve	Follow-up Curve	Treatment
1	1	26R-T; 18L-L	22R-T; 13L-L	Observation
2	1	67R-T	92R-T	Observation
3	1	18L-PT; 27R-T	18L-PT; 17R-T	Brace
4	3	46L-PT;59R T; 34L-L	46L-PT; 58R-T; 37L-L	Brace
5	5	15T-L	18L-TL	Observation
6	5	14L-L	14L-L	Observation
7	5	44L-TL	48L-TL	Observation
8	5	26L-L	25L-L	Observation
9	5	33R-TL	30R-TL	Observation
10	5	22R-T; 35L-L	20R-T; 34L-L	Observation
11	5	25R-TL	28R-TL	Brace
12	5	25L-L	23L-TL	Brace
13	5	21R-T; 38L-TL	18R-T; 34L-TL	Brace
14	5	12L-TL	15L-TL	Brace
15	5	32L-TL	32L-TL	Brace

Cobb Angle: (degrees)(L: left, R: Right) (PT: Proximal Thoracic, T: Main Thoracic, TL: Thoracolumbar, L: Lumbar)

Table 3-7- Reliability result of classifying the first and one year follow-up scan of 15 torsos

Observers	Group Classification				Subgroup Classification			
	P%	K	95% CI	Strength of agreement	P%	K	95% CI	Strength of agreement
1*	80%	0.56	0.22-0.90	Moderate	80%	0.74	0.48-0.99	Good
2	93%	0.62	0.15-1.00	Good	87%	0.81	0.56-1.00	Excellent
3	93%	0.77	0.35-1.00	Good	87%	0.82	0.61-1.00	Excellent
4*	80%	0.63	0.24-1.00	Good	40%	0.29	0.00-0.58	Fair
5*	93%	0.84	0.55-1.00	Excellent	73%	0.66	0.39-0.93	Good
Average	88%	0.70		Good	77%	0.71		Good

*: Scoliosis professional observers
P%: Percentage of agreement

3.4 Discussion

In this chapter, a novel technique was presented to quantify, visually report, and classify torso asymmetry in patients with AIS based on ST data. Three distinct groups divisible into six subgroups with different torso asymmetry patterns were

identified based on visual comparison of the asymmetry maps of the analyzed torsos. The repeatability, intra- and inter-observer, short and long-term test-rest reliability of the classification indicates that the method is repeatable. However, like other classification systems [72], categorizing some subjects that have characteristics on the boundary between different groups may become complex.

While we expected our classification system to produce excellent reliability results, we realized that there are sources of discrepancies during the process of visual categorization. The most common difficulties encountered by the observers included the distinction of subgroup A1 from subgroup B1 and subgroup A2 from subgroup B2. These discrepancies occurred when one or more small patches of asymmetry were ignored in section 1 in some trials (or by some observers) and counted in others. Another difficulty was identifying the difference between subgroups A1 and A2 and subgroups B1 and B2 when the extended deviation on the shoulder/scapula region was ignored by some observers and counted by others. However, the mean kappa value of 0.85 (range, 0.68 to 0.92) obtained for intra-observer reliability and multi-observer kappa coefficient of 0.62 calculated for inter-observer reliability demonstrates comparable reliability with respect to the Lenke classification system [76]. In their study, five surgeons who had developed the Lenke classification system used both the Lenke and the King classification for a group of patients. Kappa values of 0.83 (range, 0.79 to 1.0) and 0.92 (range, 0.83 to 1.00) were reported for the intra-observer and inter-observer reliability of classifying the curve type, respectively using the Lenke classification and 0.62 and 0.49 using the King classification [72]. However, no multi-observer kappa was reported in Lenke's study. The reliability of the present system may possibly be improved by clarifying the manual for the proposed classification system with precise values of deviation for the different categories, performing the test by scoliosis professionals, or providing more observer training.

Selecting an appropriate spectrum for the colour map of the deviation analysis assists the observer to distinguish the category. Employing a large number of colours would make the torso a compound of colours which might distract the observers, while a reduced number of colours might conceal some features of the torso deformity. Likewise, a wide range of maximum and minimum deviation would not reveal the mild deformity, while a narrow range would not illustrate the variations among the severely asymmetric torsos. Our proposed spectrum, with nine colour segments and a MaxDev of $\pm 22\text{mm}$, was selected after trying a variety of different settings for the full set of torsos models. Our chosen spectrum allows categorizing all curves encountered in this study.

The high P% for the group classification (92%) and the subgroup classification (85%) in the test-retest reliability shows that the pattern of torso deformity is nearly the same in the first and second baseline scan for the examined subjects. This means that positioning the patient during the scan and pre-processing the torso geometry for analysis were reproducible and do not significantly affect the classification based on the asymmetry analysis of the torso. This suggests that our classification system is repeatable and provides a method to group patients according to their ST asymmetry map irrespective of the time at which the data was acquired.

The P% for the group classification was greater than or equal to the corresponding value for the subgroup classification in all cases. In general, this is due to the fact that it is more difficult to classify the subjects into six groups than three. With 6 subgroups, chance agreement is also less likely than with 3 groups. With the six subgroups, the boundaries between the subgroups are more subtle, and some asymmetry maps may lie on these boundaries. It can be seen from Table 3-5A, that the number of agreements between observers for the three group classification, represented by the diagonal entries, is generally high when compared to the number of disagreements. However, in Table 3-5B, the large values in the (1,2) and (4,5)

entries indicate areas of uncertainty among the observers in distinguishing subgroup A1 from A2 and subgroup B1 from B2.

Based on the reliability coefficient values and visual comparison of the asymmetry maps between the baseline and one year follow-up scans, it was determined that the pattern of asymmetry and group classification remains constant for the majority of patients throughout a one year time interval. Even if the magnitude or severity of the deformity changed between the baseline and one year follow-up scans, the pattern of asymmetry was found to be the same. One observer (Observer 4) was found to have good reliability in the group classification for this analysis, but only fair reliability in the subgroup classification ($\kappa=0.29$). This lower reliability may be due to the difficulties in distinguishing the different subgroup categories as discussed above. However, it may also be due to differences in the torso DCM from treatment or progression of the scoliosis deformity. It was found that 40% of the discrepancies in subgroup classifications for Observer 4 were related to subjects with a change in Cobb angle of more than 4° (Subject ID 2, 3, 11 and 13 in Table 3-6).

While our classification system was found to be reliable, it is not meant as a quantitative measure of asymmetry. The STDEV of the deviation over the full torso summarizes the severity of the asymmetry; however, it does not quantify the extent of asymmetry in specific regions (i.e. areas of high asymmetry). Chapter 4 will focus on augmenting our qualitative classification system with measures that can objectively assess the severity of the deformity more appropriately within each category. In addition, the comparison between the deformities measured using the X-ray and the obtained asymmetry map will be further investigated to determine the relationship between the external deformity and the internal spinal geometry. Although the classification system was found to be reliable, the validity, and sensitivity to change of the suggested parameters should be assessed in the future.

3.5 Conclusion

Classifying the torsos based on the asymmetry map derived from ST scans has a tremendous potential to non-invasively detect torso asymmetry associated with scoliosis. Further, this classification may assist with monitoring progression non-invasively if extracted parameters reflect progression with high sensitivity in each deformity type. The asymmetry analysis and associated classification system have the potential to accurately monitor progression; the proposed system is able to draw the attention of the clinicians to areas of change and consequently may reduce the number of X-rays required for patient follow-up. Further, classification of surface deformities may guide the design of personalized braces and/or exercise treatment by identifying areas of the surface most affected by scoliosis. Bracing uses surface pressures to correct the effect of scoliosis and to prevent further progression. Many scoliosis exercise approaches focus on improving posture thereby addressing the external deformity. Therefore, the proposed classification may help direct these therapies to address the most asymmetric features for the patients.

The success in classifying the torso based on markerless ST data may lead to the development of severity measures that are specific to each group which might overcome the limitations of the current ST measures. For example, in the current ST measurements the indices are not specific to a certain curve type so changes in some patients, captured by a change in some severity indicators, are diluted when averaged with the same measurements obtained from patients with a different curve type. Our categorization method will allow the development of ST measurements specific to a subgroup of patients with a similar deformity. Furthermore, our technique does not rely on any markers and thus reduces the inherent errors associated with placing landmarks on the patients and digitizing landmarks during the analysis.

Chapter 4

Curve Predictions¹

4.1 Introduction

The spinal deformity associated to AIS influences the posture of the patient in a more or less significant way, depending on its type and severity. Assessing torso surface deformities, a task that is hardly doable using the radiographs, is valuable in clinic since it documents an important aspect in patients' point of view [13, 98]. Scoliosis curve characteristics such as location apical vertebra, number of curves, and magnitude of curve are important parameters in scoliosis management. Researchers attempted to use ST to predict the important parameters used to monitor the internal deformity in patients with scoliosis such as the Cobb angle, shape, location, severity, and axial rotation of the underlying spinal curves in order to replace or at least decrease the periodic radiographic evaluations [3, 15, 28, 47, 54, 61, 63, 99-101].

In this chapter, the 3D markerless asymmetry analysis of the full torso [102] is employed to identify the area of asymmetry and illustrate the deformities with 3D contour maps. Since the indices extracted from the proposed asymmetry analysis are measured without human intervention, the issues with marker placements are

¹ A version of this chapter has been submitted in the Journal of Spine Deformity. A. Komeili, L. Westover, E. Parent, M. El-Rich, S. Adeeb, "Correlation between a Novel Surface Topography Asymmetry Analysis and Radiographic Data in Scoliosis," Spine Deformity.

avoided. The clinical relevance and relation of DCMs to scoliosis severity, as measured by the Cobb angle, was investigated and asymmetry analysis [102] was shown to be reliable. The objectives of this chapter were: (1) to assess the accuracy of the asymmetry analysis in identifying the number, direction and location of the scoliosis curve apices, (2) to predict if the severity of the scoliotic curve belong to categories requiring different management (mild =Cobb<25°, moderate 25°<Cobb<40° and severe Cobb>40°). This chapter is organized as follows. The inclusion criteria for collecting the samples was provided in Section 4.2.1. Section 4.2.2, 4.2.3 and 4.2.4 describe the attempt to predict the curve characteristics such as number, location and direction of the scoliosis curves. The employed statistical method, to classify the severity of the curve, was investigated in Section 4.2.5. Section 4.3 presents the results of the curve characteristics prediction. Section 4.4 provides extensive discussion about the accuracy of the results. Section 4.5 summarizes the finding of this chapter and recommends directions for future research.

4.2 Materials and Methods

4.2.1 Clinical Data

Torso scans from 100 patients with AIS were selected according to selection criteria as described in Section 2.2.1. This sample included, 78% females, 10 to 18 years old, Cobb angles between 10°-69°. There were 32, 3, 13, 0, 46, and 6 subjects with Lenke 1 through Lenke 6, respectively. Torso scans of 24 additional patients with AIS meeting the same selection criteria were employed as a validation sample to assess the accuracy of the model developed for predicting the location of the curve apex from ST data. Table 4-1 shows the number and distribution of the subjects based on the location of the curve and magnitude of the Cobb angle. Since some of the

subjects had double or triple curves, the number of curves exceeds the number of subjects.

Asymmetry of the torso was investigated using the 3D markerless asymmetry analysis described in Chapter 2. To be able to quantitatively assess the local deformities the colour patches with $>\pm 3\text{mm}$ deviation were automatically isolated from the DCM. Due to symmetry about the best plane of symmetry, the corresponding red and blue deviations in each colour patch have equal deviation with opposite sign, so only one side of the torso was considered to calculate parameters used in the models predicting radiograph data. Figure 4-1 shows as an example the complete DCM and the isolated colour patches of an analyzed torso.

Table 4-1- Distribution of the curves based on the location of curve and Cobb angle value.

	Location of Curve	Mild Cobb $<25^\circ$	Moderate $25^\circ < \text{Cobb} < 40^\circ$	Severe $40^\circ < \text{Cobb}$	Total
Development sample (100 subjects)	PT	15 (10%)*	3 (2%)	2 (1%)	20
	T-TL	45 (29%)	33 (21%)	24 (15%)	102
	L	14 (9%)	12 (8%)	8 (5%)	34
Validation sample (24 subjects)	PT	1 (3%)	2 (5%)	1 (3%)	4
	T-TL	11 (28%)	10 (25%)	4 (10%)	25
	L	3 (8%)	6 (15%)	2 (5%)	11
PT: Proximal Thoracic, T-TL: thoracic/thoracolumbar, L: lumbar *: Number (Percentage)					

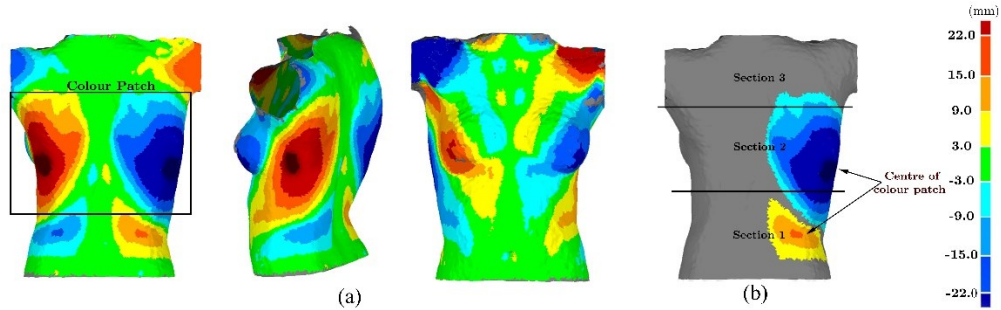


Figure 4-1-a) Full DCM of an analyzed torso from back, side, and front view, b) Colour patches isolated from the DCM

4.2.2 Number, direction, and location of curves

Since the blue and red colours represent protruded and sunken regions on the torso surface, respectively, the number and location of the blue areas were deemed to reflect the number and location of the scoliotic curve in the vertebral column. The location of the curve was determined based on the classification system introduced in Chapter 3. That is, if the centre of the colour patch is in the lower third section of the torso it represents a Lumbar (L) curve; if the centre of the colour patch is in middle one third section of the torso it represents a thoracic/thoracolumbar (T-TL) curve; and finally if the colour patch centre is located in the upper one third section of the torso it represents proximal thoracic (PT). Table 4-2 summarizes how to identify the location of curve using the subgroups.

Table 4-2-Determining the location of curve (T-TL, L) based on the subgroup category

Subgroup	Location of the colour patch centre (See Figure 4-1b)	Curve Location
A1	Section 2	T-TL
	Section 3	PT
A2	Section 1	L
A3	Section 2	T-TL
B1,C1	Section 1	L
	Section 2	T-TL
	Section 3	PT
B2	Section 1	L
	Section 2	T-TL

Three novice observers determined the number, direction and location of the curve(s) from the DCM. Standard instructions were provided to the observers. The observers were asked to determine the number, direction and location of the apical vertebra (PT, T-TL, L) using the DCM. The observers first counted the number of colour patches in the DCM. To determine the direction of the curve, observers simply determined if the blue colour was on the right or left side of the torso. Finally, the height of the torso was equally divided into three sections (visually) and observers identified the section in which the centre of the colour patch was located (see Figure 3-1). The curve location was classified as lumbar (L), thoracic/thoracolumbar (T-TL), or proximal thoracic (PT). Each measure was compared with the X-ray data to investigate the inter-method reliability between the DCMs and the radiographs.

4.2.3 Height of the apical vertebra

Beyond determining the number, direction and general location of the curve(s), finding the exact location of the apical vertebra is an important variable in the clinical applications, such as brace design, because it is the region that requires most in-brace correction and corresponds to where a pressure pad is typically used. The vertical distance between the centre of each colour patch (point with MaxDev) and

the posterior superior iliac spine (PSIS) was measured in the DCM and termed h_{ST} (Figure 4-2a). From the corresponding radiograph the vertical distance between the centre of the apical vertebra and the PSIS was measured using the calibrated axis in the radiograph and termed h_r (Figure 4-2b).

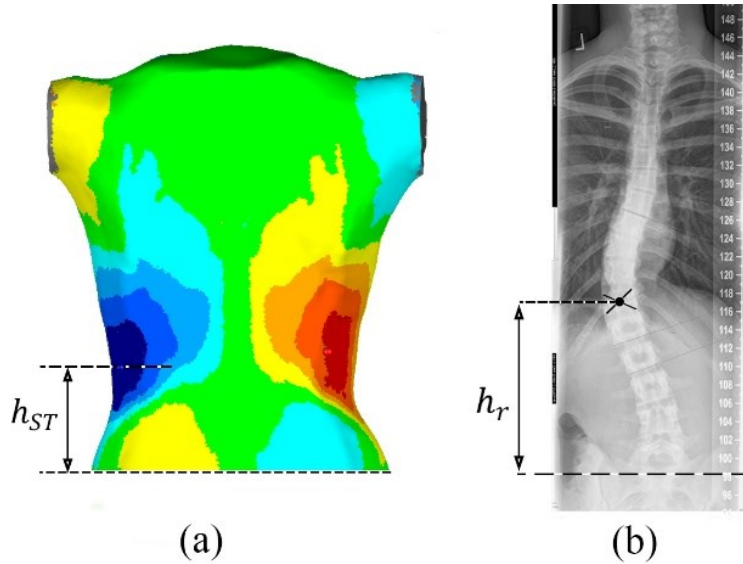


Figure 4-2- a) Vertical distance between the point with maximum deviation and PSIS measured from the DCM, b) vertical distance between apical vertebra and PSIS measured using corresponding radiograph

4.2.4 Curve magnitude

The 25° and $40\text{-}50^\circ$ Cobb angle are often considered as the threshold for mild-moderate and moderate-severe scoliosis [103]. For an isolated colour patch, the MaxDev of torso provides certainly an idea of the severity of the torso asymmetry; however, it overlooks the value of the Cobb angle. Therefore, the MaxDev and RMS of the individual point-by-point deviation (see Section 2.2.4) in the isolated colour patch area were chosen as independent parameters to predict curve severity. Our rationale to select these parameters was that there is a direct relation between the severity of Cobb angle and the deviation of vertebra and consequently deviation of the torso [104]. The MaxDev and RMS were used to classify each curve into the

following groups: severe (Cobb>40°), moderate (25°<Cobb<40°) and mild (Cobb<25°). Curves were divided into T-TL and L group based on the radiograph data and the classification tree analysis was performed separately for each group because lateral deformation of T-TL curve is transferred to the trunk surface differently via the rib cage compared with L curves. The surface predictions were tabulated against radiographic data and the accuracy of classification was estimated.

4.2.5 Statistical analysis

The inter-method (ST vs Radiograph) P% and Kappa coefficient were calculated for identifying the number and location of scoliosis curve by each observer. The analysis was repeated for a subset of subjects with Cobb angles>25°, which corresponds to a group with clinically important curves where bracing is usually recommended.

A 100-subjects cohort was used to develop a linear regression model, to identify the location of apical vertebra, of the form:

$$h_r = Ah_{st} + B \quad (4-1)$$

where, A and B are constants. The 24-subject cohort was used as a validation sample to assess the accuracy of the model. The scoliosis curves with Cobb>25° correspond to a group with clinically important curves, so analysis was repeated for the subset of subjects with Cobb angles>25°.

The classification tree technique from the IBM SPSS Statistics 21 [105] was used to determine the ability of MaxDev and RMS (as predictors) to identify the curve severity subgroup (as target) corresponding to each curve. Classification tree analysis is a powerful form of multiple variable analysis that provides unique capabilities to supplement or substitute for traditional statistical forms of analysis such as multiple linear regression. Both quantitative (such as height and weight) and qualitative (such as gender and colour) data can be accommodated in the classification tree construction. The classification tree is produced by algorithms that identify split in independent variables (predictors) into branch-like segments, which

can be used to predict, describe, or classify dependent variable (target). These segments form an inverted tree which branches out from a root node at the top of the tree. The decision rule (which is an arithmetic operation in this study) splits the data and form the branches underneath the root node. The question is “How to define the decision rule to classify the data at each node?” Typically a scoring method is employed to score every possible split on the data. Then each split is scored using a function that is aimed to measure the purity of the subset data after the split. One measure of the purity or randomness of a variable is called entropy. Entropy aims to answer ”how uncertain we are of the outcome?” Entropy essentially measures how random an outcome is. So entropy depends on the probability of all the outcomes. Suppose we have a set of possible n events p_1, p_2, \dots, p_n . The entropy of this set of events is calculated as follows [106]:

$$H(x) = H(p_1, p_2, \dots, p_n) = - \sum_{i=1}^n p_i \log_2 p_i \quad (4-2)$$

Where p_i is the probability of the i th outcome. Therefore, $H(x)$ is just calculated by summing over all possible outcomes of x , weighing by the probability of that outcome and multiplying by logarithm (base two) of the probability of the outcome. Using Eq. (4-2) it may be seen that a deterministic variable with probability of $p = 1$, has the minimum entropy equal to zero. The entropy is mainly used to measure the purity score, however another common measure is called gini index. The gini index measures the impurity score, instead of purity score, and is obtained as follows:

$$H_{\text{gini}}(x) = \sum_{i=1}^n p_i(1 - p_i) \quad (4-3)$$

The information gain (IG) is used as the criterion to define the decision rule at each node. The IG calculates the reduction in entropy when a branch is constructed using the following formula:

$$IG = Entropy(X) - Entropy(X|Y) \quad (4-4)$$

The calculation of the $H(x)$, $H_{gini}(x)$ and IG are given in the Appendix B with an example. To calculate the decision rule in each node the following steps are taken in the classification tree analysis:

- 1- All the possible thresholds are examined to split the data,
- 2- Each of them is scored using one of the measure of purity, such as gini-index,
- 3- Whichever threshold scores the best (maximum IG) is chosen to be the decision rule at that node,
- 4- Data is split according to that rule which gives two subsets, right-hand subset of data and left-hand subset of data.

If a more complex tree is required then the same procedure for the left and right-hand of the branches is repeated recursively which will decide what their sub-branches would look like. Setting a depth parameter controls the complexity of the classification tree.

In this study the classification and regression trees (CRT) method from the IBM SPSS Statistics 21 [105] was employed as the growing method to calculate the decision rule at nodes. The CRT splits the data into segments that are as homogeneous (all independent variables have the same value for the dependent variable) as possible with respect to the independent variables (here MaxDev and RMS) and exploits the gini index for calculating impurity score. To generate a simple classification tree, the maximum number of segments beneath the root node was set to 2.

The surface predictions were tabulated against the data from the radiographs. The specificity, sensitivity and accuracy were calculated for each curve severity

classification subgroup. These terms are illustrated using a conventional two-by-two (2 x 2) table as shown in Table 4-3. Let's assume the "+" and "-" signs in Table 4-3 indicate the "sick" and "normal". Then, cell "a" denotes those who are correctly diagnosed as sick by the test; in other words, the test is true positive (TP) as is the gold standard. Cell "b" represents false positive which are those who have positive results for the test but are not according to the standard (FP). Cell "c" indicates false negative those who are sick but are diagnosed as normal by test (FN). And finally, cell "d" represents true negative which are those who are correctly diagnosed normal by test (TN). Sensitivity (also called the true positive rate) is the percentage of the sick people who are correctly identified as having the condition. Specificity (sometimes called the true negative rate) is the percentage of the healthy people who are correctly identified as normal. The overall accuracy is the ratio of true predictions (a+d) to the total number of predictions (a+b+c+d).

Table 4-3- Calculation of the sensitivity and specificity

	Standard +	Standard -
Test +	a (TP)	b (FP)
Test -	c (FN)	d (TN)
Accuracy (a+d)/(a+b+c+d)	Sensitivity a/(a+c)	Specificity d/(b+d)
TP: True positive, FP: False positive, FN: False negative, TN: True negative		

4.3 Results

4.3.1 Number, direction, and location of curves

Table 4-4 shows the number of true and false prediction (false positive + false negative) for counting the number of curves and identifying the location of curves. Table 4-5 shows the P% and Kappa coefficient between the surface and radiographic data for determining the number, direction, and location of the curve from the DCMs. Improved agreement was observed when mild curves, i.e. Cobb<25°,

were excluded (58 cases), particularly for the number of curves. Curve direction was predicted with 100% agreement when a scoliosis curve was present.

Figure 4-3a compares the vertical location of the apical vertebra measured from radiographs (h_r) and DCMs (h_{st}) for 102 T-TL and 34 L curves. The predictive model for T-TL curves was $h_r = 0.90h_{st} + 69.80$ with R^2 value of 0.78. The predictive model for L curves was $h_r = 0.80h_{st} + 60.53$ with R^2 value of 0.51. The majority of outliers were found to represent mild curves. In Figure 4-3b mild curves (44 T-TL and 13 L curves) were excluded from the regression analysis and the R^2 value increased to 0.83 (predictive model: $h_r = 1.05h_{st} + 45.44$) and 0.61 (predictive model: $h_r = 0.87h_{st} + 50.37$) for T-TL and L curves, respectively. Vertical location of the apical vertebra on ST underestimated the location measured on radiograph as demonstrated by the majority of the points for both T-TL and L curves being located above the bisector line, presented with a dashed line in Figure 4-3.

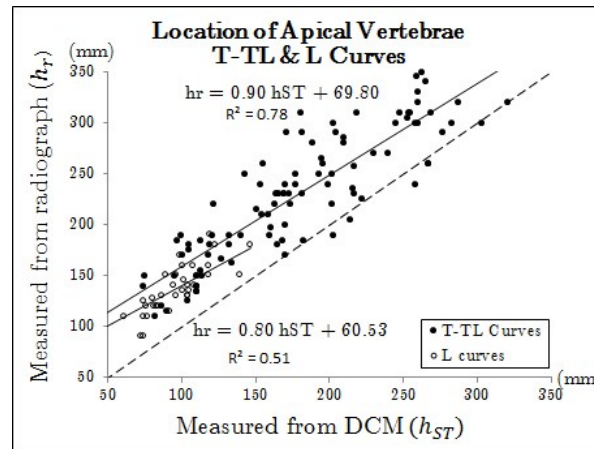
The models developed for the full range of curves (Figure 4-3a) were validated with an additional cohort of 24 subjects. The predicted location of apical vertebra was correlated to h_r with $R^2 = 0.89$ for T-TL curves and $R^2 = 0.58$ for L curves based on R^2 values (Figure 4-3c). The average difference between the predicted value and the measured value for T-TL and L curves was 17mm and 13mm, respectively.

Table 4-4- The observers' classification of the number and location of the curves.

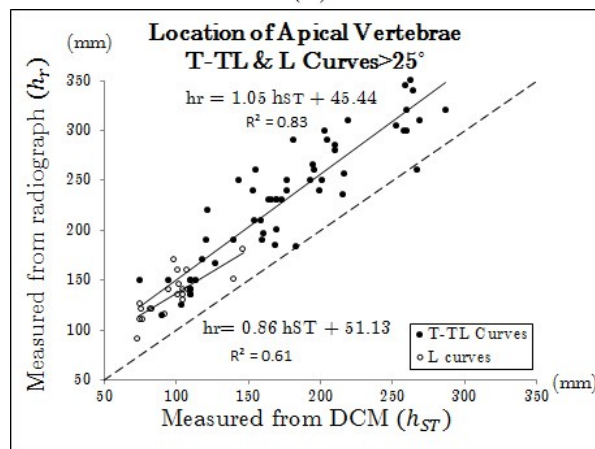
Observer	Number of curves 10°<Cobb<69°						Location of curves 10°<Cobb<69°					
	Single (43)*		Double (47)		Triple (10)		PT (20)		T-TL (102)		L (34)	
	T	F	T	F	T	F	T	F	T	F	T	F
1	26	8	31	22	3	10	16	4	96	6	20	14
2	24	9	35	21	2	9	11	9	98	4	21	13
3	30	16	27	17	2	8	11	9	86	16	22	12
Average	27	11	31	20	2	9	13	7	93	9	21	13
Observer	Number of curves Cobb>25°						Location of curves Cobb>25°					
	Single (19)		Double (22)		Triple (1)		PT (5)		T-TL (57)		L (20)	
	T	F	T	F	T	F	T	F	T	F	T	F
1	13	0	16	6	0	7	5	0	55	2	13	7
2	14	1	18	5	0	4	4	1	55	2	13	7
3	14	3	17	5	0	3	4	1	52	5	13	7
Average	14	2	17	6	0	5	4	1	54	3	13	7
PT: proximal thoracic. T-TL: thoracic/thoracolumbar, L:lumbar *: (Number); T:True, F:False												

Table 4-5- Percentage of agreement (P%) and agreement coefficient (K) between the observers classification and radiograph measurements.

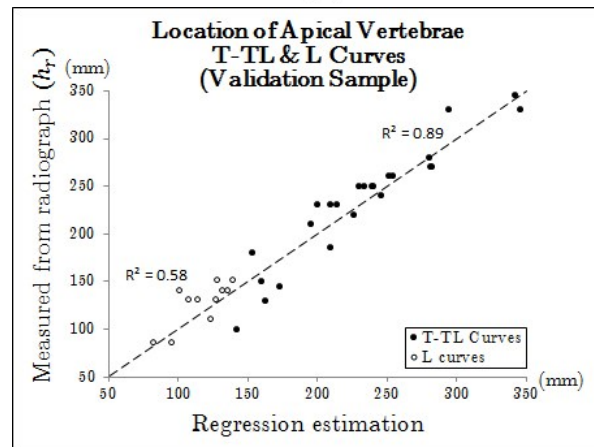
Observer	Number of curves 10°<Cobb<69°					Location of curves 10°<Cobb<69°				
	Single (43)	Double (47)	Triple (10)	K	95% CI	PT (20)	T-TL (102)	L (34)	K	95% CI
	P%					P%				
1	60%	66%	30%	0.32	0.16-0.48	80%	94%	59%	0.72	0.64-0.81
2	56%	74%	20%	0.33	0.17-0.49	55%	96%	62%	0.70	0.61-0.79
3	70%	57%	20%	0.30	0.14-0.45	55%	84%	65%	0.60	0.51-0.70
Average	62%	66%	23%	0.32		63%	92%	62%	0.67	
Observer	Number of curves Cobb>25°					Location of curves Cobb>25°				
	Single (19)	Double (22)	Triple (1)	K	95% CI	PT (5)	T-TL (57)	L (20)	K	95% CI
	P%					P%				
1	68%	73%	0%	0.47	0.25-0.69	100%	96%	70%	0.78	0.66-0.90
2	74%	82%	0%	0.57	0.35-0.79	80%	96%	65%	0.74	0.61-0.86
3	74%	77%	0%	0.52	0.28-0.75	80%	91%	70%	0.70	0.57-0.83
Average	72%	77%	0%	0.52		87%	95%	68%	0.74	
PT: proximal thoracic. T-TL: thoracic/thoracolumbar. L:lumbar P%:Percentage of agreement; K: agreement coefficient										



(a)



(b)



(c)

Figure 4-3- The prediction of the location of apical vertebra using the vertical position of the point with maximum deviation in the colour patch (a) 102 T-TL and 34 L curves, (b) 57 T-TL and 20 L curves with Cobb > 25°, (c) 24 validation sample subjects using regression line

4.3.2 Curve magnitude

Figure 4-4 shows the classification trees that were developed to identify the severity for the T-TL and L curves from the DCM data along with the results of the prediction. The accuracy of prediction for T-TL curves was 73% (74/102), with 32/45 mild curves classified correctly (71%), 22/33 moderate curves (67%), and 20/24 severe curves (83%). The accuracy of prediction for L curves was 59% (20/34), with 7/14 mild curves classified correctly (50%), 9/12 moderate curves (75%), and 4/8 severe curves (50%). Interestingly, the results showed that 95% of T-TL curves and 90% of L curves were correctly classified when the moderate and severe groups were combined and contrasted with the mild group.

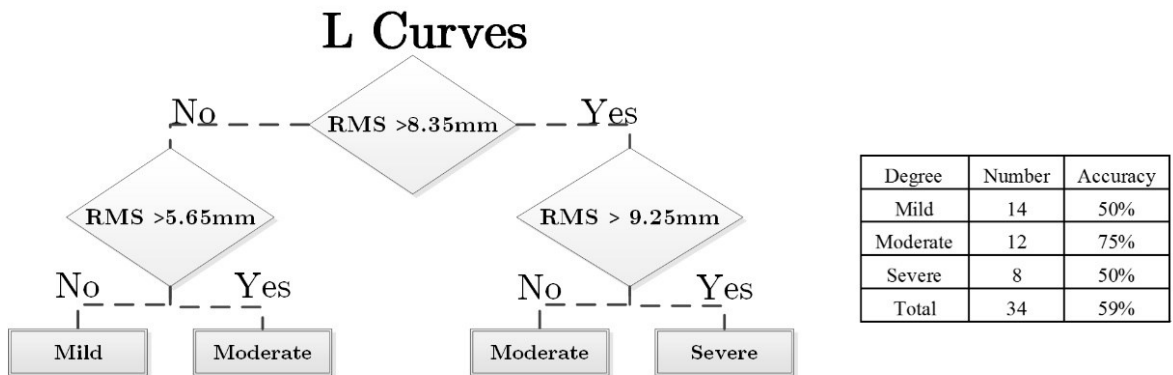
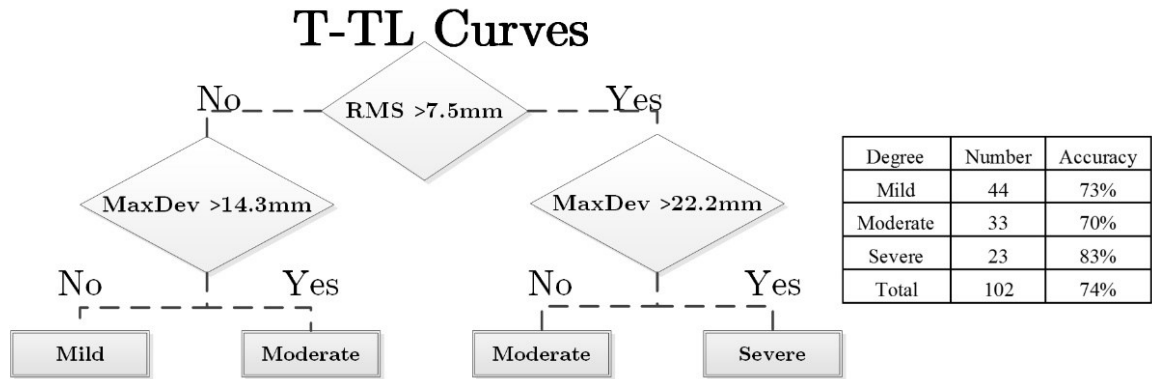


Figure 4-4- Classification trees to identify the degree of scoliosis using root mean square (RMS) and maximum deviation (MaxDev) of the colour patch for T-TL and L curves.

4.4 Discussion

This chapter presented a ST technique for identifying torso surface asymmetries associated with scoliosis and develops the correlation between the ST measures and clinically relevant radiographic parameters. DCMs were used to predict the number, direction, and location of curves, estimate the height of the apical vertebra, and predict the curve severity for a cohort of subjects with scoliosis. The developed procedure is quick and does not require manual intervention from the evaluators. This is particularly important in the fast paced environments of scoliosis clinics.

The kappa coefficient was poor when observers counted the number of curves. This is because observers often counted extra curves, mostly PT, from the DCMs. Twenty-one colour patches were identified on the shoulders (section 3), where there were no curves on the corresponding radiograph. Axial rotation of the torso or uneven shoulders may have produced colour patches in the PT region in the absence of a scoliosis curve. Less than 10% of curves were missed, all minor mild curves in patients with double scoliosis curve for which the corresponding colour patch was small. Excluding mild curves increased the average agreement to 72% and 77% for identifying the number of single and double curves. A small curve typically exhibits a small torso deformity, leading to scattered colour patches on the DCM. These patches are more difficult to identify than the clear colour patches associated with larger curves.

The direction of the curve was identified on the DCM with 100% accuracy. This indicates that this aspect of the spinal deformity translates to a torso surface deformity in a predictable manner i.e. a right curve produces an outward protrusion on the right side of the back and a left curve produces an outward protrusion on the left side of the back.

When predicting the location of the curve, T-TL curves were identified with excellent accuracy ($P\% = 92\%$), while PT and L curves were identified with 63% and 62% accuracy, respectively (Table 4-5). Excluding mild curves increased the accuracy of these predictions, particularly for PT curves. These classifications were done by novice observers with no clinical scoliosis background. We speculate that the method would be more accurate when used by experienced clinicians. Some of the curves on the boundaries, (e.g. TL), may be easier to identify for an experienced clinician with a greater understanding of the underlying anatomy. A similar classification has been reported in which 97 patients who were candidates for surgery were analyzed using the cross-sections of the torso [78]. Although both mild and moderate curves were

excluded from their analysis, only 72.2% of curves were correctly classified into three groups: major thoracic, double and triple, and lumbar major curves.

The ST measurement underestimated the vertical location of apical vertebra. The height of the MaxDev in the DCM was lower than the actual apical vertebra as indicated by the resulting prediction model and by the majority of results lying above the bisector line (Figure 4-3a, b). This relationship differs between T-TL curves and L curves, with the difference between larger for T-TL curves, where the vertebrae are connected to the ribs (Figure 4-5). The lateral deformation in the thoracic spine is transferred to the torso through the ribs, whereas in the lumbar section the vertebrae are surrounded with soft tissues which may mask a portion of the deformity particularly for small curves [47, 107]. It was found that h_r was predicted for 24 test subjects within an average of 17mm and 13mm for T-TL curves and L curves, respectively. These values are smaller than the height of one vertebra [47] in this population and therefore represent errors of prediction clinically minor in importance.

Excluding the mild curves improved the R^2 values in the regression models for both T-TL and L curves. For patients with a Cobb angle greater than 25° (where bracing is recommended) the h_{st} parameter has a significant correlation with respect to the vertical location of the apical vertebra. The location of h_{st} and pattern of colour patches in the DCM may be useful clinically for both brace design and brace adjustments.

Curve severity (mild, moderate, severe) was predicted with 73% (32/44), 70% (23/33), and 83% (20/23) accuracy for mild, moderate, and severe T-TL curves, respectively. Although 75% of moderate L curves (9/12) were correctly diagnosed (Figure 4-4), half of the mild and severe L curves were misidentified, especially when they were a part of double curves. This may be due to the small sample size for L curves, in addition to the reasons discussed earlier, or an interconnected effect of asymmetry in the T-TL region and the surface deformity in the L section. With a

double curve the prominent deviation in the upper back (section 2 or 3 Figure 4-1) dominates the asymmetry analysis. Since such a curve would be in the opposite direction as the lumbar curve in section 1, it may overshadow the relatively small deviation in the lumbar region of the DCM. Additional work is needed to include more double curves in the analysis and to study the interconnected effect of T-TL and L curves.

The ST parameters were very accurate when distinguishing moderate or severe curves from mild curves in both the T-TL (95% accuracy) and L (90% accuracy) regions. This analysis can be used when following a patient over time to identify the progression from mild scoliosis, typically requiring only observation, to moderate or severe scoliosis requiring intervention such as bracing. An increase in the curve severity identified on the DCM could be used to alert the physician of a progression so they can take required action to adjust the treatment or request an X-ray for further investigation.

The introduced asymmetry analysis demonstrated strong correlation with respect to the radiograph data in terms of direction, location, and severity of the curve. In the future, the proposed asymmetry analysis will be tested for its ability to detect $>5^\circ$ curve progression over time in patients with AIS. In the clinic, progression of 5° or more is considered progression of the deformity [108]. Previous indicators yielded at best partial results and were limited by inter and intra-observer variability [108-110].

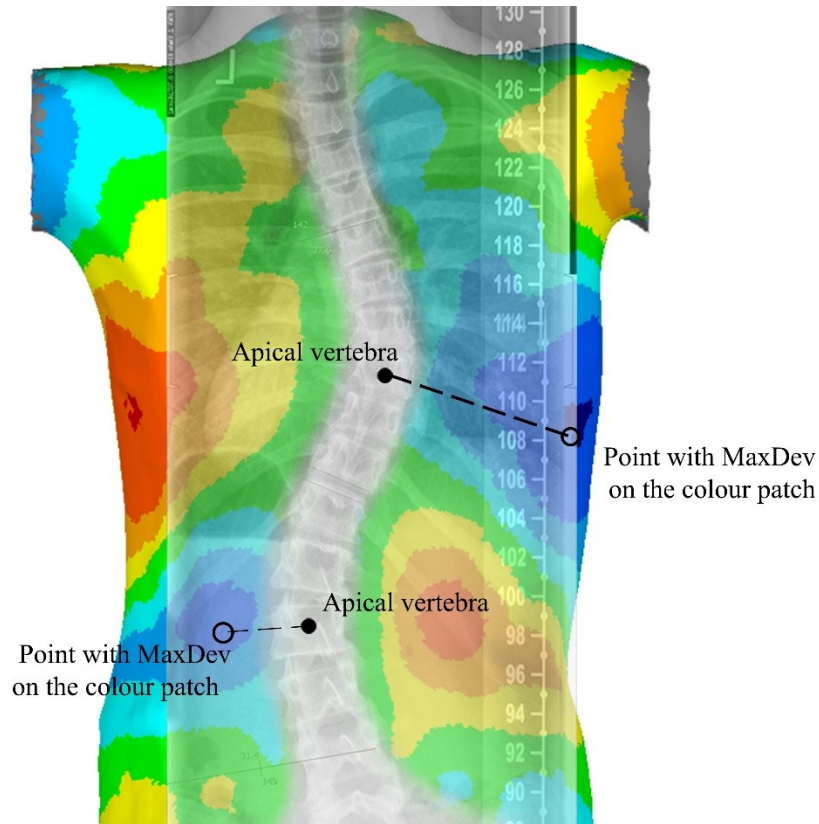


Figure 4-5- Estimated location of apical vertebra on the DCM of a patient with AIS, and exact location of the apical vertebra on the superimposed corresponding X-ray. (•): Located on the radiograph, (◦): located on the DCM.

4.5 Conclusion

Predicting the number, direction, and location of the curve may allow more informed planning of brace adjustments without exposing patients to radiation. These parameters were identified with acceptable accuracy by three novice observers who did not have any scoliosis specific training. The accuracy of the prediction of the vertical location of apical vertebra was within less than a vertebral body height for both T-TL and L curves using the DCMs.

Asymmetry of the torso associated with scoliosis results from a multivariable relationship between the torso and the spine shape, and is influenced by the alignment of the spine, ribcage, trunk rotation, body fat, morphometry and posture

[15, 89]. Previous attempts to relate torso surface geometry with the underlying spinal deformity have relied on a series of indices [47, 54, 61, 78] and have been limited in their clinical success. The spectrum of deformities associated with scoliosis cannot be fully captured by a discrete number of indices. The method presented here uses the entire torso surface and both a visual and quantitative representation of the asymmetry to better capture the torso deformity. This will enable clinicians to better predict the underlying spinal deformity from the torso surface with the aim of replacing some X-rays with non-invasive ST images. The 3D nature of the asymmetry analysis presented here can also supplement current monitoring techniques to include measures of cosmetic appearance.

The introduced parameters (h_{ST} , RMS and MaxDev) are independent of local or global coordinate-system, simple to measure, can be automatically extracted after scan acquisition, could be applied to surface geometry scanned using any ST system, and do not require surface markers placements. Predicting the vertebrae parameters from DCMs, such as the number and severity of curves, was associated with some variability for mild curves especially for the lumbar curves. However, adoption of the developed measurements may help the management of scoliosis curve by predicting the vertebrae parameters and identifying their variation.

Chapter 5 will assess the utility of the DCMs in detecting $\geq 5^\circ$ curve progression and will investigate the effectiveness of the DCMs in observing the curve progression over time.

Chapter 5

Monitoring Scoliosis¹

5.1 Introduction

High risk of progression and variable growth rate justified the use of frequent follow-up of patients with AIS until skeletal maturity [25, 111, 112]. Mild and moderate curves are monitored every 6 to 9 months to prevent further curve progression [27, 113]. Severe curves that have not yet undergone surgery are even more likely to continue progressing over time [114, 115]. Patients who had surgery may require postoperative monitoring evaluation to observe curves above and below the spinal instrumentation. Therefore, patients with AIS with different ranges of Cobb angle may receive one or two radiographs every 6 months until the end of skeletal growth [28, 29]. The X-ray dose with the associated lifetime risk of developing cancer is a problem justifying research on alternatives to the use of radiographs for monitoring the scoliosis curves [1, 81]. High correlation between the ST measurements and radiograph data motivated the researchers to take advantage of ST indices to evaluate [60, 83, 87, 102, 116-119], and monitor the internal alignments of the spine [5, 21, 27, 44, 62, 117, 120-122]. Although ST methods have been improved

¹ A version of this chapter has been submitted in The Spine Journal. Amin Komeili, Lindsey Westover, Eric Parent, Marwan El-Rich, Samer Adeeb, “Monitoring for Idiopathic Scoliosis Curve Progression Using Surface Topography Asymmetry Analysis of the Torso in Adolescents.”

significantly, they have not completely replaced radiographic assessment. Current ST methods do not evaluate the actual bone morphology and do not represent the vertebral column the way a radiograph does. However, a reliable ST method, which is able to monitor the curve progression over time and identify scoliosis curve characteristics, could reduce the number of radiographs in monitoring the scoliosis and avoid excessive ionizing radiation.

A group of ST methods only monitor specific curve types or curve magnitudes, for instance Theologis et al. [21] and Schulte et al. [27] considered only thoracic curves in their analysis. The introduction of numerous ST indices, whose physical meaning may not be readily clear to the clinicians led to the lack of agreement about the clinical value of ST methods [10, 123]. In addition, to our knowledge, few ST studies attempted to develop parameters with conceptual equivalency to radiograph parameters. Further, an accurate and easy way to implement ST technique is essential for successful non-invasive monitoring of scoliosis in patients with AIS. In this chapter the capability of the 3D markerless ST asymmetry analysis [124] to detect $\geq 5^\circ$ progression in the spinal curvature in patients with AIS over a one year follow-up interval is investigated.

5.2 Materials and Methods

5.2.1 Clinical Data

Torso scans of patients with AIS were randomly selected as described in Chapter 2. The first 100 consecutive patients who met the inclusion criteria and had the necessary data available were included in the study. The necessary data included a full torso ST scan with a corresponding out of brace X-ray at both a baseline time point and a follow-up time point within 12 ± 3 months from baseline. The X-ray and ST scans were taken on the same day.

Four patients were excluded from the analysis because their ST asymmetry colour map did not represent the scoliosis curve in the corresponding radiograph due to inaccurate measurements of Cobb angle from the radiograph or curve correction over one year, leaving 96 patients in the study. For instance, the radiograph of the second subject in Table 5-1, where thoracolumbar curve is missing in the one year follow-up, could only monitor the thoracic curve. In contrast, the corresponding ST colour map of this subject only presented an asymmetry colour patch in the thoracolumbar region. Therefore, the validity of the ST results for this subject could not be assessed and we inevitably excluded this subject from the analysis. Also, 11 individual curves from patients with double or triple curves were excluded because the surface asymmetry map did not have an area of asymmetry associated with those curves. The excluded individual curves were 10 mild curves (8 lumbar and 2 thoracic) and one moderate curve (lumbar) (Table 5-1). However the second curve in these subjects, which was the major curve in most of them, was monitored using DCMs of torso and compared to the corresponding radiograph data. All of the curves that were excluded were less than 25° except one which was the smallest in a triple curve patient with curves as large as 59° .

The final sample included 75% ($n = 72$) females and 25% ($n = 24$) males with Cobb angles between 10° - 69° . There were 32, 3, 13, 0, 42, and 6 subjects within the modified Lenke 1 through Lenke 6 curve types, respectively [125]. Data was collected from all consenting consecutive volunteers attending routine visits to the scoliosis clinic. Body mass index (BMI) was calculated for each patient using their weight in kilograms divided by their height squared in meters as measured during their clinical visit. The mean BMI for the patients was 21 (range: 13 – 34). Fifteen patients were classified as overweight, having BMI >25 . Table 5-2 shows the number and distribution of the subjects based on the location of the curve, magnitude of the

Cobb angle, and number of curve with $\geq 5^\circ$ progression. Since some of the subjects had double or triple curves, the number of curves exceeds the number of subjects.

Table 5-1- Subjects and curves that were excluded from the analysis

	Baseline Curve	Follow-up Curve	BMI	Δ Cobb $^\circ$		
				UT	T-TL	L
Excluded subjects	5R-UT ; (10L-TL)* ; 8R-L	(9L-TL) ; 7R-L	20		-1	-1
	(17R-T) ; 18L-TL	21R-T	20		4	
	(21R-T) ; 20L-TL	(15L-TL)	19		-6	
	22L-L	22R-T ; (22L-L)	21			0
Excluded curves from double or triple scoliosis curve	(11R-T) ; 10L-L	(11R-T) ; 9L-L	15		0	-1
	15L-UT ; 11R-T ; (10L-L)	15L-UT ; (12R-T) ; 12L-TL	21	0	+1	+2
	16R-T ; (13L-L)	19R-T ; 17L-L	27		+3	+4
	21L-UT ; 21R-T ; (16L-L)	21L-UT ; 18R-T ; (19L-L)	20	0	-3	+3
	19R-T ; (17L-L)	25R-T ; 24L-L	15		+6	+7
	(17R-T) ; 41L-TL	27R-T ; 48L-TL	18		+10	+7
	26R-T ; (18L-L)	22R-T ; 13L-L	20		-4	-5
	24L-UT ; 28R-T ; (22L-L)	25L-UT ; 28R-T ; 16L-L	22	+1	0	-6
	38R-TL ; (22L-L)	38R-TL ; 28L-L	17		0	+6
	35R-T ; 29L-L	21L-UT ; 30R-T ; (24L-L)	21		-5	-5
46L-UT ; 59R-T ; (34L-L)	46L-UT ; 58R-T ; 37L-L	22	0	-1	+3	

R: Right, L: Left, UT: Upper Thoracic, T: Thoracic, TL: Thoracolumbar, L: Lumbar
 (*)*: This curve did not appear in the DCM of torso, Δ Cobb $^\circ$: Curve progression,
 (-): improvement, (+) worsening.

Table 5-2- Distribution of the monitored curves based on the location of curve and Cobb angle value

	Location of Curve	Mild Cobb $<25^\circ$	Moderate $25^\circ \leq$ Cobb $<40^\circ$	Severe $40^\circ \leq$ Cobb	Total
sample (96 subjects)	T-TL	40 (7)*	33 (4)	24 (8)	97 (19)
	L	11 (1)	10 (2)	9 (4)	30 (7)

T-TL: thoracic/thoracolumbar, L: lumbar, *: Number of curves (number of curves with $\geq 5^\circ$ Cobb angle progression)

5.2.2 Surface topography

The baseline and follow-up ST scans of each individual were analyzed using the 3D markerless asymmetry analysis [124]. A macro was developed to isolate the area of asymmetry (i.e. points with $|\text{deviation}| \geq \pm 3\text{mm}$) from DCM of the whole torso to assess each scoliosis curve separately [124, 126]. The back view of two analyzed torsos with its corresponding radiograph is presented in Figure 5-1. Visual appraisal of the 96 analyzed torsos showed that the darker the DCM the larger the Cobb angle would be (Figure 5-1). Our hypothesis was that there is a direct relation between change in the asymmetry of the torso and change in the Cobb angle (ΔCobb). During AIS follow-up, the change in the maximum deviation (ΔMaxDev) of torso deformity may be a symptomatic of the ΔCobb . However, MaxDev may remain the same from the baseline to the follow-up scans and overall deviation along the torso may change. Taking into consideration the whole possible measurements profile may provide more information for tracking the ΔCobb when monitoring the scoliosis. So, in addition to ΔMaxDev , the change of the square root of mean squares (ΔRMS) of the colour patch deviations and the percentage of change for the area ($\Delta\text{A}\%$) covered by each colour patch were calculated.

5.2.3 Radiograph analysis

The corresponding baseline and follow-up radiographic Cobb angle measurements which was measured by the clinical engineer were retrieved from the clinical database to calculate the ΔCobb over the interval. All X-rays were digital and the Cobb angle was measured with the measurement tools available in the IMPAX viewing software (AGFA Healthcare, Mortsel, Belgium) that is used clinically. The reliability of the Cobb angle measurements was not investigated in this study; however, inter-observer and intra-observer reliability has been reported previously [31, 127]. A mean error of 5° has been reported in Cobb angle measurement from radiographs because the endplates, from which the Cobb angle is drawn, do not have a clear trajectory as a

single line on the radiograph [31]. To make sure that the change in Cobb angle exceeds measurement error, and consistent with accepted clinical practice, a change of $+5^\circ$ in Cobb angle was considered as the threshold to document curve progression [108, 128].

5.2.4 Statistical analysis

The classification tree technique (as explained in Section 4.2.5) from the IBM SPSS Statistics 21 [105] software was employed to determine the diagnostic accuracy of Δ RMS, Δ MaxDev and Δ A% for detecting the progression of scoliosis [129]. Patients with Δ Cobb $\geq 5^\circ$ and Δ Cobb $< 5^\circ$ were categorized in “Progression” and “Non-progression” groups, respectively.

The technique uses the selected independent variables to develop a classification tree (as explained in Section 4.2.5) that can be used to classify a given curve as “progression” or “non-progression”. Δ RMS, Δ MaxDev and Δ A% were selected as independent or predictor variables. Indeed, ST should detect all cases with progression that would require further investigations and use thresholds such that clinicians can be confident that the subjects classified as non-progression would not need immediate further investigation with a radiograph. The Classification and Regression Trees (CRT) criteria with target variable of “progression” group and maximum tree depth of 2 was selected for the classification tree, which defines the maximum number of times that the sample will be split when making the classification. The technique presented here was applied to each curve separately. Thus for a patient with a double or triple curve, each curve was analyzed for progression individually. The total number of curves analyzed was 127 (97 T-TL, 30 L). The effect of the body mass on the ability of the asymmetry analysis of the torso to detect curve progression was studied by repeating the analysis for the subset of the sample with a body mass index (BMI) < 25 which is the threshold for being

overweight at adolescence [130]. This secondary analysis tested the hypothesis that patients with more fatty tissue may have fewer ST changes over time.

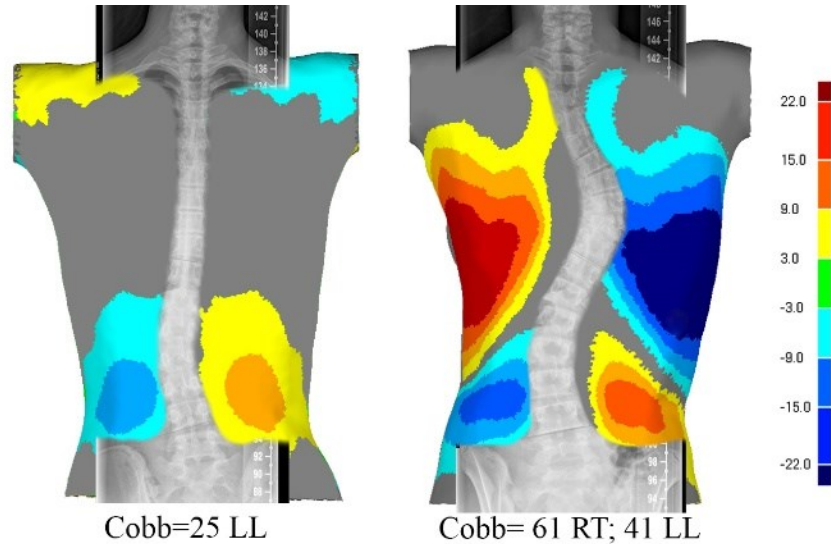


Figure 5-1- Isolated colour patch of two torsos with the corresponding radiograph. The Cobb angles was measured from the corresponding radiograph.

5.3 Results

A scatter plot of the association between the Δ RMS, Δ MaxDev and Δ A% versus the Δ Cobb is presented in Figure 5-2 for 97 T-TL and 30 L curves with identification of the cases with BMI below and above 25. Figure 5-3 shows the classification tree to classify the T-TL and L curves into “Progression” and “Non-progression” groups with the accuracy of this prediction. Based on Δ Cobb, it was found that 26 curves progressed (13 T-TL, 7 L) and 101 curves did not progress (78 T-TL, 23 L) over the interval of the study (Figure 5-3). The Δ RMS and Δ MaxDev of the colour patch were the only significant parameters to classify the T-TL curves that had progressed (Δ Cobb $\geq 5^\circ$). The Δ A% did not make a significant contribution to the model, so it was automatically dropped from the final model. The classification tree to detect T-TL curves with progression could correctly classify 13/19 (sensitivity=68.4%) of the T-TL curves that progressed and 58/78 (specificity=74.4%) of those that did not

progress. The classification tree model to detect lumbar curves with progression correctly identified 6/7 (sensitivity=85.7%) of those that progressed and 7/23 (specificity=30.4%) of the L curves that did not progress. (Figure 5-3-b)

An analysis of the classification results above showed that the majority of the misclassified curves with progression (false negative) were for subjects with BMI \geq 25. There were 5 overweight subjects with Δ Cobb \geq 5°, 4 of those were classified in “non-progression” group by the first classification tree. The subjects with BMI \geq 25 were then excluded from the analysis to investigate the effect of high BMI on the ability of ST to detect radiological curve progression. The classification tree for subjects with BMI $<$ 25 with the number of cases for each category of each decision variable, is presented in Figure 5-4. Excluding the subjects with BMI \geq 25 from the sample led to correctly classifying a similar proportion (48/67, specificity=71.6%) of curves without progression and a greater proportion (12/14, sensitivity=85.7%) of the T-TL curves with progression. Excluding the subjects with BMI \geq 25 from the sample led to correctly classifying a similar proportion (7/20, specificity=35.0%) of L curves with no progression and an improved proportion (6/6, sensitivity 100%) of L curves with progression.

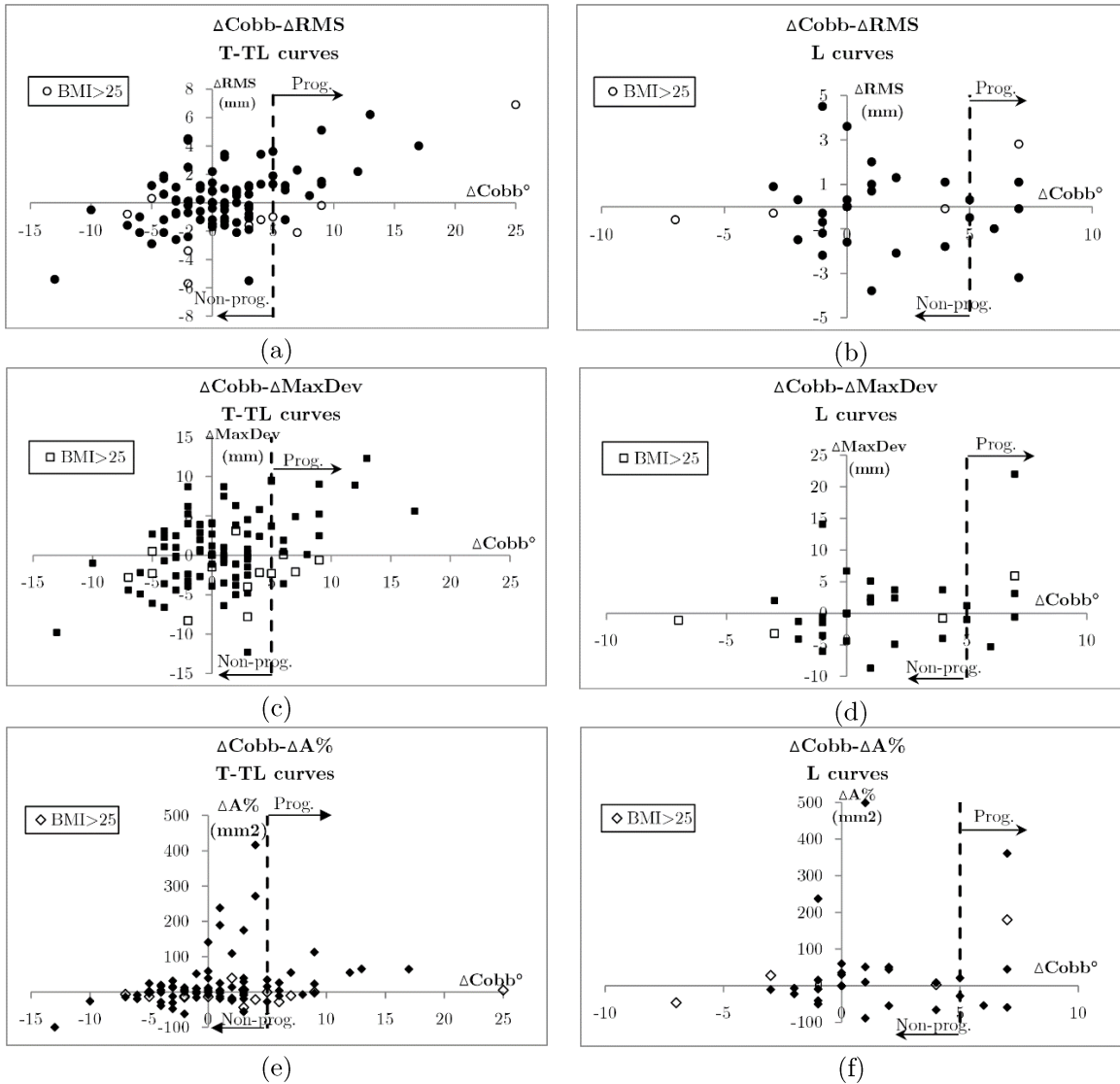


Figure 5-2- Variation of ΔRMS , ΔMaxDev and $\Delta\text{A}\%$ versus ΔCobb for 97 T-TL and 30 L curves during 12 ± 3 months follow-up. Dashed line represents the boundary between progression and non-progression based on the radiograph.

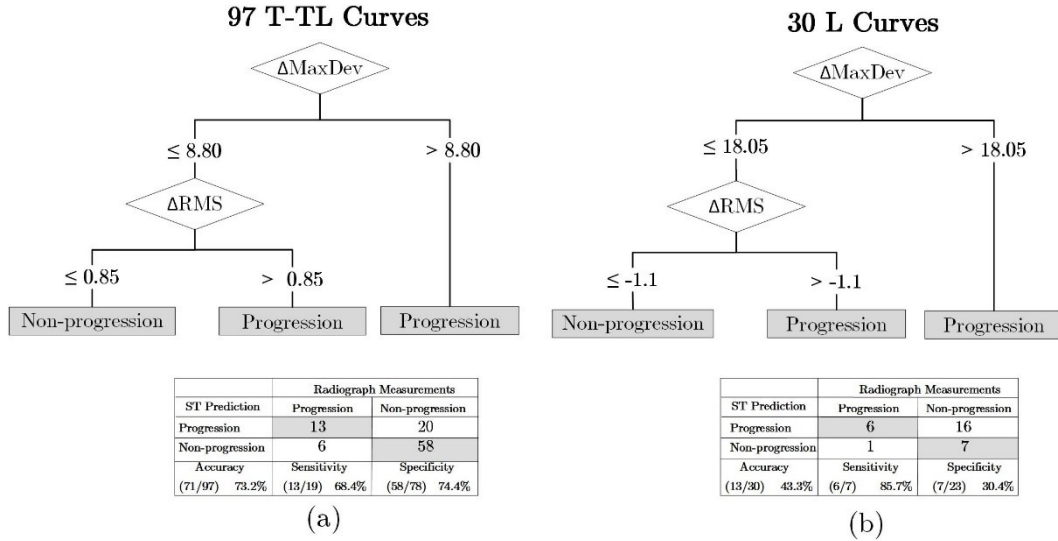


Figure 5-3- Classification tree to detect curve progression $\geq 5^\circ$ using change of root mean square (Δ RMS) and change of maximum deviation (Δ MaxDev) of the colour patch for thoracic\thoracolumbar (T-TL) and lumbar (L) curves.

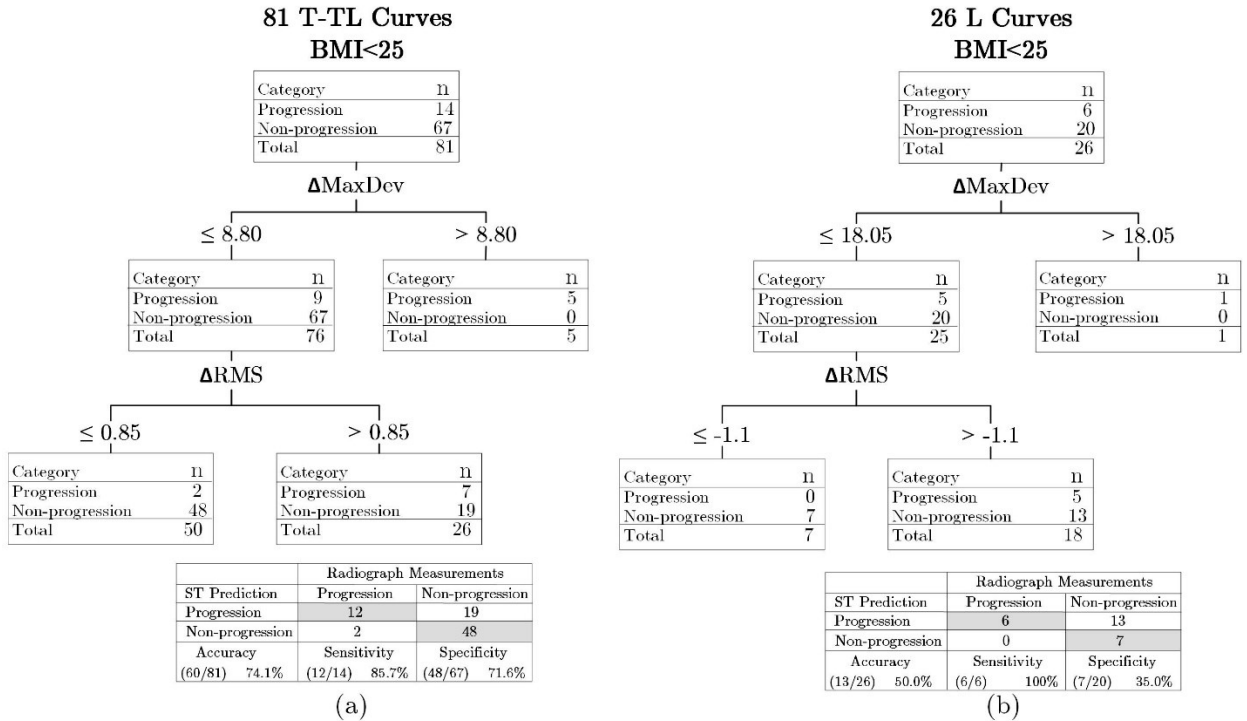


Figure 5-4- Identifying the curves with progression for patient with BMI<25 with frequency table that shows the number of cases for each category of the dependent variable.

5.4 Discussion

The variation in the torso surface asymmetry of patients with AIS over time could help identify patients with scoliosis progression exceeding 5° in thoracic and lumbar regions. The T-TL and L curves were analyzed separately. For the T-TL curves, the lateral deformation of the vertebrae in the thoracic part is transferred to the back surface through the attached ribs and causes a prominent deformation on the torso surface. In contrast, the back surface in the lumbar area is less sensitive to the vertebrae deformation due to the fact that a portion of lateral deformation in lumbar vertebrae are damped by the surrounding soft tissue [3] which justifies our analysing these regions separately.

Of the three ST parameters (ΔRMS , ΔMaxDev , $\Delta\text{A}\%$) extracted from the deviation colour map of the torso two (ΔRMS , ΔMaxDev) proved useful to predict patients with and without at least a 5° progression in the Cobb angle during a 12 ± 3 month follow-up period. Investigating the results showed that there were 9 subjects with $\Delta\text{A}\% > 50$ and $\Delta\text{Cobb} < 5^\circ$ (Figure 5-2). The correlation of $\Delta\text{A}\%$ and ΔCobb was insignificant ($R^2 = 0.016$) which led to the exclusion of $\Delta\text{A}\%$ in the classification tree for both T-TL and L curves. One explanation could be that during the follow-up period the torso growth in patients with AIS overcomes the effect of ΔCobb in the variation of the colour patch area. In addition, the radiograph of some patients who showed noticeable increase in $\Delta\text{A}\%$ but $\Delta\text{Cobb} < 5^\circ$ showed remarkable axial rotation in the vertebral column which could be the reason for the increase in ΔA . The latter observation warrants further investigation of the ability of ST parameters to detect rotation changes in patients with AIS.

The model summary table provides broad information about the specifications used to build the model and the resulting classification. Excluding the subjects with $\text{BMI} \geq 25$ led to identifying 12/14 (85.7%) and 6/6 (100%) of T-TL and L curves with progression, respectively, (Figure 5-4); indicating that as hypothesized

the method is highly sensitive to changes. This is an advantage of the classification tree, since in clinical application it is more desirable to not miss progressive curves. The goal of ST monitoring is to achieve high confidence in detecting the cases without curve progression in order to prevent exposure to unnecessary additional X-rays and reduce radiation dose. Our classification tree analysis was conducted to minimize the risk of missing curves with progression by maximizing the sensitivity for detecting the curves with progression, i.e. only 2/14 (14%) T-TL curves with progression and 0/6 (0%) of the L curves with progression were misclassified for subject with BMI<25. The classification table does, however, reveal one potential limitation of the classification tree: 19/26 (73.1%) L curves were diagnosed as having progression, however only 6/26 (23.1%) L curves had progressed which means that the model could filter only small number of the curves without progression (7/20). Our technique demonstrated that when our classification tree predicts that a patient with BMI<25 did not have curve progression using ST data there is a probability over 90% that no radiographic progression has occurred. This is clinically important and warrants a validation study to confirm if the high negative predictive value of this classification tree model can be replicated in a sample of new patients. If the negative predictive value remains as good, it may be possible to safely recommend that patients classified in the non-progression group on the basis of their ST data may avoid a radiograph at that visit.

Indeed, when the model suggested non-progression, 96% (48/50) of the T-TL curves and 100% (7/7) did not have radiological progression. This prediction value is clinically important although not perfect. The model identified correctly only 48/81 T-TL curves with no progression during the follow-up and failed to detect only 2/14 curves with progression. Although 6/6 (100%) L curves with progression were detected using the DCM of torso, due to small number of analyzed L curves, no conclusion can yet be drawn about the efficiency of the method in capturing the L

curves with progression. Further, only 7 of 13 L curves without progression were correctly identified as having no progression suggesting that it may be possible to further improve the model.

One limitation of the method is that approximately 25% of lumbar mild curves in patients with double or triple scoliosis did not appear in the DCM of the torso. Investigating the DCMs of patients listed in Table 5-1 showed that the effect of the spine curvature on external deformities in patients with double or triple scoliosis curves, especially for mild curves, tends to “balance out” between the thoracic and lumbar regions. Nevertheless, the DCM of the torso could help avoid radiographs in 85% of patients with AIS whose DCM represents all the curves observed in a baseline radiograph.

The indices extracted from our 3D markerless asymmetry analysis have some privileges over most previous shape-based indicators[15, 55, 57, 58]: our developed indices are intuitive and related to the deviation of the spine from symmetry; proposed asymmetry analysis of the full torso preserves the information of the torso and reduces the effect of posture on the torso indices [131]; they are intuitive and related to the deviation of the spine from symmetry; our proposed asymmetry analysis of the full torso preserves the information of the whole torso; the proposed asymmetry measurement method does not rely on manually placed markers and thereby eliminates the measurement variation associated with error in marker placements; not relying on marker placements also facilitates the implementation of the method in the clinic. In addition, our asymmetry analysis can be used with any ST imaging system that is able to generate a 3D model of the torso surface and is independent of coordinate system.

5.5 Conclusion

Results from this study showed that the technique is robust and clinically relevant and can be used to monitor the progression of thoracic, thoracolumbar, and lumbar scoliosis curves. Because results showed that the ability of our asymmetry analysis is better in larger curves we recommended to use the DCMs of torso for the patients with at least one previous radiograph to ensure the monitoring of all curves. We suggest a necessary radiograph if the ST asymmetry analysis classified a patient to “progression” group. The effect of body fat was also found to be significant and the method might require a different classification tree for this group of patients with higher BMI. The method could reduce 43% of radiograph acquisition by correctly identifying both minor and major curves of 41/96 patients with non-progression. Upper thoracic curves were not examined in the present study because the external appearance of the upper torso is mainly affected by axial rotation of torso and posture of the patient at the time of scanning rather than lateral deformation of the vertebrae.

Chapter 6

Mapping the Torso Deformities to the Spinal deformities

6.1 Introduction

Since prescribed medical treatment often depends more on the rate of progression than the severity of the curve [94], the patients with AIS are monitored with a series of X-ray acquisitions. As mentioned earlier in Chapter 5, in clinical applications, X-ray radiation is considered invasive and thus the frequency of its application should be minimized. The work described in this chapter aims to develop a simulation tool to predict the spinal shape from ST data for calculating the associated change in the Cobb angle. More specifically, the objective is to provide the mathematical formulation for the spinal shape in the follow-up visit, so that, as a first step, the change of Cobb angle could be predicted using fewer radiographs.

We used surface curvature analysis which is an intrinsic shape property of the surface to express the spine shape. Curvature is a local invariant, i.e. results are independent of the patient's position in space. Even though curvature is calculated easily for a curve, a computer evaluation of the surface measurement is required when we deal with surface curvature.

In this chapter the vertebrae curve of patient with AIS in the follow-up visit is predicted using the mapping technique. To do so, a mapping function is assumed between the two plane curves; one represents the median furrow midline and the other represents the vertebrae curve in the baseline radiograph scan. In classical solid mechanics the deformation of an object under applied loads is obtained by minimizing the energy of deformation. Similarly, the one-to-one mapping function between the two curves can be obtained by minimizing the “difference of curvatures” and the extension/compression between the two objects.

6.2 Material and Methods

6.2.1 Surface Curvature Analysis

The geometry of the back of the torso was described using the points recorded by laser scanners. Using the Geomagic software [92], the point object was converted to a triangle mesh employing the “Wrap” command. Points or regions of high curvature, e.g. grooves, tips, and humps are particular characteristics regarding torso shape. These characteristics can be reliably determined using curvature analysis.

Torso surface is a 2D entity in 3D space, so two curvatures in two independent directions are required for a complete description of the local shape. It can be proven that for smooth (differentiable) surfaces there are two mutually orthogonal directions on the surface, for which the curvatures are extreme. These particular curvatures are called principal curvatures κ_1 and κ_2 . For analytical surfaces, principal curvatures and their corresponding directions are defined as the eigenvalues and eigenvectors of the following matrix [96]:

$$\begin{bmatrix} L - \kappa E & M - \kappa F \\ M - \kappa F & N - \kappa G \end{bmatrix} \quad (6-1)$$

From Eq. (6-1), principal curvatures can be derived using the following single quadratic equation:

$$(EG - F^2)\kappa^2 - (EN + GL - 2FM)\kappa + (LN - M^2) = 0 \quad (6-2)$$

Where, E, F and G are the coefficient of the first fundamental form and L, M, and N are the coefficient of second fundamental form [96]. The mean and Gaussian curvatures are two additional measures of curvatures which are given by:

$$\begin{aligned} K &= \kappa_1 \times \kappa_2 \\ H &= \frac{\kappa_1 + \kappa_2}{2} \end{aligned} \quad (6-3)$$

Such a method can be used in our application to visually delineate the median furrow midline of the torso. In case of photogrammetric surface measurements, the surface is sampled at a finite number of discrete points. Consequently, a least-squares quadratic patch to the local neighbourhood of a vertex was interpolated in order to employ the formulae of Eq.(6-2) and (6-3). The Gaussian, mean, and principal curvatures were calculated and illustrated at each vertex on the back torso in the form of a contour map. There was a clear contrast between the median furrow midline and other regions of the torso when contours of minimum principal curvature were plotted.

The back view of the torso was aligned with the corresponding radiograph using the edge of shoulders and PSIS. The median furrow midline of the torso was identified by marking at least 20 points on the contours of torso curvature from bottom to top as shown in Figure 6-2. A parametric Fourier series in the form of Eq.(6-4) with a maximum of nine elements was interpolated in order to analytically present the median furrow midline.

$$\begin{aligned} y = g(t) &= a_0 + \sum_{i=1}^n a_i \cos\left(\frac{2\pi}{T} b_i t\right) + \sum_{i=1}^n c_i \sin\left(\frac{2\pi}{T} d_i t\right) \\ x &= t \quad t \in [t_{min}, t_{max}] \end{aligned} \quad (6-4)$$

where $a_i, b_i, c_i,$ and d_i are constants of Fourier series and t is the parametric variable of the median furrow midline equation. From the corresponding radiograph, the vertebra body centre was marked using the cross section of the diagonal lines of

vertebra body as shown in Figure 6-4. A similar Fourier series as described in Eq.(6-5) was fitted to analytically present the vertebrae curve in the radiograph.

$$Y = h(T) = A_0 + \sum_{i=1}^n A_i \cos\left(\frac{2\pi}{T} B_i X\right) + \sum_{i=1}^n C_i \sin\left(\frac{2\pi}{T} D_i X\right) \quad (6-5)$$

$$X = T \quad T \in [T_{min}, T_{max}]$$

where A_i, B_i, C_i, D_i are constants of Fourier series, $i = 1 \rightarrow n$, and T is the parametric variable of the vertebrae curve equation.

6.2.2 Mapping Technique

A third order polynomial function was defined as the mapping function between median furrow midline and vertebrae curve as:

$$T = \alpha_0 + \alpha_1 t + \alpha_2 t^2 + \alpha_3 t^3 \quad (6-6)$$

where $\alpha_0, \alpha_1, \alpha_2, \alpha_3$ are unknown constants to be defined using the boundary conditions of Eq.(6-7) and minimizing the optimization function. One could consider other formats for the mapping function such as a sinusoidal function. The third order polynomial function was selected in this study in order to simplify the equations and improve the processing time. The accuracy of the third order mapping function will be investigated for plane curves in Section 6.3.2. The boundary conditions of Eq.(6-7) map the start and end points of the median furrow midline to the corresponding start and end points of the vertebrae curve. The optimization function developed in this study minimizes the curvature difference between the points on curve and their corresponding mapped points on the other curve. It also tends to produce strain uniformity through the domain of analysis similar to what happens during the growth of live organs. In this thesis plane curves were used to represent the medina furrow midline and vertebra curve, however the mapping technique could be extended to use general curves in space. The following discusses the criteria the mapping is based on.

$$y(t_{min}) = Y(T_{min}) \quad (6-7)$$

$$y(t_{max}) = Y(T_{Max})$$

a) Uniformity

By uniformity we mean that a uniform extension/compression is considered between the two curves (i.e. median furrow midline and vertebra curve). An extension/compression takes place when a segment of median furrow midline is mapped to a segment of vertebrae curve with longer/shorter length. Figure 6-1 shows a non-uniform and uniform mapping between two curves. The change of length, i.e. $ds-dS$, specifies the magnitude of compression/extension of a segment during the deformation. So, the integral in Eq.(6-8) sums up the square of the magnitude of compression/extension formed by a mapping function. To understand the concept of uniformity, it may be perceived from the $S_{uniformity}$ in Eq.(6-8) that in order to make this function as small as possible the change of the length ($ds-dS$) at segments should be as uniform as possible. So the conclusion can be drawn that minimizing the “strain” is a “smoothing” process for the deformation. This criteria tends to predict a uniformly growing/shrinking pattern. In a way, this appears plausible, since in a living organs, such as bone, if any part grows much faster than others the whole body may look out of the original shape. Minimizing the integration of the square of “strain” over the interval of interest, results in maximum uniformity. The optimization function to be minimized is

$$S_{uniformity} = \int_{a_0}^{a_n} (ds - dS)^2 = \int_{a_0}^{a_n} \left(\sqrt{x'^2 + y'^2} - \sqrt{\dot{X}^2 + \dot{Y}^2} \frac{dT}{dt} \right)^2 dt \quad (6-8)$$

where (') and (·) refer to the derivative with respect to parametric parameters t and T , respectively. The unknown coefficients $\alpha_0, \alpha_1, \alpha_2, \alpha_3$ of mapping function $T = f(t)$ are obtained by minimizing the above optimization function.

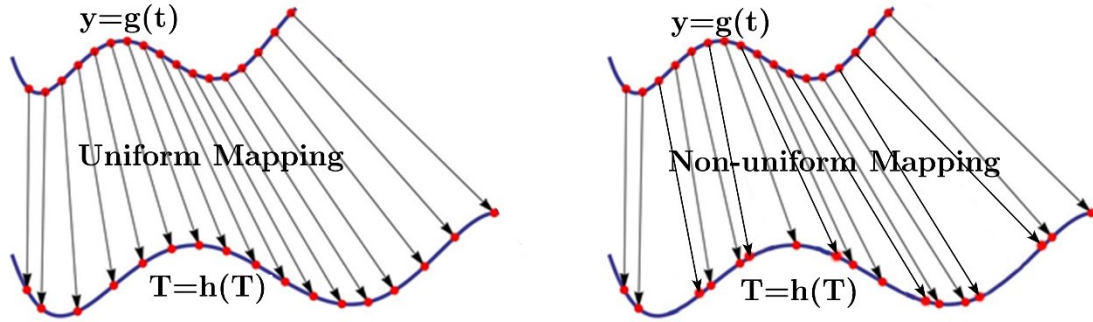


Figure 6-1- Uniform mapping versus non-uniform mapping between two plane curves

b) Curvature

It is also possible to avoid large bending during the mapping of two objects. In the one-dimensional case, this can be accomplished by minimizing the curvature all over the interval. For parametric plane curves Cartesian coordinate such as Eq.(6-4), the curvature is calculated as

$$\kappa = \frac{x'y'' - y'x''}{(x'^2 + y'^2)^{3/2}} \quad (6-9)$$

where prime (') refer to the derivative with respect to parametric parameter t . The optimization function which minimizes the difference of square of curvatures between two curves would be:

$$S_{curvature} = \int_{a_0}^{a_n} (d\kappa_1 - d\kappa_2)^2 = \int_{a_0}^{a_n} \left(\frac{x'y'' - y'x''}{(x'^2 + y'^2)^{3/2}} - \frac{\dot{X}\ddot{Y} - \dot{Y}\ddot{X}}{(\dot{X}^2 + \dot{Y}^2)^{3/2}} \frac{dT}{dt} \right)^2 dt \quad (6-10)$$

The original idea behind this function is that, the spots where large changes emerge in shapes should be mapped accordingly. For instance, in corners the sudden changes in shape of tissues, such as the end of bones, are expected to be mapped. This point of view is also easy to understand. As experience often shows, some marks on special spots of the body are likely to stay where they were after a long period of time. These spots include fingertips and other ends of the body, furrow on wrists and elbows, or the ends of bones.

c) Combination of Uniformity and Curvature

The above criteria may not be quite capable of reflecting the real situation. The minimization of strain tends to predict a uniformly distributed deformation; while the minimization of the curvature tends to predict a “concentrated” deformation. The combination of these two contradictory criteria comes out as

$$S_{Comb} = C_1 \times S_{curvature} + (1 - C_1) S_{uniformity} \quad 0 \leq C_1 \leq 1 \quad (6-11)$$

where, C_1 is the weight factor for particular units. The extra term added into the integrand increases the complexity of the analytical solution, which brings up the need for a faster and more accurate numerical solution.

In this thesis S_{Comb} function was used to obtain the unknown constants of the mapping function, by which both the curvature and extension/compression effects were considered in the mapping function. To validate the accuracy of the suggested mapping technique, it was compared to the exact mapping between the two predetermined curves in Section 6.3.2.

6.2.3 Monitoring the Worsening and Progression of Scoliosis Curve

The application of the mapping function, formulated in Section 6.2.2, in the scoliosis context is described in this section. The curvature analysis was conducted on both the baseline and follow-up ST torso scans of 100 patients. The specifications of subject selection criteria was described in Section 4.2.1. Figure 6-2 illustrates one example of the back view screenshot of curvature contours. The baseline radiograph of patients were aligned with the back view of the analyzed torso using the edge of shoulders and PSIS (see Figure 6-2). The median furrow midlines in both baseline and follow-up scans, which were shown in yellow or red in the minimum principal curvature contours of the torso, were manually marked on 20 distributed locations. In order to get a more accurate interpolation the observer made sure that the start point, end point, and point with maximum lateral deviation of median furrow midline

were marked. A Fourier series was interpolated to the selected points in each baseline and follow-up scans in order to analytically represent the median furrow midline. The vertebra body centres of the spinal column were marked on the corresponding baseline radiograph, and a Fourier series was interpolated in order to analytically represent the baseline vertebrae curve. The left configuration in Figure 6-2 shows the interpolated Fourier series of median furrow midline (black curve) in a baseline ST scan along with the interpolated Fourier series of vertebrae curve in the corresponding radiograph (yellow curve). The mapping function for each individual, which maps the interpolated median furrow midline curve to the interpolated vertebrae curve, was calculated utilizing the mapping technique described in Section 6.2.2. The vectors of the mapping function for one of the subjects are shown in Figure 6-2. This set of mapping vectors was employed on the follow-up ST scan to deform the follow-up median furrow midline and construct the predicted follow-up vertebrae curve (dashed line in Figure 6-2).

The roots of the second derivative of the vertebra curve equation in the baseline scan were calculated to locate the points of inflection. The tangent lines at these roots were drawn and the angle between the tangents was measured. This angle was named the pseudo Cobb angle (PCA) as shown in Figure 6-3. The PCA of the predicted vertebra curve in the follow-up scan were measured using the same procedure.

The classification tree analysis was conducted to design a two-category classification system. The change of the Cobb angle (ΔCobb) was labelled with nominal values of +1 and 0. The change of PCA (ΔPCA) in T-TL and L regions were examined separately as independent variables. Also, since the inclusion rate was low for the group of patients with $\text{Cobb} < 25^\circ$ (see Table 6-1), the calculation of the classification tree analysis was repeated excluding the subjects with $\text{Cobb} < 25^\circ$ with the purpose of determining the best range of the Cobb angle where the curvature

analysis and proposed mapping function techniques are most effective. Figure 6-7 shows the variation of the ΔPCA according to the variation of $\Delta Cobb$ for T-TL and L analyzed curves.

a) Monitoring the worsening ($\Delta Cobb > 0^\circ$) scoliosis curve

In this chapter the improvement and worsening of scoliosis curve, measured by the Cobb angle, was defined when respectively $\Delta Cobb \leq 0^\circ$ and $\Delta Cobb > 0^\circ$. Awareness of clinicians about the effectiveness of the ongoing treatment is one of the main advantages of determining the improvement/worsening of the scoliosis curve. The ΔPCA and $\Delta Cobb$ was calculated from baseline and follow-up scans. The accuracy of the proposed mapping technique and curvature analysis in determining the improvement/worsening of the scoliosis curve was evaluated using the classification tree analysis (see Section 4.2.5). A nominal value of 0 was assigned to the subjects with $\Delta Cobb \leq 0$, indicating the “Improved” category. A nominal value of 1 was assigned to those subjects who had $\Delta Cobb > 0^\circ$, indicating the “Worsened” category. The ΔPCA was used as an independent parameter in the classification analysis to categorize the patients into either “Improved” or “Worsened” group.

b) Monitoring the progression of scoliosis curve

Although defining the improvement/worsening of the Cobb angle is informative in scoliosis clinics, a Cobb angle variation in the range of $0-5^\circ$ is not enough by its own to persuade the clinician to change the treatment. However, a $\Delta Cobb \geq 5^\circ$ between two visits advises that the progression of scoliosis is imminent, particularly when a patient with AIS has a moderate or severe scoliosis curve [101, 114, 115]. As stated in Chapter 5; progression of a scoliosis curve, measured by the Cobb angle, was defined when $\Delta Cobb$ is $\geq 5^\circ$ over a period of 12 ± 3 months. The classification tree analysis was repeated but this time the nominal value of 0 was assigned to the subjects with $\Delta Cobb < 5^\circ$ indicating the “Non-progression” category. A nominal value of 1 was assigned to those who had $\Delta Cobb \geq 5^\circ$ indicating the “Progression” category.

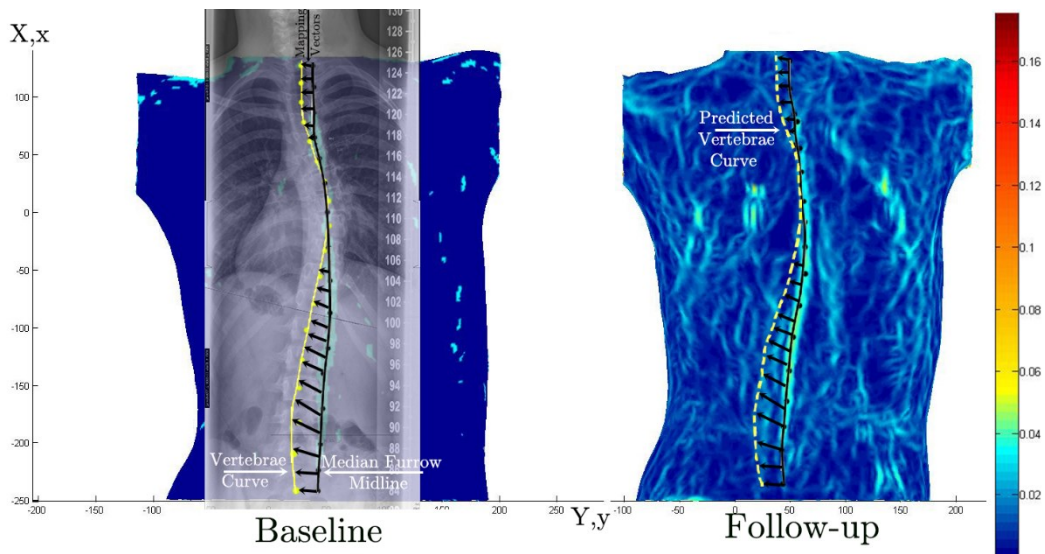


Figure 6-2- Left: curvature analysis of baseline ST scan, the black curve indicates the median furrow midline, the yellow curve connects the vertebra body centres in the corresponding radiograph, and black arrows are the mapping vectors. Right: curvature analysis of same torso after one year, the black curve indicates the median furrow midline, the dashed curve represents the predicted vertebrae curve using the mapping vectors.

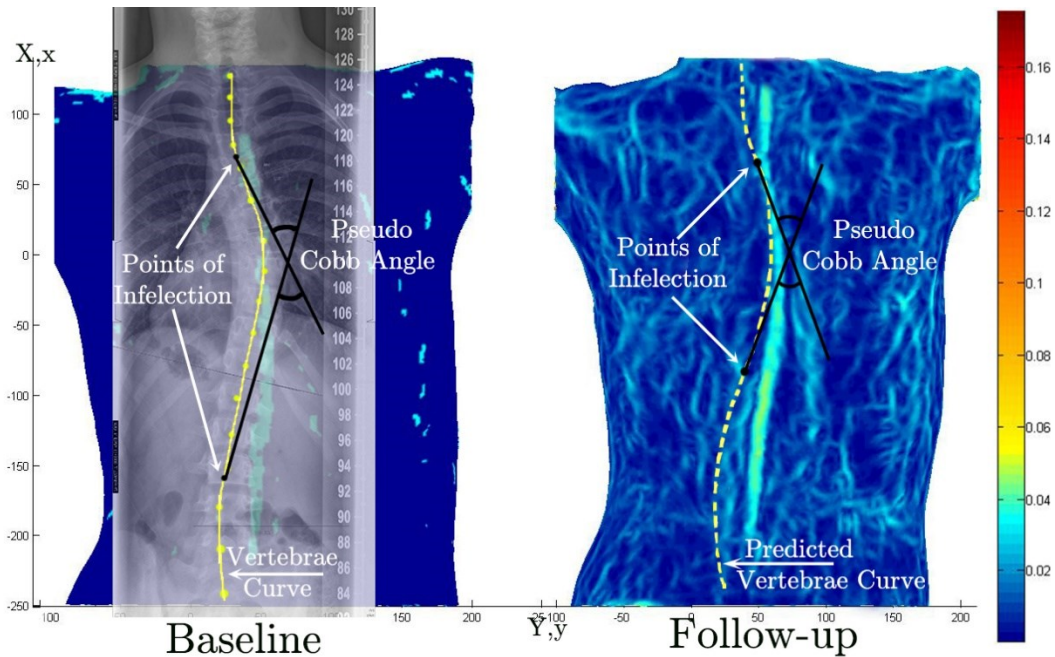


Figure 6-3- The pseudo Cobb angle (PCA) is the angle between two tangent lines extended from the points of inflection. Left: the PCA of vertebrae curve in the baseline scan. Right: the PCA of predicted vertebrae curve in the follow-up scan.

6.3 Results

6.3.1 Surface Curvature Analysis

Figure 6-4 illustrates one torso subjected to the surface curvature analysis. The elliptic and hyperbolic areas were clearly separated, i.e. median furrow midline exposed with yellow in a blue background, when the minimum curvature was plotted. Different ranges of curvature could then be distinguished by different colours. The black curve in Figure 6-4 is the Fourier series approximation of the median furrow midline. The yellow curve is the Fourier series approximation curve of the vertebrae curve. From 100 torsos subjected to the curvature analysis only 40 yielded a clear representation of the median furrow midline. In other models, the median furrow midline was imperceptible due to thick layers of fat or a flat torso at either the

thoracic or lumbar section. Figure 6-5 shows some examples where the median furrow midline could not be marked.

Table 6-1 contains the information of the Cobb angle, curve count, and BMI of the subjects that were considered in the surface curvature analysis. Those in the “excluded” row were dismissed from the mapping analysis because the observer could not place points in the median furrow midline with confidence. The percentage of included subjects, whose median furrow midline was successfully contrasted in the curvature contour of torso, is presented inside parentheses in Table 6-1. The rate of exclusion for subjects with $BMI > 25$ was 90%. Also, the torso of patients with severe scoliosis ($Cobb \geq 40^\circ$) visually presented the median furrow midline with a higher rate than mild and moderate scoliosis.

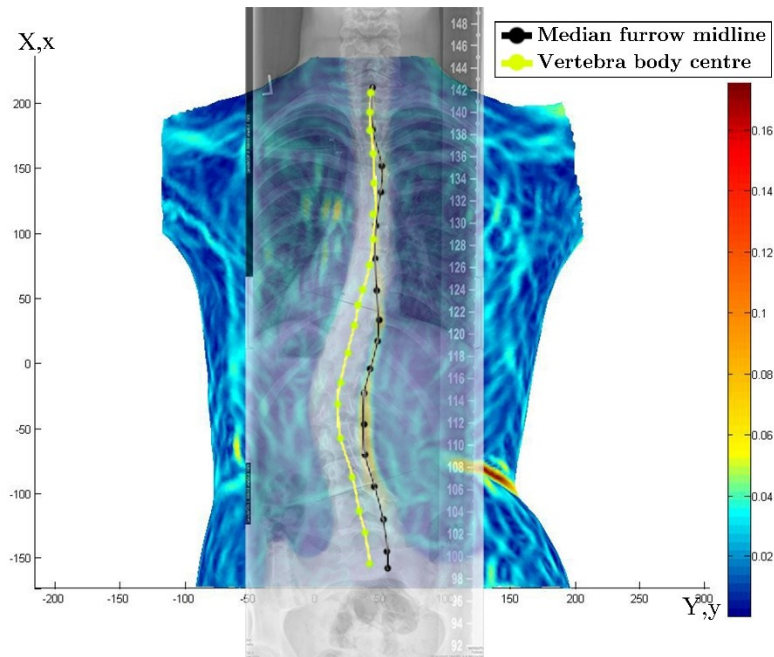


Figure 6-4- Curvature contour illustration of an analyzed torso. Black curve: Fourier series interpolation of the median furrow midline, yellow curve: Fourier series interpolation of the vertebrae body centres.

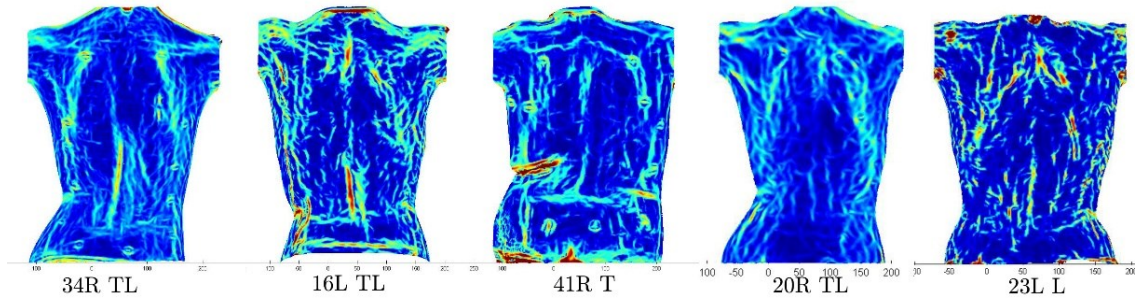


Figure 6-5-Examples of surface curvature analysis of torsos which were excluded from the investigation. The median furrow midlines were not entirely exposed in the surface curvature contour.

Table 6-1- Cobb angle, curve count, and BMI distribution of the subjects.

	Cobb<25°	25°≤Cobb<40°	Cobb≥40°	Single Curve	Double& Triple Curve	BMI<25	BMI≥25
Included	14	13	13	19	21	39	1
Excluded	31	17	12	26	34	51	9
Total	45 (30%)*	30 (43%)	25 (52%)	45 (42%)	55 (38%)	90 (43%)	10 (10%)

*: Percentage of “Included”.

6.3.2 Validation of the Mapping Function

Our validation of the mapping function technique consists of the following. A cosine curve was considered as curve 1 with the parametric equation of:

$$\begin{cases} x = t + \frac{\pi}{3} \\ y = \cos 2 \left(t + \frac{\pi}{3} \right) \end{cases} \quad -\frac{\pi}{3} \leq t \leq \frac{\pi}{3} \quad (6-12)$$

The second curve, named curve 2, was constructed by deforming curve 1 using the following deformation: uniform compression in x-direction followed by a 45° counter clockwise rotation. The left plot in Figure 6-6 depicts the resultant curves used for the validation. A mapping function was considered as described in Eq.(6-13), which is the exact mapping function, to obtain the parametric equation of curve 2. Substituting Eq.(6-13) in Eq.(6-12) and employing the assumed deformation the equation of second curve was derived as shown in Eq.(6-14).

$$T = \tan(t) \quad -\frac{\pi}{3} \leq t \leq \frac{\pi}{3} \quad (6-13)$$

$$\begin{cases} X = \frac{\cos \frac{\pi}{4} \times (\tan^{-1} T + \frac{\pi}{3}) - \sin \frac{\pi}{4} \times \cos 2(\tan^{-1} T + \frac{\pi}{3})}{2} & -\tan(\frac{\pi}{3}) \leq T \leq \tan(\frac{\pi}{3}) \\ Y = \sin \frac{\pi}{4} \times (\tan^{-1} T + \frac{\pi}{3}) + \cos \frac{\pi}{4} \times \cos 2(\tan^{-1} T + \frac{\pi}{3}) \end{cases} \quad (6-14)$$

In order to test the accuracy of the method a third order polynomial mapping function (see Eq.(6-6)) was considered as the approximate solution with unknown constants c_1, c_2, c_3, c_4 as shown in Eq.(6-6). The approximate mapping function was calculated by minimizing the Eq.(6-11) with respect to the unknown constants. A subroutine was developed in Wolfram Mathematica 9 [93] to minimize the optimization function.

Figure 6-6 illustrates the obtained mapping vectors for the two predetermined curves Eq.(6-12) and Eq.(6-14). As it may be seen in the right plot, the approximated mapping function is close to the exact solution. This demonstrates that approximate mapping function precisely resolved both rotation and extension/compression deformations.

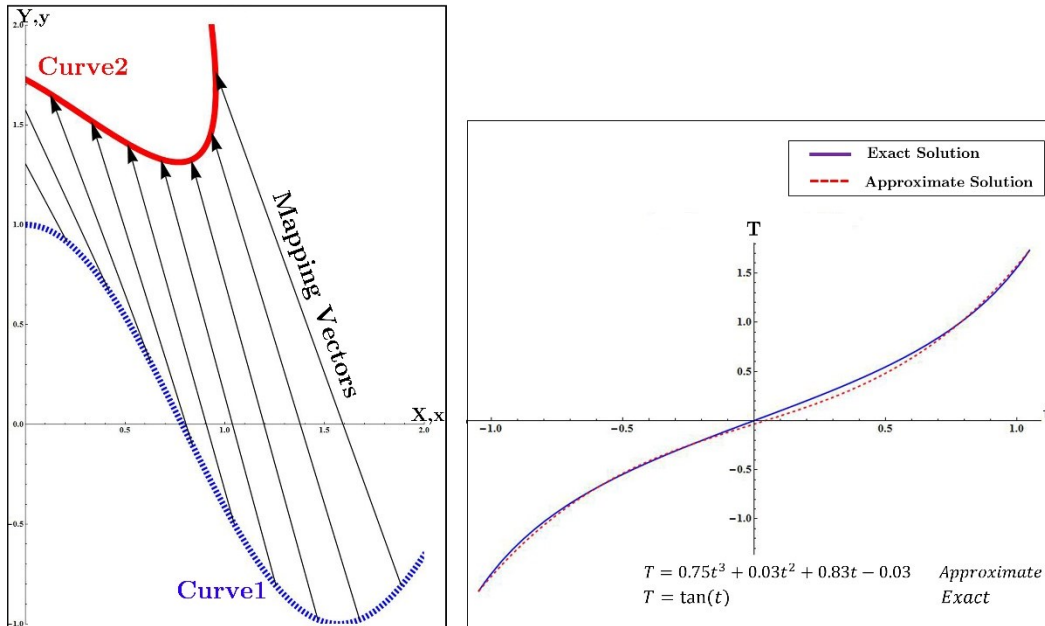


Figure 6-6- Left: The predetermined curve 1 and curve 2 are correlated through mapping vectors. Right: Comparison of exact and approximate mapping function.

6.3.3 Predicting the Change of Cobb Angle

From 40 analyzed torsos, 43 T-TL and 11 L curves were included in the follow-up analysis using the mapping technique. Figure 6-7 shows the variation of Δ PCA with respect to the variation of Δ Cobb for 43 T-TL and 11 L analyzed curves. Subjects with minor Cobb angle of $\geq 25^\circ$ are shown with filled black circle.

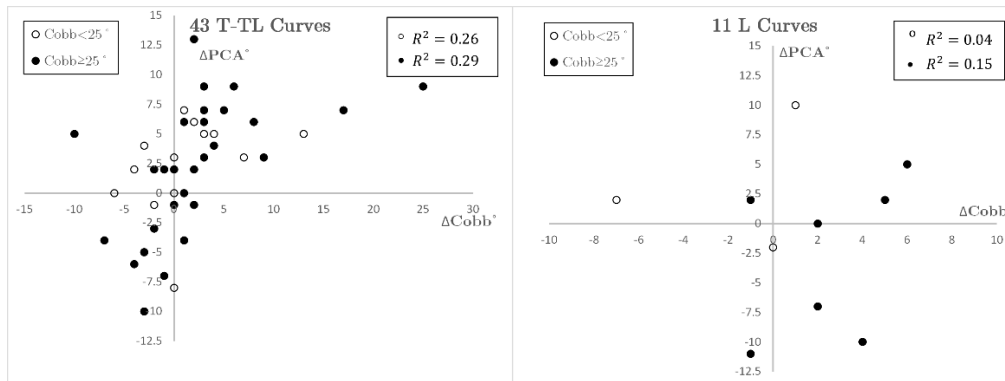


Figure 6-7- Comparing the changes of PCA (Δ PCA) with the changes of the corresponding Cobb angle (Δ Cobb).

a) Monitoring the worsening (Δ Cobb $>0^\circ$) of scoliosis curve

The classification tree obtained for 43 T-TL curves is presented in the left chart in Figure 6-8, while in the right chart classification tree of a subset of 23 T-TL curves with Cobb $>25^\circ$ is presented. In the left chart, 4 curves with Δ Cobb $>0^\circ$ were inaccurately predicted as “Improved”, which decreased the sensitivity and specificity of the classification to 82.6% and 85.0%, respectively. The accuracy of Δ PCA in predicting the Cobb angle progression was 83.7%. Excluding the T-TL curves with Cobb $<25^\circ$ did not significantly improve the accuracy. Figure 6-9 summarizes the classification of 11 L curves with the resultant accuracy, sensitivity, and specificity.

The accuracy of the prediction increased from 72.7% to 85.7% when L curves with Cobb<25° were excluded from the analysis (see right chart in Figure 6-9).

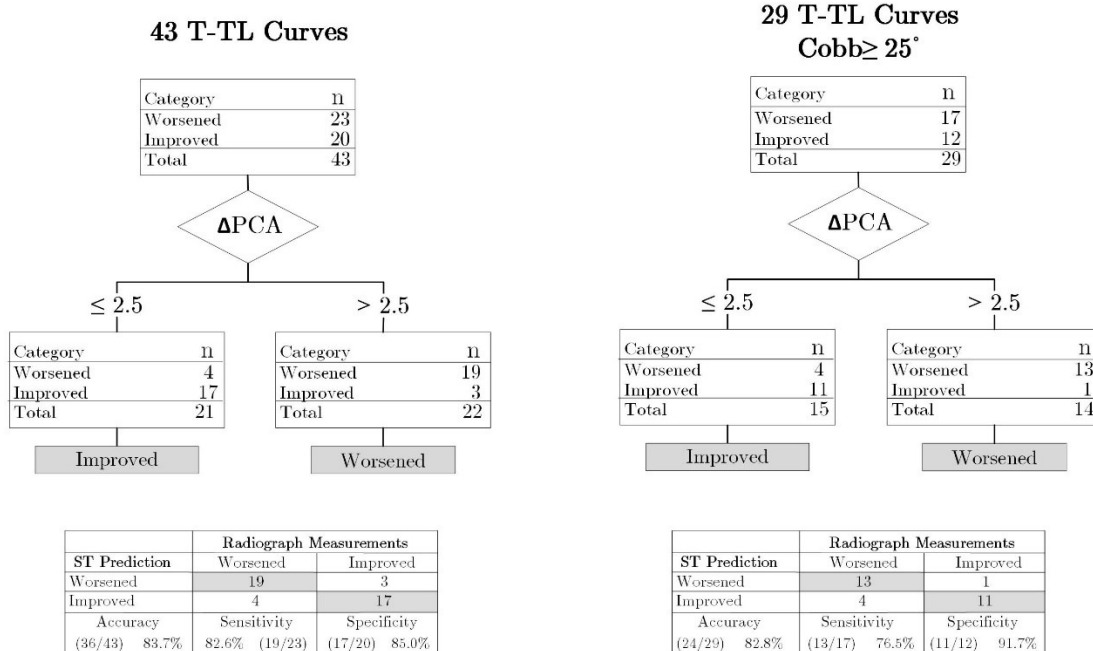


Figure 6-8- Classifying the 43 ΔPCAs in of T-TL section into “Improved” and “Worsened” groups representing ΔCobb ≤ 0° and ΔCobb > 0°, respectively.

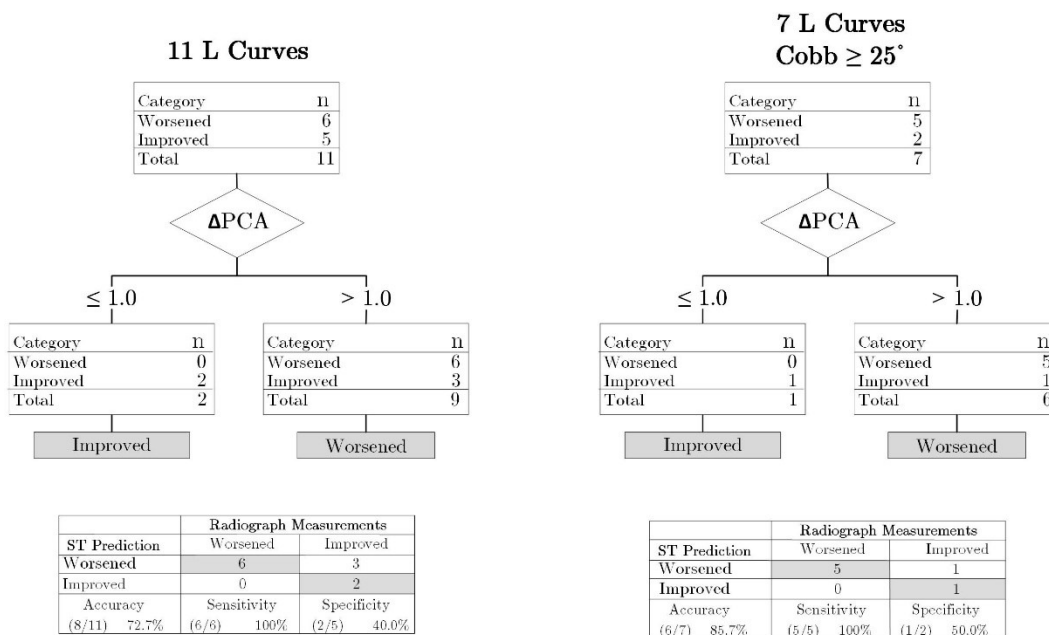


Figure 6-9- Classifying the 11 ΔPCAs in L section into “Improved” and “Worsened” groups representing ΔCobb ≤ 0° and ΔCobb > 0°, respectively.

b) Monitoring the progression ($\Delta\text{Cobb} \geq 5^\circ$) of scoliosis curve

The classification tree was performed on the 43 T-TL curves by assigning a nominal value of 1 to curves with $\Delta\text{Cobb} \geq 5^\circ$. This yielded 67.4% correct classifications with sensitivity and specificity of 100% and 60%, respectively (see Figure 6-10). Interestingly, the obtained classification system did not classify a curve with $\Delta\text{Cobb} \geq 5^\circ$ into the non-progression group. Excluding the subjects with $\text{Cobb} < 25^\circ$ from the cohort increased the accuracy of the predication to 72.4%.

From 11 analyzed L curves in the cohort only 2 progressed $\geq 5^\circ$, and the developed classification system in Figure 6-11 accurately defined them as progression. Excluding 4 L curves with $\text{Cobb} < 25^\circ$ resulted in an accuracy of 85.7% as illustrated in the right chart in Figure 6-11.

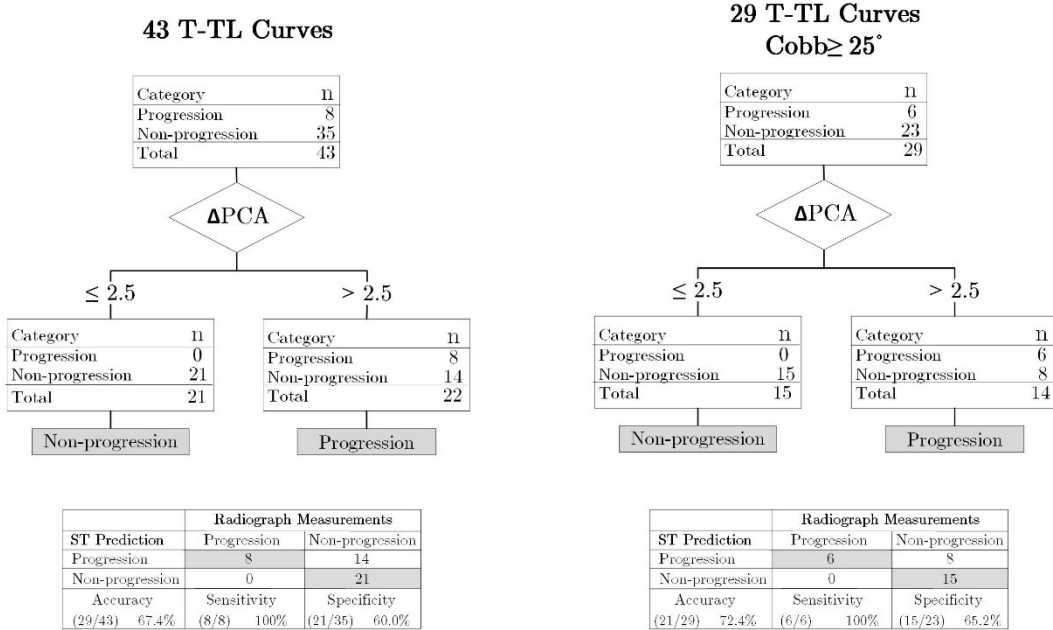


Figure 6-10- Classifying the 43 ΔPCAs in T-TL section into “Progression” and “Non-progression” groups representing ΔCobb ≥ 5° and ΔCobb < 5°, respectively.

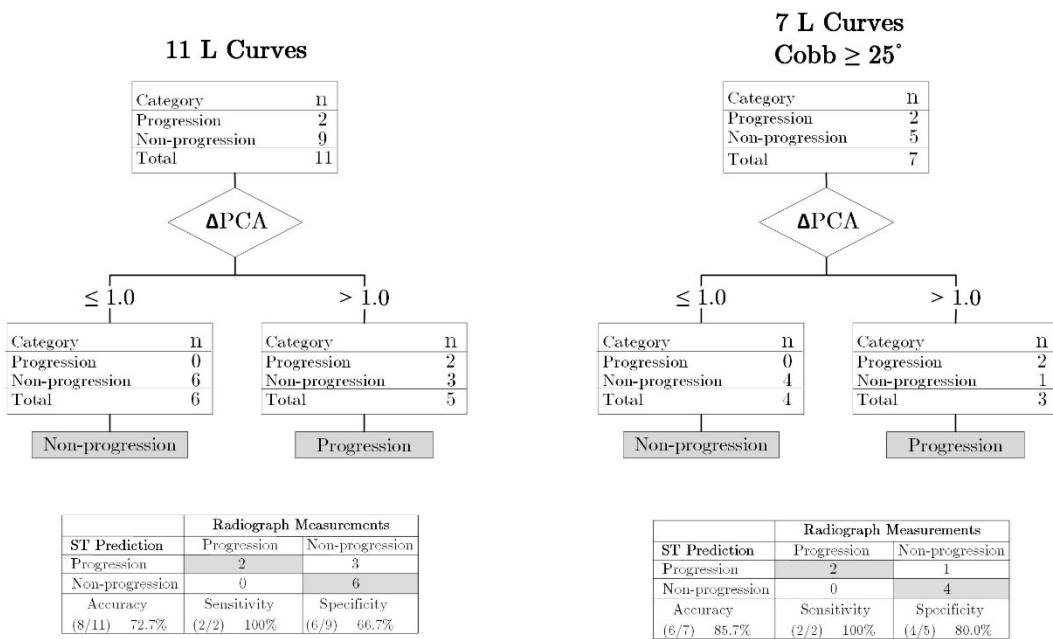


Figure 6-11- Classifying the 11 ΔPCAs in L section into “Progression” and “Non-progression” groups representing ΔCobb ≥ 5° and ΔCobb < 5°, respectively.

6.4 Discussion

From Table 6-1, it is perceived that curvature analysis is less effective on mild curves where spinous process was hardly reflected on the curvature contours of torso. In fact, it is also difficult for an expert to distinguish the median furrow midline in the torso surface of patients without palpation. Further investigation showed that, a low inclusion rate in the surface curvature analysis of mild curves also comes from the large number of patients with $BMI \geq 25$, i.e., 5 out of 31 patients with $Cobb < 25^\circ$ had $BMI > 25$. It is apparent that tracing the median furrow midline of subjects with $BMI > 25$ was the most difficult task, thus we don't recommend the surface curvature analysis for this group of patients.

The PCA introduced in this thesis is likely analogous to the computer-cobb angle introduced by Stokes et al. [64], but we measured the PCA by following the median furrow midline in the contours of torso curvature while their method involved following the line of spinous processes by palpation and marker placement.

Considering the complexity of the equations and processing time, a third order polynomial function with four unknown constants was considered as the mapping function. The mapping function was assumed to be constant over time. The running time to minimize the optimization function Eq.(6-11), using a desktop computer equipped with a core i7 CPU and 16GB of memory, was between 7 to 30 minutes depending on the number of Fourier series elements. The efficiency of the suggested mapping function could be compared to other types of equations such as logarithmic, sinusoidal, Fourier series, and etc. in terms of accuracy and processing time. For the sake of simplicity, the median furrow midline and vertebrae curve were modelled with plane curves in this study. One could use curves in 3D space and extend the concept of mapping function to 3D in order to consider out of plane deformities such as the axial rotation of the torso.

The resulted PCAs from the curvature analysis were smaller than the corresponding Cobb angles in 93% of cases. Similar behaviour was reported for computer-cobb angle in Stokes et al. study [64]. From Figure 6-7 it is observed that variation of ΔPCA and $\Delta Cobb$ are more correlated for T-TL curves than L curves. The high accuracy in the outcome of the classification tree in Figure 6-8 showed that the proposed technique properly approximated whether the Cobb angle increased or decreased over time. Further analysis of the results showed that the 4 misclassified worsened T-TL curves in Figure 6-8 had a mean Cobb angle of 46° (range 41° - 51°) with a mean $\Delta Cobb$ of $+1.5^\circ$ (range 1° - 2°). Thus, it is concluded that the classification tree might fail to observe slight worsenings of the large T-TL curves between the successive scans.

As stated before, for curve progressions less than 5° during a specified period of follow-up the physician may determine that the curve is not worsening rapidly enough and adjusting or considering a treatment may not be necessary[101]. In Figure 6-10 and Figure 6-11 the $\Delta Cobb=5^\circ$ was set as the margin of the categories in the classification tree to classify the subjects into “Progression” and “Non-progression” groups. The accuracy of the classification of 43 T-TL curves was 67.4% which shows approximately a 16% decrease compared to Figure 6-8, where using the ΔPCA 83.7% of the T-TL curves were correctly classified in the “Improved” and “Worsened” categories. Even though the classification tree in Figure 6-10 gave relatively suboptimal performance, its excellence is that it yielded to a zero false prediction in the non-progression group, i.e. false negative=0. In other words, the risk of missing a progression curve was zero when the classification tree in Figure 6-10 was used. The accuracy of the classification system in identifying the 5° progression of 11 L curves was higher than T-TL curves, however, we did not conclude a solid decision about the reliability of the developed classification due to low numbers of investigated curves. However, the current outcome of the technique is promising to

approximate the progression of scoliotic deformities of L curves, given observations on the external trunk. Further work is suggested to conduct a clinical validation of the mapping technique using a large database of scoliosis patients.

6.5 Conclusion

A particular advantage of the surface curvature analysis in the detection of median furrow midline is that the method is independent of any precautions concerning markers. Furthermore, similar to the asymmetry analysis, the curvature analysis is coordinate free. So, different positioning of the vision system between the visits does not impact the outcome. Consequently, the surface curvature analysis might be especially useful in the study of scoliosis.

We assumed that the mapping function of the baseline scan, which correlates with the median furrow midline to the vertebrae curve, and mapping function of the follow-up scans are identical. This allowed us to use the calculated mapping function from the baseline scans in order to deform the median furrow midline of the torso in the follow-up ST scan and construct the follow-up vertebrae curve. This assumption, of course, contains inaccuracy since the patients with AIS are in their most active growing period and there may be significant changes in height and weight between observations. However, more frequent observations may help to minimize the error of this assumption.

A Fourier series with a maximum of nine elements was used to analytically represent the interpolated curves. Developing a more general equation to fit a curve on the control points of the median furrow midline and vertebra body centres will improve the accuracy of the technique.

We noted that the performance of our surface curvature analysis was weaker for subjects with double or triple curves than for subjects with single curve. This aspect of the proposed system could be enhanced by adjusting the posture of the

patients at time of scanning along with an additional set of descriptors for this group of patients. One limitation of the introduced surface curvature analysis is its high exclusion rate coming from either the likely flat torso in the median furrow midline section or probably the insufficient precision of the acquisition system. This is enough to consider the use of the mapping function technique as a supplement tool in monitoring the progression of scoliosis in patients with AIS. However, a high accuracy in detecting the worsened/improved curves in Figure 6-8, and zero false prediction in determining the non-progression curves in Figure 6-10 showed that the proposed Δ PCA parameter could be an adequate supplement for other predictive parameters. The use of Δ PCA parameter combined with the Δ MaxDev and Δ RMS, which were introduced in chapter 5, appears to hold promise for the monitoring of the scoliosis curve. Further work in this direction will improve the performance of the proposed mapping function.

The mapping function yielded promising results on the training samples. However, it may end up with a different estimation accuracy on a new set of samples. As future work, one can validate the functionality of the proposed mapping technique on a larger data set.

Chapter 7

Summary and Conclusion

7.1 Conclusion

7.1.1 3D Markerless Asymmetry Analysis

This study proposed a new 3D ST analysis of the torso deformities which eliminated the marker placing step in the management of scoliosis. In this study, four VIVID 910 3D laser scanners (KONICA MINOLTA Sensing Inc.) were used to record the coordinate of the torso, however any acquisition system which is able to record the coordinate of the torso could be used to reconstruct the torso model. The proposed asymmetry analysis was independent of the direction and location of the origin of the coordinate system. This characteristic facilitates the application of our ST technique so that it can be used with existing ST equipment in other scoliosis clinics as long as they are able to capture the full torso coordinates. The markerless feature of the developed asymmetry analysis allows analysing the pre-obtained full torso ST scans of individuals which were captured earlier in the clinic. Therefore, our ST technique could immediately monitor patients who have had at least one full torso ST scan in their previous visits. In contrast, marker dependent methods require landmarks on specific locations to assess the asymmetry of the torso, so the previous ST scans that don't highlight the location of the necessary markers would be useless.

An appropriate spectrum for the colour map of the deviation analysis was selected to assist in distinguishing the categories. The best range and number of the

colours in the spectrum were selected such that it could reveal mild scoliosis, meanwhile illustrate the variations among the severely asymmetric torsos. The presented DCM of the torso is the first true 3D illustration of the torso asymmetry which considers the entire torso information while other ST methods employ a limited number of markers as the representative of the entire torso. The asymmetry of the torso was calculated globally, i.e. the asymmetry of the breast affects the calculation; however, local deformities can be isolated for local assessments and further investigations. The visual representation of the torso asymmetry in the DCMs facilitates patients' understanding of the interaction between treatment and asymmetry of the torso and may motivates them to complete the treatment.

In addition, the application of the proposed asymmetry analysis is not limited specifically to scoliosis. Investigation of the asymmetry of other body parts, such as breasts which presumed to be a symmetric organ in normal persons [132] is an example of the applicability of the suggested method in other practices.

7.1.2 Classification System

This study highlighted the need to have a classification system for torso deformities to provide appropriate information to clinicians and help them select the best treatment option. Three broad classification groups subdivided into a total of six subgroups were identified among the asymmetry maps (Appendix A). The classification system categorized the asymmetry patterns of the torso surface based on the location and number of the asymmetries. The high reliability rate of the classification system demonstrated the repeatability of the method. The mean kappa coefficient for the intra- and inter-observer reliability of four observers who classified 46 subjects with AIS in three broad groups were 0.85 and 0.62, indicating excellent and good reliability, respectively (Table 3-4). While the reliability tests demonstrated that the method is repeatable, comparing the 15 one year follow-up ST scans with their corresponding baseline scans showed that the method potentially could

document the progression of the scoliosis curve. The kappa coefficient and percentage of agreement were 0.70 (range: 0.56 to 0.84) and 0.71 (range: 0.29 to 0.82), respectively, when five observers classified 30 models from the 15 pairs of the torso models (baseline and one year follow-up) (Table 3-7). The source of discrepancies during the process of visual categorization was the distinction of the subgroup A1 from B1 and subgroup A2 from B2. This incongruity was likely because one or more colour patches of asymmetry were ignored in section 1 in some trials and counted in others (Section 3.4).

7.1.3 Measurements

The reliability study of the classification indicated that the DCM of torso derived from the asymmetry analysis was reliable within reasonable limits. We therefore proceeded to use the DCM of the torso and associated asymmetry indices in an attempt to relate surface and spinal deformity. After considering several torso asymmetry indices two indices of torso asymmetry, MaxDev and RMS, were selected to correlate the torso asymmetry to the spine curvature. The selected indices were measured from the DCM of the torso without manual intervention so the reliability of the indices was already satisfied. The visual appraising of the DCM determined the number and direction of the spine curvature. In simple words, the number of colour patches through the height of torso corresponded to the number of scoliosis curves. The direction of the blue patch, which represents the protruded area of the torso, corresponded to the direction of the scoliosis curve. This is an exclusive feature of the DCM which simplified the task of interpreting the outcomes of the ST technique. A tangible result will be more useful and applicable for clinicians. Three novice observers determined the number and location of the scoliosis curve from the DCM of 100 patients' torsos. When observers determined the number of scoliosis curve with Cobb>25° the average percentage of agreement, between observers' identification and radiograph measurement, was 72%, 77%, and 0% for single(19), double(22), and

triple(1) curves, respectively (Table 4-5). Investigating the reason of the inconsistency in identifying the triple curves showed that small scattered colour patches on the proximal thoracic of DCM, which could be due to axial rotation of the torso or inclined posture of the patient at the time of scanning, were counted as an extra curve by some observers. The observers determined the direction of curve with 100% agreement when a scoliosis curve was present.

The location of the apical vertebra, which is an important factor to determine the location of the pressure pads for in-brace correction, was predicted using the linear regression analysis for T-TL and L curves. The location of the point with MaxDev (h_{st}) in the DCM of the 100 torsos correlated well to the location of the apical vertebra (h_r) in the corresponding radiograph with $R^2 = 0.78$ and $R^2 = 0.51$ for T-TL and L curves, respectively. Better correlations with $R^2 = 0.83$ and $R^2 = 0.61$ were achieved when only curves with Cobb $> 25^\circ$ were considered (Figure 4-3). The validity of the obtained regression lines was examined by predicting the location of apical vertebra in 24 validation sample subjects which resulted in $R^2 = 0.89$ and $R^2 = 0.58$ for T-TL and L curves, respectively. As regression line equations denote in Figure 4-3, the location of apical vertebra was underestimated, likely because the lateral deformation of the vertebrae transferred to the torso surface through inclined ribs. The estimation of location of the apical vertebra was accurate within ± 1 vertebral level in all cases with an average difference of $\pm 17\text{mm}$ and $\pm 13\text{mm}$ for T-TL curves and L curves, respectively.

The underlying spinal curvature was relatively localized compared to the asymmetry of the torso surface, likely due to compensatory effects such as trunk rotation, body fat, ribcage and morphometry [15, 89]. Hence, the accuracy of the Cobb angle estimation from the DCMs is still insufficient to support the belief that ST could be a reliable replacement for radiographic Cobb measurements. Despite this limitation, the magnitude of the Cobb angle was estimated in the three ranges of

Cobb $<25^\circ$, $25^\circ \leq$ Cobb $<40^\circ$, and $40^\circ \leq$ Cobb representing mild, moderate, and severe scoliosis. The MaxDev and RMS of the colour patch were selected as independent variables and the corresponding Cobb angles from the radiographs were selected as dependent variable in the classification tree analysis (see Section4.2.5). Using a classification tree with a depth of 2 we could classify the magnitude of the Cobb angle for T-TL curves into mild, moderate, and severe groups with the average accuracy of 74%. As expected the average accuracy of the Cobb angle prediction for L curves was lower. Investigating the results showed that the inconsistency in classifying the L curves occurred mostly in patients with double scoliosis curves. We reported that the interconnected effect of asymmetry in the T-TL region on the surface deformity of the L region might be the reason for getting a lower accuracy in prediction of the Cobb angle in the L region. Surprisingly, the classification tree is strongly accurate in distinguishing $>25^\circ$ (moderate or severe) curves from the $<25^\circ$ curves in both T-TL (95% accuracy) and L (90% accuracy) curves. With this level of accuracy, requesting extra X-rays to determine whether a mild curve corresponds to a different level of severity or not, is deemed unnecessary.

Overall, we have presented an original assessment method using a 3D markerless ST as a reference modality. The indices derived from the DCM of the torso such as MaxDev, RMS, PCA, and h_{ST} expressed strong correlation to the radiographic measurements, encouraging their use in attempting to identify whether curve progression has occurred between consecutive visits of patient to the scoliosis clinic. This correlation was likely attributable to the use of full torso dataset rather than presenting the torso attributes with a limited number of landmarks. The high correlation between the ST indices and scoliotic spinal deformity may also be useful in the design and evaluation of braces in the management of scoliosis.

7.1.4 Curve Monitoring

The high degree of correlation between ST indices and radiograph data was a promising finding and suggested that this relation is not merely coincidental and encouraged the use of developed ST indices in monitoring the scoliosis curve over time. The results of the prediction of the number and location of scoliosis curve in Table 4-5 indicated that the DCM of the torso might not represent corresponding colour patches on the torso surface especially when a scoliosis curve with a Cobb $<25^{\circ}$ exists. In order to ensure all scoliosis curves are being monitored we recommended the method for study of individual curve progression when a baseline X-ray was available. The baseline and follow-up of both ST and radiograph scans of 96 patients with AIS were considered to investigate the ability of the method in identifying the curves with at least 5° progression. The follow-up scans used in this study were taken 12 ± 3 month after the first scan. The scoliosis curves in the dataset were subdivided in to thoracic/thoracolumbar and lumbar groups in order to optimize the Δ Cobb estimation. Several plausible ST parameters were examined, such as $\Delta A\%$, Δ MaxDev, Δ RMS and etc., to predict the change of the Cobb angle. However, since the Cobb angle is the clinicians' single gold standard for the radiographic assessment of scoliosis, we were interested in reducing the number of topographic indices as much as possible by eliminating the redundant indices that poorly correlated to the change of the Cobb angle. Only Δ MaxDev and Δ RMS indices of the colour patch were found to be appropriate in identifying whether the scoliosis curve progressed at least 5° or not (Figure 5-2). A classification tree analysis categorized T-TL curves in "progression" and "non-progression" groups with 73.2% accuracy (Figure 5-3). There were 19 T-TL curves with Δ Cobb $\geq 5^{\circ}$ and the classification tree could identify 13 of them with sensitivity of 68.4%. Exploring the DCM of those 6 miss-categorized patients denoted considerable fat on the torso surface. Excluding the patients with BMI >25 , which is the standard threshold of overweight, from the classification tree

analysis increased the accuracy and sensitivity to 74.1% and 85.7%, respectively. This implies that failing to identify the T-TL curves with $\Delta\text{Cobb} \geq 5^\circ$ likely resulted from the softening of asymmetry deformities by skin fat. With this level of sensitivity only 2 out of 14 T-TL curves with $\Delta\text{Cobb} \geq 5^\circ$ in patients with $\text{BMI} < 25$ were not identified as “progression”. This level of accuracy approached clinical usefulness in detection of $\geq 5^\circ$ difference in the Cobb angle.

A separate classification tree analysis was conducted for L curves using the ΔMaxDev and ΔRMS of the DCM colour patch in the lumbar section of the torso. The effect of body fat was similarly found significant in the prediction of the ΔCobb for the lumbar curves. The accuracy and sensitivity of the classification tree for the L curves in patients with $\text{BMI} < 25$ were 50% and 100%, respectively (Figure 5-4). Although the classification tree successfully identified all of the L curves with $\Delta\text{Cobb} > 5^\circ$, further investigation is required to include more L curves in the analysis. The noticeable improvement of sensitivity after excluding the subjects with $\text{BMI} > 25$ demonstrated that the high level of body fat effectively influences the change of torso asymmetry. So we proposed to study patients with $\text{BMI} > 25$ in a separate group and consider more descriptive ST parameters in the classification tree analysis.

Although the DCM of the torso represented a colour patch on the scapula area (section 3 in Figure 3-1), the indices of asymmetry analysis failed to monitor the upper thoracic curves. Several reasons were speculated such as axial rotation of the torso; i.e. since the upper torso is wider, even small axial rotation of the torso may cause significant asymmetry on the shoulders. The presence of a colour patch on section 3 of subjects whose radiographs data did not show any upper thoracic curve supports the fact that the asymmetry deformities on section 3 are formed mainly due to the axial rotation of torso rather than lateral deformation of the upper thoracic vertebrae. Also, the green scapula in the DCM of the 5 analyzed normal torsos ensured that the integrated data noise and posture of subjects do not significantly

influence the asymmetry patterns. These findings are in agreement with other ST methods, where the correlation analysis has shown a higher redundancy between the torso deviation and the axial rotational components [133]. From a clinical perspective, these results showed qualitatively that scoliosis is associated with axial rotation and asymmetric lateral deviation of the torso.

Considering the fact that patients with upper thoracic curves along with the patients with double scoliosis curves who were missing one of their curves in the DCM of the torso were considered as failure, the method could reduce 43% of radiation dose by identifying 41/96 patients with non-progression in both T-TL and L curves.

Chapter 6 proved the concepts of a technique for monitoring Cobb angle variation associated with scoliosis using a mapping function. Surface curvature analysis and mapping functions techniques were employed as an alternative tool for monitoring the scoliosis curve. The median furrow midline was followed using contours of minimum curvature on the back torso of subjects. The weakness of the surface curvature analysis was its high exclusion rate, i.e. from 100 analyzed subjects, only 40 resulted in visual representation of the complete median furrow midline. This was not far-fetched because the curvature of the torso at the median furrow midline could be smoothed by several factors such as body fat and posture. Fourier series plane curves were fitted to the median furrow midline of the analyzed torso and vertebrae body centres from the corresponding radiograph. A third order polynomial mapping function correlated these curves considering the curvature and uniformity as the criteria of the mapping. The obtained mapping function for each individual was employed to deform the median furrow midline in the follow-up scan of the torso to predict the follow-up vertebrae curve by which the pseudo Cobb angle was measured. The Δ PCA parameter was a good predictor of Δ Cobb according to the obtained accuracy in Figure 6-8 and Figure 6-10. We believe that once the Δ PCA index is

coupled with other indices such as ΔMaxDev and ΔRMS , confidence in the prediction of the ΔCobb will increase. In this study, a variety of polynomial functions with different orders were examined and finally a third order polynomial function was found to be the best assumption based on the accuracy of the resulting mapping and processing time. The format of the the mapping function could be improved by examining different types of equations for mapping function such as logarithmic and/or sinusoidal.

7.2 Future Work

Our research has shown that ST can be used to: classify scoliosis based on torso asymmetries [124], identify several scoliosis curve parameters [102], and identify non-progressive curves without the need for radiographs [134]. However, in order to fully use the power of our techniques in a clinical setting, work is still needed in four main areas.

In the first area, we need to understand how asymmetries manifest themselves in normal subjects. For example, right handed athletes may have a larger right torso compared to their left torso. Such a pattern of asymmetry is different from the scoliosis patterns observed in our previous classification. We have identified a 3mm threshold, below which asymmetries can be assumed normal [124, 135]. However, using a smaller threshold will allow us to visualize the asymmetry patterns of normal subjects. By comparing the resulting patterns of normal adolescents with those of scoliotic patients, we can gain more insight into the differences between normal and scoliotic asymmetries.

Axial rotation of the torso is one of the meaningful parameters in management of scoliosis which was not accounted for in the content of this thesis. The correlation of the axial rotation to the Cobb angle was proved in the literature [99]. In this thesis, the colour patch in section 3 of the DCM is deemed to originate from the axial rotation of the torso. However, it is not yet completely clear how axial

rotation of the torso should be evaluated from the torso DCM. Thus, future research on this topic will involve developing a technique for such evaluation.

As discussed in Section 7.1.1, the proposed asymmetry technique could be utilized to investigate the deviation of symmetric body parts such as breasts [132]. Breast asymmetry is very prevalent in scoliosis patients, its assessment and study should not be neglected. Breast asymmetry analysis could be beneficial for two reasons, first it is one of the important signs of abnormalities that a subject can identify and second, it is an important factor during the period of physical development and associated concerns with self-perceived body image. The documentation of breast asymmetry type has the potential to guide the proposal of measurements as scoliosis deformities progress. In previous studies, breast asymmetry was observed with relation to scoliosis; however, these studies did not fully examine the correlation between the two as they did not attempt to describe the overall location and pattern of the asymmetry. The primary focus of these studies was merely on the asymmetry [136] or predominantly on the volume of the breast [137-139]. In Chapter 1, our asymmetry scoliosis patterns were based on the visualization of each of the back asymmetries and breast asymmetries separately. However, we believe that there is a strong link between those asymmetries and the curve location and magnitude. In a preliminary study, we assessed breast asymmetry in 25 patients with AIS using the proposed asymmetry analysis. We proposed a breast asymmetry classification, and assessed its reliability [132]. However, we were not able to find an association between breast asymmetry classification and the Lenke curve type [76]. Our proposed classification of the breast asymmetry can be further used to develop parameters for quantifying different types of breast asymmetry. The documentation of breast asymmetry type can be useful for patients and doctors when trying to evaluate and plan for potential cosmetic and/or reconstructive surgery. In the future,

one could explore breast asymmetry as a qualitative and quantitative measure of scoliosis.

Our technique showed that torso data could be integrated into a set of clinically understandable torso asymmetry indices and that a classification tree presented with these input indices could monitor the progression of scoliosis T-TL and L curves [134]. The clinical data in this study was used as training samples to discover potentially predictive relationships and develop the predictive models such as decision trees, and mapping function. New cases are required to investigate the prediction quality of the predictive models. A concern regarding the classification tree taxonomy was the low number of L curves in the dataset. As a further improvement, more patients with lumbar scoliosis curve will be analyzed in the future to ensure that asymmetry indices in the lumbar section could accurately document the curve progression. As our dataset grows, we intend to further analyze more patients with $BMI > 25$ and develop relevant asymmetry indices in order to optimize the monitoring of scoliosis curve progression in this subgroup.

While the mapping technique proposed in this dissertation provides a guideline to future research, the outcome of our research suggest many more specific open questions and directions. So, research remains to be done on topics mapping of surface deformities to the internal deformities, such as to try generalize the mapping function in order to consider the out of plane deformations in the equation of mapped curves, and to consider a time dependent mapping function in order to simulate the growth effect.

Finally, we need to clearly identify the situations where ST can be utilized to replace unnecessary radiographs. We have shown that we are able to identify curve severity [140], curve parameters [140], and curve progression [134] with good to excellent accuracy using the techniques of this dissertation. The next challenge will be to apply ST parameters to related questions regarding the use of this method in

clinical settings that arose once it was shown that DCM of torso could be consistently related to spinal deformity. For example, how indices of the torso could be used in designing scoliosis braces, and could a 3D representation of torso asymmetry make any improvement in the rate of patients' compliance with their scoliosis techniques. In addition, our algorithms have currently been prepared by engineering students and need to be translated into automatic algorithms that clinicians can directly apply and utilize. Developing a user-friendly interface software along with the clinical trial of the technique could be the subject of future studies with the goal of diagnosing and monitoring scoliosis with nothing more than non-invasive scans of the torso surface.

Appendix A

Instruction Manual for Classification

Reliability test User Manual

General Information

The primary goal of this test is to assess the reliability of a markerless 3D surface topography method in classifying the torso asymmetry of patients with scoliosis. The torso of the patients illustrated with three main colours:

Green: represents normal torso

Blue: represents protruded area of the torso with an outward deformation.

Red: represents the intended area of the torso with an inward deformation.

The objective of this reliability test is to assess the clarity and precision of the proposed classification. In this test, participants are asked to categorize analyzed torsos into 6 categories.

Torso Sections

The height of the torso (L) is divided into 3 sections as shown in Fig.1. Section 1 cuts the torso from the PSIS and mainly contains the lumbar vertebrae. Section 2 mainly includes the thoracic/thoracolumbar vertebrae and is located between $L/3$ and $2L/3$ from the PSIS. Finally, section 3 covers the top one-third of the torso length.

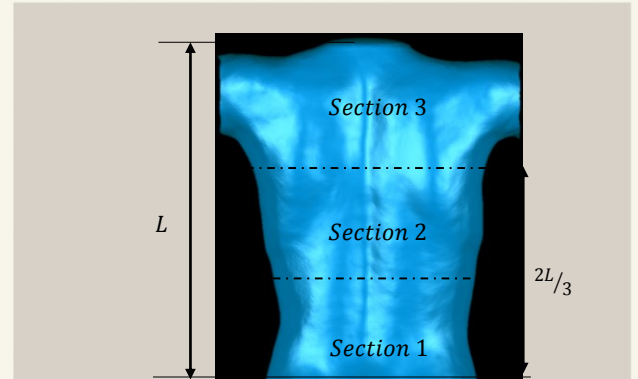


Figure 1. Definition of torso sections

Torso Classification



The asymmetry analysis expresses the torso deformities with contour colours. There are 3 main colours in the contours. The green colour indicates non-deformed regions of the torso. Therefore a completely green torso represents a normal subject whom is expected to have a fairly symmetric torso. Blue and red colours are representing an outward and inward deformation in the torso, respectively. The pair of corresponding red and blue colour is called a colour patch.

Six signatures have been developed to classify the torso deformation based on the number and location of the colour patches obtained from the deviation analysis. These signatures can be categorized into group A, B, and C with two, three, and four colour patches, respectively. Developed signatures with their descriptions are

Reliability test

User Manual

Table 7- Developed signatures of the torso with description

	Subgroup	Description of individual colour patches
Group A (2 Asymmetry patches)	A1 	First Patch: located in sections 1* and 2 with the centre of deformation close to the boundary between sections 1 and 2 representing thoracic/thoracolumbar curves. Second Patch: located in section 3 and characterizes shoulder asymmetry
	A2 	First Patch: same as subgroup A1. Second Patch: located in section 3 with the centre of the patch located close to the scapula
	A3 	First Patch: located strictly in section 1 representing lumbar curves Second Patch: located strictly in section 3 and characterizes shoulder asymmetry
Group B (3 asymmetry patches)	B1 	First Patch: located strictly in section 1 representing lumbar curves Second Patch: located in sections 1 and 2 with the centre of deformation located close to the boundary between sections 1 and 2 representing thoracic and thoracolumbar curves Third Patch: located in section 3 and characterizes shoulder asymmetry
	B2 	First and Second Patches: same as subgroup B1. Third Patch: located in section 3 with the centre of the patch located close to the scapula
Group C (4 asymmetry patches)	C1 	First, Second and Third Patches: located in and between sections 1 and 2 Fourth Patch: located strictly in section 3 and characterizes shoulder asymmetry
*Sections 1, 2 and 3 represent the bottom, middle and top thirds of the torso respectively.		
Test Description		

You are presented with front and back view of the 46 torsos subjected to the asymmetry analysis. Look at each torso and try to match them with one of the suggested signatures in Table 1. The pictures might match more than one group or even none of them. In these cases considering the location of the colour centre and ignoring the minor and scattered colour patches try to find the best class.

Terms and Conditions

- 1- Start from the first page of the booklet and continue through the last page in order.
- 2- Don't come back to the subject that you have classified already to change it.
- 3- Complete the test without taking a break.

Reliability test User Manual

Introduction to Scoliosis

Scoliosis is a medical condition associated with lateral deviation and axial rotation of the spine. On a posterior-anterior X-ray a normal spine appears straight; however a spine with scoliosis appears curved in a C or S-shape (Figure 2). Figure 3 shows several different curve patterns due to scoliosis. The severity of the curve is monitored over time to identify patients whose deformity has progressed so that treatment can be offered.

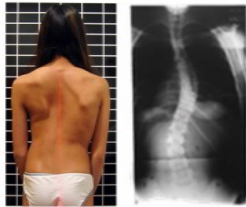


Figure 2- Asymmetric torso and X-ray of scoliosis patient

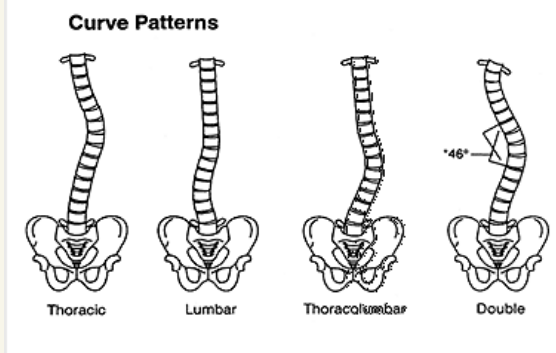


Figure 3-Different curve patterns of scoliosis

Scoliosis is also associated with an external deformity causing the patient's torso to appear asymmetric and rotated. This external deformity is often more bothersome to patients, affecting their quality of life. Surface topography can be used to assess the torso surface asymmetry. The torso of the patients with scoliosis can be classified into groups based on their "asymmetry pattern" allowing specific surface topography measurements to be developed for each group.

Classification Tips

The first step to classify a torso in this test is to count the number of curves. The pair of blue and red colours (colour patch) through the height of torso represents the number of curves. Figure 4 shows one example of counting the number of colour patches.

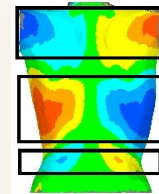


Figure 4- Counting colour patches of the torso

Counting the colour patches is confusing in some cases as illustrated in Figure 5. The following tips may help to distinguish the colour patches:

- I. Small colour patches located on the edge of the torso in section 1 are not counted (Figure 5-a), unless they have a dark blue or red colour or extended to the centre of section 1. (Figure 5-b,c,d).
- II. Small scattered colours may be due to abnormal muscle growth, so they are dismissed (Figure 5-e).
- III. Only one curve counted in the section 3, even there are more than one colours in this region. (Figure 5-f)

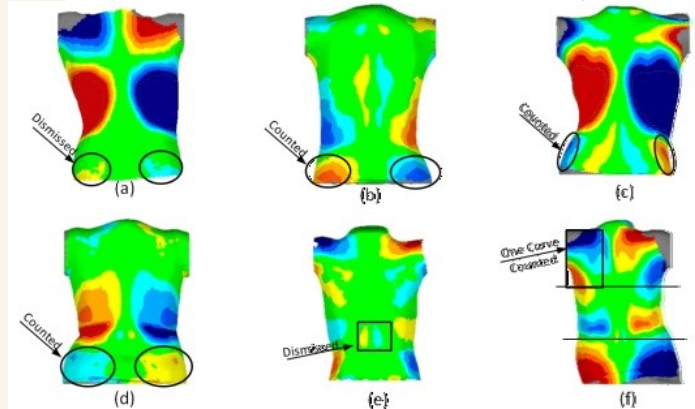


Figure 5-a) Small and mild colour patches on the edge of section 1. b&c) Severe deformation on the edge of section 1. d) Deformation extended to the centre of section 1. e) Small scattered colour patches. f) Two deformations in section 3.

Appendix B

Entropy and Information Gain

Entropy is a measure of how random a variable is. It is sometimes equated to the purity or impurity of a variable. A high entropy means that sampling is from a uniform distribution, therefore there is an equal chance of obtaining any possible value. Low entropy means that the distribution varies, it has peaks and valleys. Suppose we have a set of possible events p_1, p_2, \dots, p_n . The entropy of a set of events is expressed as [106]:

$$H(x) = H(p_1, p_2, \dots, p_n) = - \sum_{i=1}^n p_i \log_2 p_i \quad (\text{B } 1)$$

where p_i is the probability of the i th outcome. The logarithm base 2 makes the units of the entropy bits. The gini index measures the impurity score, and is obtained as follows:

$$H_{\text{gini}}(x) = \sum_{i=1}^n p_i(1 - p_i) \quad (\text{B } 2)$$

Let's consider the distribution of pseudo ΔRMS and $\Delta MaxDev$ of 18 patients with scoliosis as shown in Figure B 1. We aim to categorize patients into progression (red points) and non-progression (blue points) groups using classification tree. As Figure B 1 illustrates, there are 10 blue and 8 red events, therefore the probability of outcome blue and red are 10/18 and 8/18, respectively. The entropy of the distribution is

$$H(x) = H(p_1, p_2) = - \sum_{i=1}^n p_i \log_2 p_i = \quad (\text{B } 3)$$

$$-\left(\frac{10}{18}\log_2\frac{10}{18} + \frac{8}{18}\log_2\frac{8}{18}\right) = 0.99 \text{ bits}$$

Now let's consider one split for the ΔRMS attribute, where the data points are divided into those points that fall at $\Delta RMS < 0.5$ (subset 1), and those points that falls at $\Delta RMS \geq 0.5$ (subset 2) as shown in Figure B 2. These are the subsets that we would split into at the next level of the tree as illustrated in Figure B 3. In subset 1 there are 10 blue and 3 red points. So the probability of the outcome red and blue in subset 1 would be 10/13 and 3/13, respectively. Subset 2 encompass only 5 red points, so the distribution is deterministic and the probability of the outcome red and blue in subset 2 would be 1 and 0, respectively. Hence, the entropy of subset 1 and subset 2 are respectively

$$\begin{aligned} H_{sub1}(x) = H(p_1, p_2) &= - \sum_{i=1}^2 p_i \log_2 p_i = \\ &= -\left(\frac{10}{13}\log_2\frac{10}{13} + \frac{3}{13}\log_2\frac{3}{13}\right) = 0.78 \text{ bits} \end{aligned} \tag{B 4}$$

$$\begin{aligned} H_{sub2}(x) = H(p_2) &= - \sum_{i=1}^1 p_i \log_2 p_i = \\ &= -\left(\frac{5}{5}\log_2\frac{5}{5}\right) = 0 \text{ bits} \end{aligned} \tag{B 5}$$

Considering the number of data points in each subset, the fraction of the subset 1 and subset 2 would be 13/18 and 5/18, respectively. The information gain (IG) parameter is calculated as the weighted difference of entropies in each branch. We calculate the probability that we go down to the subset 1 (which is 13/18) times the difference of entropies in subset 1 (which is 0.99-0.77). We add to it the probability that we go down to subset 2 (which is 5/18) times the difference of entropies on subset 2 (which is 0.99-0). Thus, the IG is expressed as

$$IG = \frac{13}{18} \times (0.99 - 0.77) + \frac{5}{18} \times (0.99 - 0) = 0.43 \text{ bits} \tag{B 6}$$

A classic representation of IG is

$$IG = H(x) - H(x, y) \tag{B 7}$$

$$= \sum p(s,c) \times \log \left[\frac{p(s,c)}{p(s)} p(c) \right] = H(x) - \sum p(s,c) \times \log \frac{p(s)}{p(c)}$$

Where s is the split variable (left or right) and c is the class variable (in this case blue or red).

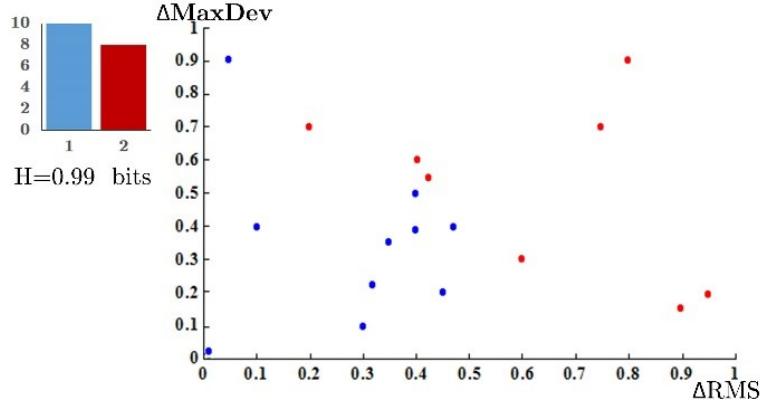


Figure B 1- Distribution of pseudo ΔRMS and $\Delta MaxDev$ of 18 patients with scoliosis.

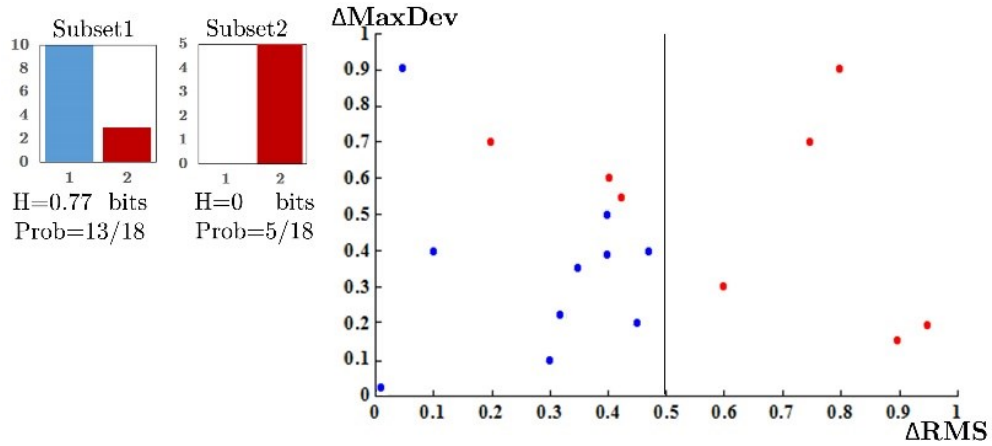


Figure B 2- Splitting the data points using decision rule of $\Delta RMS < 0.5$, and corresponding entropies at each subset.

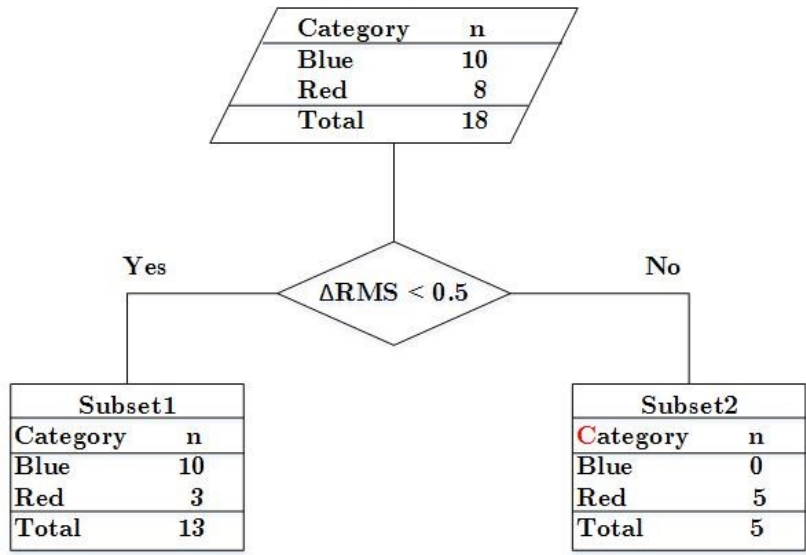


Figure B 3- Classification tree representation of the Figure B 2.

References

References

- [1] A. R. Levy, M. S. Goldberg, N. E. Mayo, J. A. Hanley and B. Poitras, "Reducing the lifetime risk of cancer from spinal radiographs among people with adolescent idiopathic scoliosis," *Spine (Phila Pa. 1976)*, vol. 21, pp. 1540-7; discussion 1548, Jul 1, 1996.
- [2] R. A. Dickson, "Spinal deformity--adolescent idiopathic scoliosis. Nonoperative treatment," *Spine (Phila Pa. 1976)*, vol. 24, pp. 2601-2606, Dec 15, 1999.
- [3] J. G. Thometz, R. Lamdan, X. C. Liu and R. Lyon, "Relationship between Quantec measurement and Cobb angle in patients with idiopathic scoliosis," *J. Pediatr. Orthop.*, vol. 20, pp. 512-516, Jul-Aug, 2000.
- [4] Y. Yoshino, M. Tsukiji and H. Takasaki, "Moiré topography by means of a grating hologram," *Appl. Opt.*, vol. 15, pp. 2414-2417, 10/01, 1976.
- [5] A. R. Turner-Smith, J. D. Harris, G. R. Houghton and R. J. Jefferson, "A method for analysis of back shape in scoliosis," *J. Biomech.*, vol. 21, pp. 497-509, 1988.
- [6] S. A. Sakka, S. Macindoe and M. H. Mehta, "Correlation of the quantec scanner measurements with X-ray measurements in scoliosis authors", in *Studies in Health Technology and Informatics, Volume 37: Research into Spinal Deformities 1* Anonymous pp. 313-317.
- [7] J. Thometz, X. C. Liu and G. F. Harris, "Computerized evaluation of the surface measurement of kyphosis and lordosis in idiopathic scoliosis," in *Engineering in Medicine and Biology Society, 1998. Proceedings of the 20th Annual International Conference of the IEEE*, 1998, pp. 2507-2508 vol.5.
- [8] D. K. Tessakov and A. S. Naumovich, "Diagnostic value of video rasterstereography of the spine," in *Research into Spinal Deformities 1.*, Sevastik JS, Ed. Amsterdam: IOS Press, 1997, pp. 277-278.
- [9] V. W. Lin and C. M. Bono, "Spinal cord medicine, principles and practice," in , V. W. Lin, D. D. Cardenas, N. C. Cutter, F. S. Frost, M. C. Hammond, L. B. Lindblom,

I. Perakash, R. Waters and R. M. Woolsey, Eds. New York: Demos Medical Publishing, 2003, .

[10] G. C. Lam, D. L. Hill, L. H. Le, J. V. Raso and E. H. Lou, "Vertebral rotation measurement: a summary and comparison of common radiographic and CT methods," *Scoliosis*, vol. 3, pp. 16-7161-3-16, Nov 2, 2008.

[11] E. J. Rogala, D. S. Drummond and J. Gurr, "Scoliosis: incidence and natural history. A prospective epidemiological study," *The Journal of Bone & Joint Surgery*, vol. 60, pp. 173-176, 03/01, 1978.

[12] M. Emrani, R. Kirdeikis, P. Igwe, D. Hill and S. Adeeb, "Surface reconstruction of torsos with and without scoliosis," *J. Biomech.*, vol. 42, pp. 2200-2204, Sep 18, 2009.

[13] M. Tones, N. Moss and D. W. Polly Jr, "A review of quality of life and psychosocial issues in scoliosis," *Spine (Phila Pa. 1976)*, vol. 31, pp. 3027-3038, Dec 15, 2006.

[14] D. L. Hill, D. C. Berg, V. J. Raso, E. Lou, N. G. Durdle, J. K. Mahood and M. J. Moreau, "Evaluation of a laser scanner for surface topography," *Stud. Health Technol. Inform.*, vol. 88, pp. 90-94, 2002.

[15] C. J. Goldberg, M. Kaliszer, D. P. Moore, E. E. Fogarty and F. E. Dowling, "Surface topography, Cobb angles, and cosmetic change in scoliosis," *Spine (Phila Pa. 1976)*, vol. 26, pp. E55-63, Feb 15, 2001.

[16] Mayfield Clinic & Spine Institute. (2013). *Anatomy of the spine*. Available: <http://www.mayfieldclinic.com/PE-AnatSpine.htm#.Uoe5KoY1N8k>.

[17] B. V. Reamy and J. B. Slakey, "Adolescent idiopathic scoliosis: review and current concepts," *Am. Fam. Physician*, vol. 64, pp. 111-116, Jul 1, 2001.

[18] R. J. Cobb, "Outline for study of scoliosis." *American Academy of Orthopaedic Surgeons*, pp. 261-275, 1948.

[19] H. Wu, P. Poncet, J. Harder, F. Cheriet, H. Labelle, R. F. Zernicke and J. L. Ronsky, "PREDICTION OF SCOLIOSIS PROGRESSION IN TIME SERIES USING ARTIFICIAL INTELLIGENCE TECHNIQUES," *Journal of Bone & Joint Surgery, British Volume*, vol. 90-B, pp. 100-101, March 01, 2008.

- [20] D. G. Little, K. M. Song, D. Katz and J. A. Herring, "Relationship of peak height velocity to other maturity indicators in idiopathic scoliosis in girls," *J. Bone Joint Surg. Am.*, vol. 82, pp. 685-693, May, 2000.
- [21] T. N. Theologis, J. C. Fairbank, A. R. Turner-Smith and T. Pantazopoulos, "Early detection of progression in adolescent idiopathic scoliosis by measurement of changes in back shape with the Integrated Shape Imaging System scanner," *Spine (Phila Pa. 1976)*, vol. 22, pp. 1223-7; discussion 1228, Jun 1, 1997.
- [22] C. J. Goldberg, F. E. Dowling, J. E. Hall and J. B. Emans, "A statistical comparison between natural history of idiopathic scoliosis and brace treatment in skeletally immature adolescent girls," *Spine (Phila Pa. 1976)*, vol. 18, pp. 902-908, Jun 1, 1993.
- [23] M. S. Goldberg, N. E. Mayo, B. Poitras, S. Scott and J. Hanley, "The Ste-Justine Adolescent Idiopathic Scoliosis Cohort Study. Part II: Perception of health, self and body image, and participation in physical activities," *Spine (Phila Pa. 1976)*, vol. 19, pp. 1562-1572, Jul 15, 1994.
- [24] B. S. Richards, R. M. Bernstein, C. R. D'Amato and G. H. Thompson, "Standardization of criteria for adolescent idiopathic scoliosis brace studies: SRS Committee on Bracing and Nonoperative Management," *Spine (Phila Pa. 1976)*, vol. 30, pp. 2068-75; discussion 2076-7, Sep 15, 2005.
- [25] P. N. Soucacos, K. Zacharis, J. Gelalis, K. Soultanis, N. Kalos, A. Beris, T. Xenakis and E. O. Johnson, "Assessment of curve progression in idiopathic scoliosis," *Eur. Spine J.*, vol. 7, pp. 270-277, 1998.
- [26] L. Ramirez, N. G. Durdle, V. J. Raso and D. L. Hill, "A support vector machines classifier to assess the severity of idiopathic scoliosis from surface topography," *Information Technology in Biomedicine, IEEE Transactions On*, vol. 10, pp. 84-91, 2006.
- [27] T. L. Schulte, E. Hierholzer, A. Boerke, T. Lerner, U. Liljenqvist, V. Bullmann and L. Hackenberg, "Raster stereography versus radiography in the long-term follow-up of idiopathic scoliosis," *J. Spinal. Disord. Tech.*, vol. 21, pp. 23-28, Feb, 2008.
- [28] V. Pazos, F. Cheriet, L. Song, H. Labelle and J. Dansereau, "Accuracy assessment of human trunk surface 3D reconstructions from an optical digitising system," *Med. Biol. Eng. Comput.*, vol. 43, pp. 11-15, Jan, 2005.

- [29] W. W. Greulich and S. I. Pyle, *Radiographic Atlas of Skeletal Development of the Hand and Wrist*. Stanford University Press, 1959.
- [30] S. Ulkatan, M. Neuwirth, F. Bitan, C. Minardi, A. Kokoszka and V. Deletis, "Monitoring of scoliosis surgery with epidurally recorded motor evoked potentials (D wave) revealed false results," *Clinical Neurophysiology*, vol. 117, pp. 2093-2101, 9, 2006.
- [31] M. Gstoettner, K. Sekyra, N. Walochnik, P. Winter, R. Wachter and C. M. Bach, "Inter- and intraobserver reliability assessment of the Cobb angle: manual versus digital measurement tools," *Eur. Spine J.*, vol. 16, pp. 1587-1592, Oct, 2007.
- [32] T. Thulbourne and R. Gillespie, "The rib hump in idiopathic scoliosis. Measurement, analysis and response to treatment," *J. Bone Joint Surg. Br.*, vol. 58, pp. 64-71, Feb, 1976.
- [33] I. A. Stokes, "Three-dimensional terminology of spinal deformity. A report presented to the Scoliosis Research Society by the Scoliosis Research Society Working Group on 3-D terminology of spinal deformity," *Spine (Phila Pa. 1976)*, vol. 19, pp. 236-248, Jan 15, 1994.
- [34] G. R. Viviani, L. Budgell, C. Dok and P. Tugwell, "Assessment of accuracy of the scoliosis school screening examination," *Am. J. Public Health*, vol. 74, pp. 497-498, May, 1984.
- [35] C. M. Ronckers, M. M. Doody, J. E. Lonstein, M. Stovall and C. E. Land, "Multiple diagnostic X-rays for spine deformities and risk of breast cancer," *Cancer Epidemiol. Biomarkers Prev.*, vol. 17, pp. 605-613, Mar, 2008.
- [36] G. M. Ardran, R. Coates, R. A. Dickson, A. Dixon-Brown and F. M. Harding, "Assessment of scoliosis in children: low dose radiographic technique," *British Journal of Radiology*, vol. 53, pp. 146-147, February 01, 1980.
- [37] S. Don, "Radiosensitivity of children: potential for overexposure in CR and DR and magnitude of doses in ordinary radiographic examinations," *Pediatr. Radiol.*, vol. 34 Suppl 3, pp. S167-72; discussion S234-41, Oct, 2004.
- [38] M. Bethesda, "Induction of thyroid cancer by ionizing radiation," National Council on Radiation Protection and Measurements., Tech. Rep. 80, 1985.

- [39] D. A. Hoffman, J. E. Lonstein, M. M. Morin, W. Visscher, B. S. Harris 3rd and J. D. Boice Jr, "Breast cancer in women with scoliosis exposed to multiple diagnostic x rays," *J. Natl. Cancer Inst.*, vol. 81, pp. 1307-1312, Sep 6, 1989.
- [40] S. M. Lai, M. Asher and D. Burton, "Estimating SRS-22 quality of life measures with SF-36: application in idiopathic scoliosis," *Spine (Phila Pa. 1976)*, vol. 31, pp. 473-478, Feb 15, 2006.
- [41] R. K. Pratt, R. G. Burwell, A. A. Cole and J. K. Webb, "Patient and parental perception of adolescent idiopathic scoliosis before and after surgery in comparison with surface and radiographic measurements," *Spine (Phila Pa. 1976)*, vol. 27, pp. 1543-50; discussion 1551-2, Jul 15, 2002.
- [42] X. C. Liu, J. G. Thometz, R. M. Lyon and J. Klein, "Functional classification of patients with idiopathic scoliosis assessed by the Quantec system: a discriminant functional analysis to determine patient curve magnitude," *Spine (Phila Pa. 1976)*, vol. 26, pp. 1274-8; discussion 1279, Jun 1, 2001.
- [43] M. A. Asher and D. C. Burton, "Adolescent idiopathic scoliosis: natural history and long term treatment effects," *Scoliosis*, vol. 1, pp. 2, Mar 31, 2006.
- [44] I. Weisz, R. J. Jefferson, A. R. Turner-Smith, G. R. Houghton and J. D. Harris, "ISIS scanning: a useful assessment technique in the management of scoliosis," *Spine (Phila Pa. 1976)*, vol. 13, pp. 405-408, Apr, 1988.
- [45] E. G. Dawson, M. A. Kropf, G. Purcell, J. M. Kabo, L. E. Kanim and C. Burt, "Optoelectronic evaluation of trunk deformity in scoliosis," *Spine (Phila Pa. 1976)*, vol. 18, pp. 326-331, Mar 1, 1993.
- [46] P. Poncet, S. Delorme, J. L. Ronsky, J. Dansereau, G. Clynch, J. Harder, R. D. Dewar, H. Labelle, P. H. Gu and R. F. Zernicke, "Reconstruction of laser-scanned 3D torso topography and stereoradiographical spine and rib-cage geometry in scoliosis," *Comput. Methods Biomech. Biomed. Engin.*, vol. 4, pp. 59-75, 2000.
- [47] I. A. Stokes and M. S. Moreland, "Concordance of back surface asymmetry and spine shape in idiopathic scoliosis," *Spine (Phila Pa. 1976)*, vol. 14, pp. 73-78, Jan, 1989.
- [48] X. C. Liu, J. G. Thometz, R. M. Lyon and L. McGrady, "Effects of trunk position on back surface-contour measured by raster

stereophotography," *Am. J. Orthop. (Belle Mead NJ)*, vol. 31, pp. 402-406, Jul, 2002.

[49] I. A. F. Stokes, J. G. Armstrong and M. S. Moreland, "Spinal deformity and back surface asymmetry in idiopathic scoliosis," *J. Orthop. Res.*, vol. 6, pp. 129-137, 1988.

[50] W. P. Bunnell, "An objective criterion for scoliosis screening," *J. Bone Joint Surg. Am.*, vol. 66, pp. 1381-1387, Dec, 1984.

[51] M. S. Moreland, M. H. Pope, D. G. Wilder, I. Stokes and J. W. Frymoyer, "Moire fringe topography of the human body," *Med. Instrum.*, vol. 15, pp. 129-132, Mar-Apr, 1981.

[52] E. Hierholzer and W. Frobin, "Rasterstereography measurement and curvature analysis of the body surface of patients with spinal deformities. in: Moreland MS, pope MH, armstrong GWD (eds) Moire," in *Fringe Topography and Spinal Deformity* Anonymous New York: Pergamon Press, 1981, pp. 267-276.

[53] V. J. Raso, E. Lou, D. L. Hill, J. K. Mahood, M. J. Moreau and N. G. Durdle, "Trunk distortion in adolescent idiopathic scoliosis," *J. Pediatr. Orthop.*, vol. 18, pp. 222-226, Mar-Apr, 1998.

[54] P. O. Ajemba, A. Kumar, N. G. Durdle and V. J. Raso, "Quantifying torso deformity in scoliosis," pp. 614450-614450, March 2, 2006.

[55] P. O. Ajemba, N. G. Durdle, D. L. Hill and V. J. Raso, "A Torso-Imaging System to Quantify the Deformity Associated With Scoliosis," *Instrumentation and Measurement, IEEE Transactions On*, vol. 56, pp. 1520-1526, 2007.

[56] P. Ajemba, N. Durdle, D. Hill and J. Raso, "Classifying torso deformity in scoliosis using orthogonal maps of the torso," *Med. Biol. Eng. Comput.*, vol. 45, pp. 575-584, Jun, 2007.

[57] P. O. Ajemba, N. G. Durdle and V. J. Raso, "Characterizing torso shape deformity in scoliosis using structured splines models," *IEEE Trans. Biomed. Eng.*, vol. 56, pp. 1652-1662, Jun, 2009.

[58] P. Patias, T. B. Grivas, A. Kaspiris, C. Aggouris and E. Drakoutos, "A review of the trunk surface metrics used as Scoliosis and other deformities evaluation indices," *Scoliosis*, vol. 5, pp. 12-7161-5-12, Jun 29, 2010.

- [59] J. L. Jaremko, P. Poncet, J. Ronsky, J. Harder, J. Dansereau, H. Labelle and R. F. Zernicke, "Indices of torso asymmetry related to spinal deformity in scoliosis," *Clin. Biomech. (Bristol, Avon)*, vol. 17, pp. 559-568, Oct, 2002.
- [60] J. L. Jaremko, P. Poncet, J. Ronsky, J. Harder, J. Dansereau, H. Labelle and R. F. Zernicke, "Genetic algorithm-neural network estimation of cobb angle from torso asymmetry in scoliosis," *J. Biomech. Eng.*, vol. 124, pp. 496-503, Oct, 2002.
- [61] J. L. Jaremko, P. Poncet, J. Ronsky, J. Harder, J. Dansereau, H. Labelle and R. F. Zernicke, "Estimation of spinal deformity in scoliosis from torso surface cross sections," *Spine (Phila Pa. 1976)*, vol. 26, pp. 1583-1591, Jul 15, 2001.
- [62] C. Bergeron, F. Cheriet, J. Ronsky, R. Zernicke and H. Labelle, "Prediction of anterior scoliotic spinal curve from trunk surface using support vector regression," *Eng Appl Artif Intell*, vol. 18, pp. 973-983, dec, 2005.
- [63] M. F. Minguez, M. Buendia, R. M. Cibrian, R. Salvador, M. Laguia, A. Martin and F. Gomar, "Quantifier variables of the back surface deformity obtained with a noninvasive structured light method: evaluation of their usefulness in idiopathic scoliosis diagnosis," *Eur. Spine J.*, vol. 16, pp. 73-82, Jan, 2007.
- [64] I. A. Stokes and M. S. Moreland, "Measurement of the shape of the surface of the back in patients with scoliosis. The standing and forward-bending positions," *J. Bone Joint Surg. Am.*, vol. 69, pp. 203-211, Feb, 1987.
- [65] B. Drerup and E. Hierholzer, "Assessment of scoliotic deformity from back shape asymmetry using an improved mathematical model," *Clin. Biomech. (Bristol, Avon)*, vol. 11, pp. 376-383, Oct, 1996.
- [66] H. K. Wong, P. Balasubramaniam, U. Rajan and S. Y. Chng, "Direct spinal curvature digitization in scoliosis screening--a comparative study with Moire contourgraphy," *J. Spinal Disord.*, vol. 10, pp. 185-192, Jun, 1997.
- [67] J. E. Herzenberg, N. A. Waanders, R. F. Closkey, A. B. Schultz and R. N. Hensinger, "Cobb angle versus spinous process angle in adolescent idiopathic scoliosis. The relationship of the anterior and posterior deformities," *Spine (Phila Pa. 1976)*, vol. 15, pp. 874-879, Sep, 1990.
- [68] P. Knott, S. Mardjetko, M. Rollet, S. Baute, M. Riemenschneider and L. Muncie, "Evaluation of the reproducibility of the formetric 4D measurements for scoliosis," *Scoliosis*, vol. 5, 2010.

- [69] J. M. Frerich, K. Hertzler, P. Knott and S. Mardjetko, "Comparison of radiographic and surface topography measurements in adolescents with idiopathic scoliosis," *Open Orthop. J.*, vol. 6, pp. 261-265, 2012.
- [70] H. Wu, J. L. Ronsky, F. Cheriet, J. Kupper, J. Harder, D. Xue and R. F. Zernicke, "Prediction of scoliosis progression with serial three-dimensional spinal curves and the artificial progression surface technique," *Med. Biol. Eng. Comput.*, vol. 48, pp. 1065-1075, Nov, 2010.
- [71] I. V. Ponseti and B. Friedman, "Prognosis in idiopathic scoliosis," *The Journal of Bone & Joint Surgery*, vol. 32, pp. 381-395, April 1, 1950.
- [72] H. A. King, J. H. Moe, D. S. Bradford and R. B. Winter, "The selection of fusion levels in thoracic idiopathic scoliosis," *J. Bone Joint Surg. Am.*, vol. 65, pp. 1302-1313, Dec, 1983.
- [73] L. G. LENKE, R. R. BETZ, K. H. BRIDWELL, D. H. CLEMENTS, J. HARMS, T. G. LOWE and H. L. SHUFFLEBARGER, "Intraobserver and Interobserver Reliability of the Classification of Thoracic Adolescent Idiopathic Scoliosis*†," *The Journal of Bone & Joint Surgery*, vol. 80, pp. 1097-1106, August 1, 1998.
- [74] E. F. Robinson and W. D. Wade, "Statistical assessment of two methods of measuring scoliosis before treatment," *Can. Med. Assoc. J.*, vol. 129, pp. 839-841, Oct 15, 1983.
- [75] A. C. Kittleson and L. W. Lim, "Measurement of scoliosis," *Am. J. Roentgenol. Radium Ther. Nucl. Med.*, vol. 108, pp. 775-777, Apr, 1970.
- [76] L. G. Lenke, R. R. Betz, J. Harms, K. H. Bridwell, D. H. Clements, T. G. Lowe and K. Blanke, "Adolescent Idiopathic Scoliosis A New Classification to Determine Extent of Spinal Arthrodesis," *The Journal of Bone & Joint Surgery*, vol. 83, pp. 1169-1181, August 1, 2001.
- [77] L. G. Lenke, R. R. Betz, T. R. Haher, M. A. Lapp, A. A. Merola, J. Harms and H. L. Shufflebarger, "Multisurgeon assessment of surgical decision-making in adolescent idiopathic scoliosis: curve classification, operative approach, and fusion levels," *Spine (Phila Pa. 1976)*, vol. 26, pp. 2347-2353, Nov 1, 2001.
- [78] L. Seoud, M. M. Adankon, H. Labelle, J. Dansereau and F. Cheriet, "Prediction of scoliosis curve type based on the analysis of trunk surface topography," in

Biomedical Imaging: From Nano to Macro, 2010 IEEE International Symposium On, 2010, pp. 408-411.

[79] M. M. Adankon, J. Dansereau, H. Labelle and F. Cheriet, "Non invasive classification system of scoliosis curve types using least-squares support vector machines," *Artif. Intell. Med.*, vol. 56, pp. 99-107, Oct, 2012.

[80] M. H. Mehta, "The rib-vertebra angle in the early diagnosis between resolving and progressive infantile scoliosis," *J. Bone Joint Surg. Br.*, vol. 54, pp. 230-243, May, 1972.

[81] N. J. Oxborrow, "Assessing the child with scoliosis: the role of surface topography," *Archives of Disease in Childhood*, vol. 83, pp. 453-455, November 01, 2000.

[82] M. M. Adankon, N. Chihab, J. Dansereau, H. Labelle and F. Cheriet, "Scoliosis follow-up using noninvasive trunk surface acquisition," *IEEE Trans. Biomed. Eng.*, vol. 60, pp. 2262-2270, Aug, 2013.

[83] P. G. Korovessis and M. V. Stamatakis, "Prediction of scoliotic cobb angle with the use of the scoliometer," *Spine (Phila Pa. 1976)*, vol. 21, pp. 1661-1666, Jul 15, 1996.

[84] H. Wu, P. Poncet, J. Harder, F. Cheriet, H. Labelle, R. F. Zernicke and J. L. Ronsky, "Prediction of scoliosis progression in time series using artificial intelligence techniques," *Journal of Bone & Joint Surgery, British Volume*, vol. 90-B, pp. 100-101, March 01, 2008.

[85] D. W. Murray and C. J. Bulstrode, "The development of adolescent idiopathic scoliosis," *Eur. Spine J.*, vol. 5, pp. 251-257, 1996.

[86] M. Ylikoski, "Spinal growth and progression of adolescent idiopathic scoliosis," *Eur. Spine J.*, vol. 1, pp. 236-239, Mar, 1993.

[87] L. Samuelsson and L. Noren, "Trunk rotation in scoliosis. The influence of curve type and direction in 150 children," *Acta Orthop. Scand.*, vol. 68, pp. 273-276, Jun, 1997.

[88] E. C. Parent, P. Q. Zhang, D. Hill, M. Moreau, D. Hedden and E. Lou, "Sensitivity-to-change of Full Torso Surface Topography Measurements in Adolescents with Idiopathic Scoliosis and a Main Thoracic Curve," *Stud. Health Technol. Inform.*, vol. 176, pp. 484, 2012.

- [89] P. O. Ajemba, N. G. Durdle, D. L. Hill and V. J. Raso, "Validating an imaging and analysis system for assessing torso deformities," *Comput. Biol. Med.*, vol. 38, pp. 294-303, Mar, 2008.
- [90] N. Tardif, P. Poncet, J. L. Ronsky, J. Dansereau and R. F. Zernicke, "Evaluation of an Integrated Laser Imaging/X-Ray Technique for Torso Asymmetry Measurement in Scoliosis." *Archives of Physiology and Biochemistry*, vol. 108, pp. 200, 2000.
- [91] Konica Minolta Inc., "Polygon Editing Tool," 2012.
- [92] Geomagic Inc., "Geomagic Qualify," 2013.
- [93] Wolfram Research Inc., "Wolfram Mathematica 9," 2012.
- [94] F. Cheriet, D. Jiang and N. F. Stewart, "Modelling of scoliotic deformities." *Int.J.Model.Simul.*, vol. 27, pp. 171-180, 2007.
- [95] J. S. Smith, C. I. Shaffrey, C. Kuntz 4th and P. V. Mummaneni, "Classification systems for adolescent and adult scoliosis," *Neurosurgery*, vol. 63, pp. 16-24, Sep, 2008.
- [96] K. L. Gwet, *Handbook of Inter-Rater Reliability : The Definitive Guide to Measuring the Extent of Agreement among Raters*. Gaithersburg, MD: Advanced Analytics, LLC, 2012.
- [97] J. Cohen, "A Coefficient of Agreement for Nominal Scales," *Educational and Psychological Measurement*, vol. 20, 1960.
- [98] M. Asher, S. M. Lai, D. Burton and B. Manna, "The influence of spine and trunk deformity on preoperative idiopathic scoliosis patients' health-related quality of life questionnaire responses," *Spine (Phila Pa. 1976)*, vol. 29, pp. 861-868, Apr 15, 2004.
- [99] L. Hackenberg, E. Hierholzer, W. Potzl, C. Gotze and U. Liljenqvist, "Rasterstereographic back shape analysis in idiopathic scoliosis after posterior correction and fusion," *Clin. Biomech. (Bristol, Avon)*, vol. 18, pp. 883-889, Dec, 2003.
- [100] D. Ovadia, E. Bar-On, B. Fragniere, M. Rigo, D. Dickman, J. Leitner, S. Wientroub and J. Dubousset, "Radiation-free quantitative assessment of scoliosis: a multi center prospective study," *Eur. Spine J.*, vol. 16, pp. 97-105, Jan, 2007.

- [101] N. Suzuki, Inami K., T. Ono, K. Kohno and M. A. Asher, "Analysis of Posterior Trunk Symmetry Index (POTSI) in Scoliosis. Part 1," *Studies in Health Technology and Informatics*, vol. 59, pp. 81-84, 1999.
- [102] A. Komeili, L. Westover, E. Parent, M. Moreau, M. El-Rich and S. Adeeb, "A Novel Surface Topography Technique to Evaluate Torso Asymmetry in Adolescent Idiopathic Scoliosis," *13th Annual Scientific Conference of the Canadian Spine Society*, 2013.
- [103] B. P. Yawn and R. A. Yawn, "The estimated cost of school scoliosis screening," *Spine (Phila Pa. 1976)*, vol. 25, pp. 2387-2391, Sep 15, 2000.
- [104] M. Rigo and E. D'Agata, "Comparison between subjective perception of trunk deformity (TAPS) and objective assessment of back asymmetry (surface topography)," *Scoliosis*, vol. 8, 2013.
- [105] IBM Corp., "IBM SPSS Statistics 21," 2012.
- [106] G. Meghabghab and A. Kandel, *Search Engines, Link Analysis, and User's Web Behavior*. Springer, 2008.
- [107] N. D. Scutt, P. H. Dangerfield and J. C. Dorgan, "The relationship between surface and radiological deformity in adolescent idiopathic scoliosis: effect of change in body position," *Eur. Spine J.*, vol. 5, pp. 85-90, 1996.
- [108] J. Lonstein and J. Carlson, "The prediction of curve progression in untreated idiopathic scoliosis during growth," *The Journal of Bone & Joint Surgery*, vol. 66, pp. 1061-1071, September 1, 1984.
- [109] L. E. Peterson and A. L. Nachemson, "Prediction of progression of the curve in girls who have adolescent idiopathic scoliosis of moderate severity. Logistic regression analysis based on data from The Brace Study of the Scoliosis Research Society," *J. Bone Joint Surg. Am.*, vol. 77, pp. 823-827, Jun, 1995.
- [110] G. Duval-Beaupere and T. Lamireau, "Scoliosis at less than 30 degrees. Properties of the evolutivity (risk of progression)," *Spine (Phila Pa. 1976)*, vol. 10, pp. 421-424, Jun, 1985.
- [111] K. J. Tan, M. M. Moe, R. Vaithinathan and H. K. Wong, "Curve progression in idiopathic scoliosis: follow-up study to skeletal maturity," *Spine (Phila Pa. 1976)*, vol. 34, pp. 697-700, Apr 1, 2009.

- [112] C. F. Lee, D. Y. Fong, K. M. Cheung, J. C. Cheng, B. K. Ng, T. P. Lam, P. S. Yip and K. D. Luk, "A new risk classification rule for curve progression in adolescent idiopathic scoliosis," *Spine J.*, vol. 12, pp. 989-995, Nov, 2012.
- [113] J. Van Goethem, A. Van Campenhout, L. van den Hauwe and P. M. Parizel, "Scoliosis," *Neuroimaging Clin. N. Am.*, vol. 17, pp. 105-115, 2, 2007.
- [114] L. A. Karol, C. E. Johnston, R. H. Browne and M. Madison, "Progression of the curve in boys who have idiopathic scoliosis," *The Journal of Bone & Joint Surgery*, vol. 75, pp. 1804-1810, 12/01, 1993.
- [115] M. C. Cassella and J. E. Hall, "Current treatment approaches in the nonoperative and operative management of adolescent idiopathic scoliosis," *Phys. Ther.*, vol. 71, pp. 897-909, Dec, 1991.
- [116] N. Suzuki, T. Ono, M. Tezuka and S. Kamiishi, "Moiré topography and back shape analysis-clinical application," in *International Symposium on Three Dimensional Scoliotic Deformities*, Stuttgart: Gustav Fisher Verlag, 1992, pp. 124-128.
- [117] X. Liu, J. C. Tassone, J. G. Thometz, L. C. Paulsen, R. M. Lyon, C. Marquez-Barrientos, S. Tarima and P. R. Johnson, "Development of a 3-Dimensional Back Contour Imaging System for Monitoring Scoliosis Progression in Children," *Spine Deformity*, vol. 1, pp. 102-107, 03/01, 2013.
- [118] J. L. Jaremko, P. Poncet, J. Ronsky, J. Harder, J. Dansereau, H. Labelle and R. F. Zernicke, "Comparison of Cobb angles measured manually, calculated from 3-D spinal reconstruction, and estimated from torso asymmetry," *Comput. Methods Biomech. Biomed. Engin.*, vol. 5, pp. 277-281, Aug, 2002.
- [119] S. C. Huang, "Cut-off point of the Scoliometer in school scoliosis screening," *Spine (Phila Pa. 1976)*, vol. 22, pp. 1985-1989, Sep 1, 1997.
- [120] R. Lyon, X. Liu and J. Thometz, "Reduced need for spinal radiographs with use of a raster stereography." in *35th Annual Meeting of the Scoliosis Research Society*, Australia, October 18-21 2000, pp. 18-21.
- [121] H. Weiss and S. Seibel, "Can surface topography replace radiography in the management of patients with scoliosis?" *Hard Tissue*, vol. 2, pp. 19, 2013.

- [122] S. S. Klos, X. C. Liu, R. M. Lyon, J. C. Tassone and J. G. Thometz, "Reliability of a functional classification system in the monitoring of patients with idiopathic scoliosis," *Spine (Phila Pa. 1976)*, vol. 32, pp. 1662-1666, Jul 1, 2007.
- [123] Y. Petit, C. Aubin and H. Labelle, "Three-dimensional imaging for the surgical treatment of idiopathic scoliosis in adolescents," *Canadian Journal of Surgery*, vol. 45, pp. 453-458, 2002.
- [124] A. Komeili, L. Westover, E. Parent, M. Moreau, M. El-Rich and S. Adeeb, "Surface topography asymmetry maps categorizing external deformity in scoliosis," *The Spine Journal*, 2014.
- [125] E. C. Parent, R. Dang, D. Hill, J. Mahood, M. Moreau, J. Raso and E. Lou, "Score distribution of the scoliosis research society-22 questionnaire in subgroups of patients of all ages with idiopathic scoliosis," *Spine (Phila Pa. 1976)*, vol. 35, pp. 568-577, Mar 1, 2010.
- [126] A. Komeili, L. Westover, E. Parent, M. El-Rich and S. Adeeb, "Correlation between a Novel Surface Topography Asymmetry Analysis and Radiographic Data on Scoliosis Curvatures," *Spine*, 2014.
- [127] S. Allen, E. Parent, M. Khorasani, D. L. Hill, E. Lou and J. V. Raso, "Validity and reliability of active shape models for the estimation of cobb angle in patients with adolescent idiopathic scoliosis," *J. Digit. Imaging*, vol. 21, pp. 208-218, Jun, 2008.
- [128] H. L. Brooks, S. P. Azen, E. Gerberg, R. Brooks and L. Chan, "Scoliosis: A prospective epidemiological study," *J. Bone Joint Surg. Am.*, vol. 57, pp. 968-972, Oct, 1975.
- [129] A. Komeili, E. Parent, M. El-Rich and S. Adeeb, "Monitoring the thoracic/thoracolumbar scoliosis curves progression using surface topography asymmetry analysis of the torso in adolescents," in *IMAST 21st International Meeting on Advanced Spine Techniques*, Valencia, Spain, 2014, pp. 144.
- [130] M. Mohokum, S. Mendoza, W. Udo, H. Sitter, J. R. Paletta and A. Skwara, "Reproducibility of rasterstereography for kyphotic and lordotic angles, trunk length, and trunk inclination: a reliability study," *Spine (Phila Pa. 1976)*, vol. 35, pp. 1353-1358, Jun 15, 2010.

- [131] P. O. Ajemba, N. G. Durdle and V. James Raso, "Clinical monitoring of torso deformities in scoliosis using structured splines models," *Med. Biol. Eng. Comput.*, vol. 46, pp. 1201-1208, Dec, 2008.
- [132] A. Trovato, A. Komeili, L. Westover, E. Parent, M. Moreau, S. Adeeb and E. Sepúlveda, "Examination of the breast asymmetry associated with adolescent idiopathic scoliosis using surface topography methods," *Scoliosis*, vol. 8, pp. 1-2, 09/18, 2013.
- [133] L. Seoud, J. Dansereau, H. Labelle and F. Cheriet, "Multilevel analysis of trunk surface measurements for noninvasive assessment of scoliosis deformities," *Spine (Phila Pa. 1976)*, vol. 37, pp. E1045-53, Aug 1, 2012.
- [134] A. Komeili, L. Westover, E. Parent, M. Moreau, M. El-Rich and S. Adeeb, "Monitoring for Idiopathic Scoliosis Curve Progression Using Surface Topography Asymmetry Analysis of the Torso in Adolescents," *The Spine Journal*, 2014.
- [135] S. Hill, E. Franco-Sepulveda, A. Komeili, A. Trovato, E. Parent, D. Hill, E. Lou and S. Adeeb, "Assessing asymmetry using reflection and rotoinversion in biomedical engineering applications," *Proc. Inst. Mech. Eng. H.*, vol. 228, pp. 523-529, Apr 11, 2014.
- [136] H. Normelli, J. A. Sevastik, G. Ljung and A. M. Jonsson-Soderstrom, "The symmetry of the breasts in normal and scoliotic girls," *Spine (Phila Pa. 1976)*, vol. 11, pp. 749-752, Sep, 1986.
- [137] C. Denoel, M. F. Aguirre, G. Bianco, P. H. Mahaudens, R. Vanwijck, S. Garson, R. Sinna and A. Debrun, "Idiopathic scoliosis and breast asymmetry," *J. Plast. Reconstr. Aesthet. Surg.*, vol. 62, pp. 1303-1308, Oct, 2009.
- [138] T. Eidlitz-Markus, M. Mukamel, Y. Haimi-Cohen, J. Amir and A. Zeharia, "Breast asymmetry during adolescence: physiologic and non-physiologic causes," *Isr. Med. Assoc. J.*, vol. 12, pp. 203-206, Apr, 2010.
- [139] F. C. Tsai, M. S. Hsieh, C. K. Liao and S. T. Wu, "Correlation between scoliosis and breast asymmetries in women undergoing augmentation mammoplasty," *Aesthetic Plast. Surg.*, vol. 34, pp. 374-380, Jun, 2010.
- [140] A. Komeili, L. Westover, E. F. Sepulveda, E. Parent, M. Moreau, M. El-Rich and S. Adeeb, "Assessment of torso deformities using 3D markerless asymmetry analysis and its clinical applications," *Scoliosis*, vol. 8, 2013.

